INTERACTIONS OF MINERAL SURFACES AND ADSORBATES: A COMPUTATIONAL MODELING APPROACH

by

Subhashis Biswas

A dissertation submitted in partial fulfillment
of the requirements for the degree of
Doctor of Philosophy
(Geology)
in the University of Michigan
2008

Doctoral Committee:

Associate Professor Udo Becker, Chair
Professor Rodney C. Ewing
Professor Kim F. Hayes
Professor Stephen E. Kesler
Professor David H. Kohn

Dedication

To all those people, whose little contributions have made this journey possible and enjoyable

Acknowledgement

First I would like to thank my advisor Udo Becker. He has given me the opportunity to explore science at a different level, and he has made the working environment really enjoyable. His enthusiasm on every aspect of research is so contagious that it has always helped me to give my best. I have learned and explored various aspects of biomineralization, surface science and computational mineralogy under Udo's guidance, and I think this will help me to mature as a research scientist in my career. Thank you Udo, for everything.

I would like to thank all my committee members, Prof. Ewing, Prof. Hayes, Prof. Kesler and Prof. Kohn for their valuable suggestions and guidance. My outlook and perception of mineralogy and Mineral science was given a total new direction by Professor Rod Ewing and Udo Becker. I have enjoyed discussing mineral science, and other aspects of science in general with Prof Becker and Prof Ewing and it helped me broaden my scientific horizon. I would like to mention special thanks to Prof Steve Kesler. He was my first ever teacher in a Geological Science course, and he was the first person who have inspired me in joining Geological Sciences. His wealth of knowledge in the field of geochemistry, economic geology and environmental science influenced my interest in my research to a great extent.

I would like to thank Professor Kim Hayes, who is also the cognate member in my committee. His suggestions and inputs have strengthened my work with calcite

biomineralization, as well as work with $As(OH)_3$ adsorption on galena surface. I would also like to thank Prof. David Kohn, for his guidance with my work in hydroxyapatite project. I have learned a great extent about bone tissue engineering, and scaffold formation from his research. I have grown increased interest in carbonate substitution in hydroxyapatite and related experimental work during my PhD working with Dr. Kohn and Sharon Segvich.

I am so honored and fortunate to have such wonderful committee members, such a wealth of experience and knowledge around me.

A special thanks to my good friend and colleague, Sharon Segvich. We started our collaboration on the hydroxyapatite project from 2004 fall semester, and we enjoyed so much doing research together. Sharon is an excellent experimentalist in the field of bone tissue engineering, and she enhanced my knowledge of bone growth and regeneration immensely. She helped me regarding the modeling and simulation of different peptides on hydroxyapatite surface. Her new technique for calculating hydration energies of peptides using Gaussian03 helped my calculation of hydration energies in various small peptides. Her constant help and suggestion on various chapters of my thesis is highly appreciated. Thank you Sharon, it has been wonderful experience working with you.

I would like to thank Jian-wei Wang, for his valuable inputs and suggestions in working with calcite seed crystallizations in 3-D network. His expertise and suggestions with aqueous systems and force-field has been of great help.

I would like to thank all my group members, Martin Reich, Frannie Skomurski, Darius Dixon, Lindsay Shuller, Devon Renock, Elizabeth Anderson for helping me with

heart whenever required, and for making the work environment so much enjoyable. The camaraderie between us was excellent and something to cherish for rest of my life. Without you, it would not have been possible to complete my research.

I would like to thank the Department of Geological Science, all faculty members, graduate students and staff members I came across with, to make graduate school such a nice and enjoyable place. A special thanks to Anne Hudon for taking care of all official and administrative matters with such ease, and making life so easy during my stay at the department. I have also received great help from all other staff members, and would like to express thanks to them as well. I would like to thank Mike Messina, whose constant effort to make our computational working environment better was of immense help.

I should mention my fellow graduate students in the department. You are truly good friends and good person by heart. I consider myself so privileged to have friends like you in graduate school. I thank you for your help in both academic and non-academic front, and for making me feel at home always. I sincerely express my gratitude to all of you.

Finally, I would like to thank my family members and friends, whose constant support and encouragement has brought me this far, and I hope to carry forward their wishes.

Table of Contents

LIST OF FIGURES

LIST OF TABLES

Chapter 1

Introduction

Environmental science and environmental geology investigate the phenomena and processes occurring at the Earth's surface, both at the macroscopic and microscopic scale. Mineral surface science is a tool to understand environmentally relevant geochemical processes at the micro and nano-scale. Two important processes that occur on surfaces are crystal growth and dissolution. Crystal growth on surfaces can be controlled by the presence of organic molecules and templates, which can influence dissolution rates and the morphology of minerals. It is well known that some organic molecules, such as phosphonic and carboxylic acids, have the ability to retard or totally inhibit crystal growth from solution [Pina et al, 2004, this paper is co-authored by S. Biswas; Becker et al, 2005]. In addition to the geochemical importance of growth inhibitors, growth inhibition is of particular interest in industrial processes where the growth of undesirable crystalline solids must be prevented (e.g., barite scale formation in off-shore oil wells, formation of various scales in water treatment processes).

The structure of mineral surfaces and minerals change at the nano, micro, and macro-scale due to the adsorption of organic and/or inorganic molecules at the surface, specifically on active growth sites on these surfaces such as steps and kinks. However, in order to understand, predict, and control crystal growth, we need to understand the molecular mechanisms that govern the inhibitor–crystal interaction. Incorporation of different elements (e.g., iron) into specific functional structures (e.g., siderophores) that match the topography of the surface needs to be understood in order to explain morphology-controlled crystal growth and dissolution as it is observed, e.g., in biomineralization processes.

In the past, adsorption of molecules to mineral surfaces has been indirectly investigated from bulk experiments. Measurements of crystallization rates in the presence of inhibitors have been attributed to the adsorption of molecules to active growth sites on surfaces. Surface techniques such as AFM provide the opportunity to study the effect of inhibitors on crystal growth in situ at a nanometer scale, and they allow direct measurements of growth rates. However, the actual energetics of the adsorption and the adsorbate structure on different surface sites needs to be determined using computational methods. The energy of the surface, the adsorption energy of organic molecules to the mineral surface, variation of adsorption energies of the growth-inhibitor at different surface sites (kink, step, edge, and terrace) can be calculated using empirical force-field and quantum mechanical methods. The computational expense of the latter is prohibitive to be applied to systems of thousands of atoms as used in computational biomineralization studies. Therefore, quantum-mechanical methods mainly serve to derive and test the force fields used in empirical methods or to study electron transfer

processes in smaller systems. Computational modeling of the adsorption of growth inhibitors and modifiers onto mineral surfaces and performing static energy minimizations and molecular dynamics simulations allows us to determine the energies required for the growth inhibition and adsorption of these molecules to mineral surfaces and their possible structural attachment and formation.

The main theme of this thesis is the interaction of adsorbates with mineral surfaces. Adsorbates can be divided into two categories, organic and inorganic adsorbates. The major part of my work deals with organic adsorbates on mineral surfaces. Organic adsorbates are mostly associated with biological systems in the environment. These biological systems/organisms induce mineral deposition in natural environments. In other words, biologically-mediated activities of these organisms lead to mineral nucleation and growth. This process is called biomineralization. There are two types of biomineralization depending on the level of biological control, (i) **biologically induced mineralization** and (ii) **biologically controlled mineralization**. The type of biomineralization that is studied during this research is biologically controlled mineralization.

Biologically induced mineralization occurs as a result of chemical changes in the environment of an organism, which can promote mineral precipitation as in the case of coral formation.

In **biologically controlled mineralization** morphologically complex structures nucleate and grow in concert with a genetically programmed macromolecular matrix of proteins, polysaccharides, and lipids. The resulting mineral micro-architectures fulfill specific physiological functions such as the addition of stiffness and strength to skeletal

tissues. These ‘‘biomaterials’’ can have remarkable physical properties that can often not be imitated by even sophisticated synthetic materials. Synthetic materials that make use of the interactions between organic matrices and inorganic crystals are called biomimetic materials and designing these biomimetic materials is one of the fastest-growing subjects in materials engineering [Shin et al, 2003].

Mostly carbonates and phosphates, and to a minor degree oxides, sulfates, and sulfides can be formed by biomineralization processes. Of these, the calcium carbonates, calcite and aragonite, have the most widespread occurrence in nature and form through either type of biomineralization.

A stable interface between the organic matrix and the nucleating surface of the biomineral is needed for biomineralization to occur. Certain thermodynamic and physical properties of the two surfaces forming the interface are required to match to form a stable interface, such as polarity, electrostatic potential, lattice geometry, and topography. This process of structural and physico-chemical matching of two types of surfaces has been investigated by various researchers [Sethmann et al, 2005, Mann, 2001]. Scientists have done experimental work to address the mechanism of growth of inorganic nucleating surface under the influence of an organic matrix [Pina et al., 1998, Orme et al, 2001, Addadi et al, 1985]. These studies helped to address the growth morphologies of nucleating mineral surfaces. To further understand biomineralization, it is necessary to study various properties of organic matrices along with mineral surface growth morphologies. Chapter 2 describes different properties of peptides, which can be part of organic matrices promoting biomineralization. Such peptides can induce selective stabilization of surface steps on nucleating mineral surfaces. The peptides studied in

Chapter 2 are small representatives of large organic matrices that govern the inorganic nucleating mineral formation during biomineralization. Thus, information on the behavior of these peptides in the selective stabilization of mineral surface steps can further the understanding of organic matrix mediated inorganic nucleus stabilization. The two main hypotheses that are tested in Chapter 2 are:

- *Can interfacial (adsorption) energies of specific peptides on particular calcite surfaces elucidate the selectivity for particular calcite surfaces and surface steps during biomineral formation?*
- *What role do side chain functional groups of the peptides play in the selective adsorption of peptides to inorganic nucleating mineral surfaces?*

The inorganic nucleating mineral surface studied in Chapters 2 and 3 is calcite (104). Calcite is a rhombohedral polymorph of calcium carbonate ($CaCO_3$). DNA, which is a double-stranded helix consisting of polymers found in the nucleus of the cell of living organisms, controls the initial biomineralization process by transferring its genetic information to proteins in the outer cell wall [Dickerson et al, 2004]. When an organism forms a template in its exoskeleton, it is thought to be an image of the genetic information carried in its DNA. Thus, the mineral deposition on the exoskeleton of the organism can be related to its DNA pattern. According to the central dogma of molecular biology, translation of DNA forms RNA, and transcription of RNA forms proteins [Crick, 1970]. Proteins are polymers of amino acids linked via peptide bonds in a specific sequence. Proteins are large complex molecules and, therefore, computationally expensive to study. In order to make the system more accessible to a molecular-simulations approach, the role of proteins in this study was simplified by peptides of

different chain lengths. Such an approach allows to determine the influence of individual functional groups that “control” mineralization when biologically-controlled mineralization is studied. Proteins are made up of amino-acids in particular sequences and consist of various functional groups in their side chain. These functional groups can be of acidic or alkaline nature, and they can be bulky and, thus, may pose steric hindrance to the mineral-adsorbate interaction. Functional groups carry a specific charge depending on pH and the pKa values of the functional groups of particular amino acids which can influence mineral deposition.

In Chapter 2, selective adsorption of peptides to specific surface steps are investigated. We study the interaction of small peptides (3-amino acid and 12-amino acid long) with the calcite {104} family of faces, which are the most stable faces of calcite. The peptides investigated have different structures and different protonation states. The molecular modelling study of peptide-calcite interaction in this chapter elucidates the effect of electrostatic and van-der-Waals adsorbate-mineral interaction and the potential steric hindrance during the alignment of peptides on calcite surfaces and surface steps. The latter process determines how peptides adopt different structural orientations during mineral-adsorbate interaction. Since all of these processes take place in an aqueous environment, the effect of hydration is taken into account in our calculations.

Peptide-calcite interactions in two-dimensions are the subject of Chapter 3, while in Chapter 2, the selectivity of the peptides for specific surface steps can be considered to be in one-dimensional approach along the surface step. This selectivity of calcite surface occurs during the formation of biomineral. The two-dimensional interface used in Chapter 3 is mimicked by calcite seed nuclei in contact with compressed biofilms.

Biofilms are representative of organic matrices in nature that induce mineral seed nucleation at the onset of biomineral formation. Langmuir films have been used in the past in experimental approaches not only to control the growth of different calcium carbonate polymorphs but also to create crystallographically well-defined organic-carbonate interfaces [Mann, 1988]. Previous studies have investigated the formation of calcite seed nuclei from supersaturated calcium carbonate solutions in contact with Langmuir films [Buijnsters et al, 2001]. We are one of the first to generate computer models of such periodic Langmuir films using amphiphilic organic molecules that have long hydrophobic carbon chains and a polar head-groups. In the experiments, the distances between the polar head groups are controlled using microscopic pistons. In our computer experiments, this setup is simulated by applying an external pressure. Under conditions, where the separation of the functional groups agrees with the distances of Ca^{2+} ions on a particular carbonate surface, nulceation of calcium carbonate seeds can be facilitated. The main hypotheses tested in Chapter 3 are:

- *What surface of calcite can form a stable interface under compressed biofilms in an aqueous medium?*
- *How can the structural and functional aspects of organic molecules in biofilms play a role in stable calcite seed nucleus formation?*

The stability of the organic(Langmuir film)-inorganic(calcite surface) interface is studied in Chapter 3 to find the most favorable interface of calcite that can be formed under biofilms. This approach was chosen because the actual timescale of calcite seed formation in experiments is much longer than the timescale of computational modeling, which makes real-time molecular-dynamics simulations of growth-seed formation under

Langmuir films prohibitive. Thus, the simulations in Chapter 3 start with nuclei that have different interfaces with the organic matrix and their respective stabilities are investigated. In this setup, the aqueous environment is calculated using a molecular dynamics approach of the surrounding water. This captures more closely biomineralization in nature, where crystal growth occurs after the crystal nucleus is developed and the mineral keeps growing from such a nucleus.

Chapter 4 deals with a type of biomineralization as it occurs in the formation of bones and teeth**.** Biominerals can nucleate and grow in concert with the macromolecular structure of biological molecules like proteins, lipids, and polysaccharides. The resulting mineral architectures (controlled biominerals in this case) perform specific physiological functions such as bone regeneration and provide mechanical strength to the bone tissue. Thus, understanding biomineral formation at a molecular level is important for tissue engineering, and this knowledge can help us optimize ways to restructure bone growth that is specific for a particular organism. In this context, Chapter 4 describes possible interactions of bioactive surfaces with biomaterials that cause cell adhesion during bone-tissue regeneration. The main aspect of bone-tissue engineering is attaining the original functionality of the damaged tissue. To achieve this, cell adhesion to synthetic support (e.g., biomaterials) via bioactive surfaces is required to happen. The bioactive surfaces can be extracellular proteins, cell-mediated synthetic proteins, or bio-engineered motifs. All these three types of bioactive surfaces interact with the biomaterial (e.g., carbonated hydroxyapatite in bone [Garcia et. al, 2005]). This biological molecule-inorganic mineral interaction leads to a series of cellular events including cell-adhesion that finally lead to bone-tissue regeneration [Garcia et al, 2005, Burdick et al, 2002]. Thus, it is important to

understand the interaction between bioactive surfaces (proteins) and biomaterial (carbonated hydroxyapatite) in order to understand bone-tissue engineering, because these interactions are stepping stone of the bone tissue regeneration process. In Chapter 4, the biological organic molecule adsorbates chosen are peptides from various sources that contribute in bone formation. RGD (arg-gly-asp) is a ubiquitous protein, YIGSR (tyr-ile-gly-ser-arg) is derived from laminin, and E_7PRGDT is derived from bone-sialoprotein [Loh et al, 2000, Iwamoto et al, 1987, Itoh et al, 2002]. The role of these peptides in cell-adhesion has been studied experimentally [Okamoto et al, 1998, Gilbert et. al, 2000]. However, the orientation of these peptides alongside a biomaterial surface is still fairly unknown. In Chapter 4, the main hypothesis that is tested is:

- *Can interfacial (adsorption) energies of specific peptides on particular hydroxyapatite surfaces elucidate the influence of peptide orientation on particular hydroxyapatite surfaces and surface step-locations during peptide-biomaterial interaction prior to cell-adhesion?*

Hydroxyapatite is chosen as biomaterials surface as relaxed hydroxyapatite surface represents the actual biomaterial component of bone, i.e., carbonated hydroxyapatite [Astala et. al, 2005]. Hydroxyapatite and carbonated hydroxyapatite are the main components of bone-minerals. Hydroxyapatite has a hexagonal structure and has different surfaces where organic molecules can get adsorbed. A stoichiometric, charge-neutral, and dipole-free hydroxyapatite (001) surface was constructed for these studies, and empirical potentials were employed to study the organic molecule-inorganic mineral surface interactions. In addition to flat (001) terraces, surface steps parallel to [010] on the (001) surface were created to analyze peptide interactions with and their orientation along these

steps. This work is an initial study of the adsorption mechanism of peptides on hydroxyapatite surfaces, which evaluates the interfacial structure of bioactive surface and hydroxyapatite (001) face. There are other faces such as (100), (010), and (213) of the hydroxyapatite and carbonated hydroxyapatite that can be studied to determine different possible faces of biomaterials surfaces present in bone where peptides can interact to trigger cell-adhesion during bone-tissue engineering. These faces are on the side of the tabular hexagonal prism form of the hydroxyapatite crystal, and peptides can easily access and interact with these faces during bioactive surface-biomaterial interaction prior to cell-adhesion.

This work and additional modeling on peptide-carbonated hydroxyapatite interaction in the future using other peptides, surfaces, and steps on these will help us address complex bone-formation questions. This will lead to a more interdisciplinary approach where biominerals can be used extensively as medical implants.

In contrast to the empirical force-field calculations on organic matter-mineral interactions, a quantum-mechanical approach has been used in Chapter 5 to evaluate electron-transfer processes through semiconducting mineral surfaces between adsorbed redox couples. In systems where electron transfer occurs, such as semiconducting minerals like galena, and redox couples like oxides and As(III) species, a quantum mechanical approach is required (Chapter 5).

In natural environments, water, especially groundwater carries various amounts of dissolved and suspended species. When the groundwater comes in contact with the minerals, these species can interact with the mineral. Arsenic is one example of such an element that is carried by groundwater. Arsenic can be useful and important, but also

poisonous. Its mobility in groundwater, its poisoning effect, its use in medicinal applications, its use in extraction of iron from iron core, and many more other geochemical and industrial aspects have made this element an important subject for research and exploration. As(III) is more soluble and mobile in solution than As(V) [Dixit et. al, 2003]. As(III) is also more toxic than its oxidized counterpart. The most common natural As(III) species in groundwater is $As(OH)_3$. To minimize the concentration of As in groundwater, it is necessary that $As(OH)_3$ gets adsorbed to mineral surfaces and subsequently oxidized while oxidation in solution is often kinetically hindered. Thus, one needs to understand the redox chemistry of different As species in the solution and in their adsorbate state. As(V) gets more strongly adsorbed to iron and aluminum hydroxides than As(III), which is weakly adsorbed to these minerals in an oxidizing environment. Research by Bostick et al [2003] on As-sulfide/oxide interaction on galena and sphalerite at different pH values has shown that As(III) species adsorb to galena surfaces, though the exact mechanism is unknown. Becker et al. [2001] have studied the promotion of galena oxidation due to the co-adsorption of Fe^{3+} and dissociated water, which is an example of the proximity effect. This reaction mechanism of the proximity effect can be used to explain the adsorption of As(III) species on galena surfaces. In Chapter 5, we have used molecular modeling techniques to study the adsorption and potential oxidation of As(III) species on galena surfaces using proximity effect theory. This theory describes how the chemical reaction of one surface site influences the electronic structure and reactivity of neighboring or nearby sites by spin polarization and electron /charge exchange. This perturbation of the electronic structure

can mobilize another species on the surface in another surface site and promote its adsorption. Thus, Chapter 5 addresses the question:

- *Does the presence of an oxidizing species, such as ferric iron or oxygen, influence the adsorption of As(III) species on the galena surface?*

The information gained from this study will help us understand the redox chemistry and mobility As(III) species in ground water.

References

Addadi L, Weiner S: **Interactions between Acidic Proteins and Crystals: Stereochemical Requirements in Biomineralization.** *Proceedings of the National Academy of Sciences* 1985, **82:** 4110-4114.

Astala R, Stott MJ: **First principle investigation of mineral component of bone: CO_3 substitution in hydroxyapatite.** *Chemistry of Materials* 2005, **17:** 4125-4133

Becker U, Biswas S, Kendall T, Risthaus P, Putnis CV, Pina CM: **Interactions between mineral surfaces and dissolved species: From monovalent ions to complex organic molecules.** *American Journal of Science* 2005, **305**: 791-825.

Becker U, Rosso KM, Hochella MF**: The proximity effect on semiconducting mineral surfaces: a new aspect of mineral surface reactivity and surface complexation theory?** *Geochimica Cosmochimica Acta* 2001, **65:** 2641-2649

Bostick BC, Fendorf S, Manning BA: **Arsenite adsorption on galena (PbS) and sphalerite (ZnS).** *Geochimica et Cosmochimica Acta* 2003, **67:** 895-907.

Buijnsters PJJA, Donners JJJM, Hill SJ, Heywood BR, Nolte RJM, Zwanenburg B, Sommerdijk NAJM: **Oriented crystallization of calcium carbonate under self-organized monolayers of amide-containing phospholipids**. *Langmuir*, 2001, **17**: 3623-3628

Burdick JA, Anseth KS: **Photoencapsulation of osteoblasts in injectable RGD-modified PEG hydrogels for bone tissue engineering.** *Biomaterials* 2002, **23:** 4315-4323

Crick F: **Central dogma of molecular biology.** *Nature* 1970, **227:** 561-563.

Dixit S, Hering JG: **Comparison of Arsenic(V) and Arsenic(III) Sorption onto Iron Oxide Minerals: Implications for Arsenic Mobility.** *Environmental Science & Technology* 2003, **37:** 4182-4189

Dickerson RE: **DNA structures from A to Z.** *Methods in Enzymology* 1992, **211:** 67-111.

Garcia AJ, Reyes CD: **Bio-adhesive Surfaces to Promote Osteoblast Differentiation and Bone Formation.** *Journal of Dental Research* 2005, **84:** 407-413.

Gilbert M, Shaw WJ, Long JR, Nelson K, Drobny GP, Giachelli CM, Stayton PS: **Chimeric Peptides of Statherin and Osteopontin That Bind Hydroxyapatite and Mediate Cell Adhesion**. *Journal of Biological Chemistry* 2000, **275**: 16213-16218

Itoh D, Yoneda S, Kuroda S, Kondo H, Umezawa A, Ohya K, Ohyama T, Kasugai S: **Enhancement of osteogenesis on hydroxyapatite surface coated with synthetic peptide (EEEEEEEPRGDT) *in vitro.*** *Journal of Biomedical Materials Research* 2002, **62**: 292-298

Iwamoto Y, Robey FA, Graf J, Sasaki M, Kleinman FA, Yamada Y, Martin GR: **YIGSR, a synthetic laminin pentapeptide, inhibits experimental metastasis formation.** *Science* 1987 **238:** 1132-1134

Loh LC, Locke D, Melnychuk R, Laferte S: **The RGD Sequence in the Cytomegalovirus DNA PolymeraseAccessory Protein Can Mediate Cell Adhesion.** *Virology* 2000, **272:** 302-314

Mann S: **Molecular recognition in biomineralization.** *Nature* 1988, **332:**119-124.

Mann S: **Biomineralization: Principles and Concepts in Bioinorganic Materials Chemistry.** *Oxford University Press*, 2001.

Okamoto K, Matsuura T, Hosokawa R, Akagawa Y: **RGD peptides regulate the specific adhesion scheme of osteoblasts to hydroxyapatite but not to titanium**. *Journal of Dental Research* 1998, 77: 481-487.

Orme CA, Noy A, Wierzbicki A, McBride MT, Grantham M, Teng HH, Dove PM, DeYoreo JJ: **Formation of chiral morphologies through selective binding of amino acids to calcite surface steps.** *Nature* 2001, **411**: 775-779

Pina CM, Putnis CV, Becker U, Biswas S, Carroll EC, Bosbach D, Putnis A: **The inhibition of barite growth by phosphonates: determination of adsorption isotherms by atomic force microscopy**. *Surface Science* 2004, **553**: 61–74.

Pina CM, Becker U, Risthaus P, Bosbach D, Putnis A: **Molecular-scale mechanisms of crystal growth in barite.** *Nature* 1998, **395:** 483-486

Rezwan K, Chen QZ, Blaker JJ, Boccaccini AR: **Biodegradable and bioactive porous polymer/inorganic composite scaffolds for bone tissue engineering.** *Biomaterials* 2006 **27:** 3413-3431

Sethmann I, Putnis A, Grassmann O, Lobmann P: **Observation of nano-clustered calcite growth via a transient phase mediated by organic polyanions: A close match for biomineralization.** *American Mineralogist* 2005, **90**: 1213-1217.

Shin H, Jo S, Mikos AG: **Biomimetic materials for tissue engineering.** *Biomaterials* 2003 **24:** 4353-4364

Chapter 2

Interactions of mineral surfaces with polypetides: an insight into the influence of amino acids on calcite biomineralization

Introduction

Most of the minerals that grow as a result of biological processes are comprised of carbonates, silicates, phosphates, and, to a smaller degree, of sulphates [Ringwood et al, 1996]. Weathering and complex biological and chemical interactions have led to the re-precipitation of dissolved minerals into sedimentary rocks. The emergence of primitive organisms promoted the processing of dissolved mineral constituents in the marine environment where both prokaryotic and eukaryotic organisms have the ability to produce mineralized skeletal elements. Thus, the resulting minerals of biogenic origin comprise a large portion of the Earth's crust and represent a large storage of sequestered carbonate, silicate, and phosphate ions. The majority of carbonates occur as calcite, typically produced by plankton and invertebrates. Organic macromolecules appear to be an integral part of most calcium carbonate biominerals. It is known

that biological carbonate formation is in large measure a process mediated by organic matrices. In extracellular mineralization, the cell produces a macromolecular matrix outside the cell in an area that will become the site of mineralization [Skinner, 2005; Mann, 1988]. The term matrix refers to a group of macromolecules comprised of proteins, polysaccharides, and glycoproteins that assemble to form a three-dimensional framework. Organic matrix frameworks can provide binding sites for the components of a mineral, thereby selectively nucleating specific crystallographic faces [Buijnsters et al, 2004]. Organic carrier molecules can help to produce local supersaturation with respect to a certain mineral phase to be precipitated. Organic templates determine the morphology of the biominerals, and the structure of the organic template is responsible for producing growth nuclei in the mineral phase. A well-studied example of this is coccolithophores, which deposit calcite as their mineral phase. Calcite is a rhombohedral polymorph of calcium carbonate ($CaCO_3$). The lowest-energy faces of pure calcite are the {104} family of faces [Henriksen et al, 2004]. DNA, which is a double-stranded helix consisting of polymers found in the nucleus of the cell of living organisms [Dickerson et al, 2004], controls the initial biomineralization process by transferring its genetic information to proteins in the outer cell wall [Kornberg, Nobel prize in chemistry, 2006]. When an organism forms a template in its exoskeleton, it is thought to be an image of the genetic information carried in its DNA. Thus, the mineral deposition on the exoskeleton of the organism can be related to its DNA pattern. According to the central dogma of molecular biology, translation of DNA forms RNA, and transcription of RNA forms proteins [Crick, 1970]. Proteins are polymers of amino acids linked via peptide bonds in a

specific sequence. The synthesis of protein from RNA allows genomic techniques to be applied in protein studies. Thus, the sequencing of amino acids in a protein is a direct reflection of the DNA base-pair sequence present in the gene of a living organism [Crick et al, 1961]. Therefore, the study of the interaction of polypeptides (containing amino acids) with calcite surfaces can help us understand the structural matching of interfaces between the organic matrix-and the inorganic mineral surface during biomineralization. Combination of our study with the experimental AFM work on thermodynamics of calcite growth will strengthen our understanding of calcite biomineralization at molecular level [Teng et al, 1998].

Here, we have looked into different properties of peptide, which are part of organic matrix in the biomineralization process, that induce selectivity in the inorganic nucleating mineral surface during biomineral formation. The peptides that are studied in this chapter are small representative of large organic matrices that govern the inorganic nucleating mineral formation during biomineralization. So, behavior of these peptides in selective stabilization of mineral surface steps would provide a good understanding of organic matrix mediated inorganic nucleus stabilization in general. The main hypothesis that is tested in this chapter is whether interfacial(adsorption) energies of the peptides on particular calcite surfaces can elucidate on selectivity of calcite surface and surface steps during biomineral formation. The other hypothesis we have tested here is what role the side chain functional groups of the peptides play in selective adsorption on inorganic nucleating mineral surface.

The interaction of oligomers/polypeptide chains on (104) calcite surfaces as a precursor of biomineralization has been studied in this chapter. Our main objective is to find suitable orientations of amino-acid residues in these peptide chains, where these peptide chains align themselves parallel to flat calcite surfaces or parallel to a step on these surfaces. This type of one-dimensional matching between a calcite surface step and a protein chain may be one mechanism to control the shape of biominerals. Structural matching at inorganic-organic interfaces is a key concept for oriented nucleation in biomineralization. The stereochemical relation between the coordination environments of ions on specific crystal faces (Ca^{2+} and CO_3^{2-} in this case) and the arrangement of ligands (i.e., peptide residues, oligomers) around ions bound to the surface is a potential factor for organic nucleation and selectivity of biominerals. If the distance between the repeating unit residues in the adsorbent matches the distance between the repeating units in the adsorbate surface and if the polarities of organic template and mineral surface/step match, the adsorbing long-chain polymer or oligomeric organic compound can lie parallel to the surface step and, thus, stabilize the interface. The most favorable interfacial energy between a pair of organic matrix-inorganic nucleating surface leads to formation of a stable biomineral.

Methods

Choice of amino acid sequence in small protein oligomers

As a precursor of biomineralization, we are studying the interaction of oligomers/polypeptide chains on the {104} calcite family of faces. Our main objective is to find suitable orientations of amino-acid residues in these peptide chains

and where these peptide chains align themselves parallel to the calcite surface. By evaluating the adsorption energies of different peptide sequences on calcite steps, we are trying to find the most suitable of such sequences to promote the controlled growth of surfaces whose growth may start from these steps.

In order to find a suitable polypeptide sequence for optimal adsorption, one has to note that translation from the DNA to polypeptide sequences involves the conversion of a four base code (ATCG) into twenty different amino acids. A codon or *triplet of bases* specifies a given amino acid [Crick et al, 1961]. Most amino acids are specified by more than one codon. The conversion of codon information into proteins is conducted by means of the RNA. Each transfer-RNA (tRNA) has an anticodon, which can base pair with a codon. Some anticodons have modified bases that can pair with more than one codon, specifying the same amino acid; this means that we do not need 61 different tRNA molecules for all 61 codons.

In order to avoid steric hindrances of complex polypeptides, we chose to work initially with 3-amino acid long small-chain oligopeptides to study their interaction with calcite surface steps. Since a given amino acid requires 3 bases to be expressed, we can apply the A-T G-C rule, commonly known as Chargaff's rule [Chargaff et al, 1948]. Chargaff's rule states that the molar ratio of A (adenine) to T (thymine) and of G (guanine) to C (cytosine) is always approximately equal in a DNA molecule. Chargaff's Rule is true as a result of the strict hydrogen bond forming rules in base pairing. For every G in a double-strand of DNA, there must be an accompanying complementary C; similarly, for each A, there is a complementary paired T (U-uracil for RNA).

The base pairs chosen for the current study with their anticodons and corresponding amino acid according to their expression are listed in Table 2.1.

The amino acids listed in Table 2.1 have different functional groups as side chains, and, consequently, their functional groups have different pKa values. The α-carboxylic acid groups have pKa values from 1.77-2.58, and the α-amino groups have pKa values in the range 9.0-10.60 [Lim et al, 1991]. The side-chain functional groups have varying pKa values, depending on the strength of their respective conjugate acids and/or bases. Lysine, tyrosine, and arginine have pKa values over 10 such that they need highly alkaline conditions to be deprotonated. In our study, we apply protonated and deprotonated functional groups, thus varying pH conditions from acidic to alkaline in our models.

We are using empirical force-field methods to study the adsorption of peptides containing the above-mentioned amino-acids on calcite (104) surfaces and surface steps. Using the Cerius^2 software (Accelrys Inc.), we have created calcite (104) surfaces and surface steps along periodic bond chains parallel to the symmetry-equivalent [48-1] and [4-4-1] directions. All Coulomb interactions between the 3-amino-acid peptide molecule and mineral cluster atoms are included as well as all interactions within the molecule (except for 1–2, nearest neighbor, and 1–3, second nearest neighbor, interactions, which are treated using Morse and three-body potentials, respectively) and within the calcite cluster, which is achieved by setting the cut-off radius to 200 Å, which is significantly larger than the dimensions of the cluster. The calcite cluster contains 700 atoms, i.e., 140 $CaCO_3$ units. The Ca^{2+} and CO_3^{2-} ions are arranged in such a way that there is no net dipole moment either

perpendicular or parallel to the calcite {104} faces. This is achieved by the steps that bound the cluster being parallel to [48-1] ([4-4-1]) which is equivalent to having a cluster that is terminated by a face that is symmetry equivalent to the (104) face. In other words, the cluster is a nano-version of the typical rhombohedron of calcite found in nature. In order to create steps on the upper surface, the upper layer consists of 15x16 surface unit cells whereas lower layer consists of 15x22 surface unit cells for polar surface steps (Ca^{2+} present on the step edge). For non-polar surface steps which are parallel to [48-1] ([4-4-1]), 14x12 surface unit cells in the lower layer and 14x8 surface unit cells in the upper layer were chosen. For the non-polar step, there are alternating Ca^{2+} and CO_3^{2-} ions along the step edge. We can have two types of non-polar surface steps, creating an acute angle and an obtuse angle. We also created polar surface steps parallel to both [42-1] and [010] step direction, and in each of these cases, the steps can be terminated by either Ca^{2+} or CO_3^{2-} ions. We have calculated adsorption energies for each of these surface step scenarios mentioned above and adsorption to flat terraces.

The CALCITE force field was developed in this study to calculate the interactions within the organic molecules and for interactions between the organic molecule and the substrate. This CALCITE force field uses the potentials listed in Table 2.2 (a core-only potential set was derived to simulate interactions within the calcite). Interactions within the organic molecules and between the calcite and the organic molecules are based on the UNIVERSAL1.02 force field [Rappe et al, 1991].

The force field list in Table 2.2 controls the interaction between carbon and oxygen atoms in the carbonate group and the O-C-O angle, and the inversion

potential determines how planar the carbonate group is as a consequence of distortion caused by surface relaxation or adsorption. It also accounts for the bond stretching action between the carbon and oxygen atoms and van der Waals interaction between them. In order to find the absolute energy minimum with its corresponding structure of a molecule adsorbed to the surface, the molecules were brought close to the surface manually in different orientations. From each starting position, the minimizer of Cerius[2] was used to optimize the position.

The charge distribution within the peptide molecules was calculated using the QEq [Rappe et al, 1991] charge equilibration scheme. Subsequently, the respective (according to the deprotonation state) number of protons was removed and the corresponding positive charge was adjusted by evenly distributing the charge difference due to deprotonation over the remaining charged molecule. The individual atomic charges from this initial charge distribution were not changed in subsequent adsorption calculations. This is important because redistributing the charges within a calculation or in between adsorption energy calculations introduces arbitrary fluctuations in the calculated adsorption energies. This approach is justified because none of the reactions discussed in this study involves significant charge transfer. The charges of atoms in the calcite are those listed in Table 2.2.

Molecular dynamics simulations at 300 K were performed to avoid trapping the adsorbate in a local energy minimum before and during optimization. These dynamics simulations were performed using a constant *NVE* ensemble. This is the most suitable ensemble for the setup that we used with constant number of atoms (constant N), non-periodic system (thus using V rather than P), and an adiabatic

approach (constant E). The structure is allowed to evolve in time, by solving Newton's equation of motion. Every 100 steps, velocities are rescaled if the averaged temperature goes outside the specific window around the target temperature. The dynamic time step is 0.001 ps, and for each MD run, we run 500 steps.

In order to investigate the interaction between a specific protein that may trigger the biomineralization of some coccolithophorids and the calcite surface or a calcite step, we increased the complexity of our calculation from 3-amino-acid peptide residues to 12-amino-acid peptide residues. For this setup, we used the protein GPA (glycophorin A), which is a calcium-binding protein in the coccolithophorid *Emiliania Huxleyi* [Corstjens et al., 1995]. GPA contains high percentages of constituent glutamic acid, proline, and alanine. With one deviation, an amino acid stretch of 35 residues is repeated in GPA. This repeat unit contains a sequence of 12 amino acids showing homology with the Ca^{2+}-binding loop of EF-hand motifs [Kawasaki et al, 1995]. The amino acid sequence of this 12-amino acid residue is **pro-glu-val-pro-glu-gly-ala-val-asp-thr-ala-ile.**

All the above mentioned adsorption calculations involving 3-amino acid residue and 12-amino acid residue peptides are initially performed in vacuum conditions. To understand the adsorption in natural biomineralization processes, we must consider aqueous environment. Researchers have found that physisorption of water is energetically most favorable on calcite (104) surface, and the stepped planes are found to be good models for growth steps on the experimental (104) surface [de Leeuw et al, 1997; Kerisit et al, 2004]. As we are studying the adsorption of peptide on calcite (104) surface, and we are mainly focused on the behavior of the peptides,

and interaction of its' functional groups with mineral surface atoms, we need to calculate hydration energies of these peptides when they attach to the mineral surface. We use quantum mechanical calculations using Gaussian03 [Frisch et al, 2004] to calculate the hydration energy of the 3-amino acid residue peptides. We use a 3-21g basis set and a dielectric continuum approach [Cances et al, 1997] with a dielectric constant of water of 78.39. A molecular dynamics approach with hundreds of water molecules for tens of different configurations would have been to computationally expensive. The hydration energy of the 12-amino acid residue peptide with complex side chain structure is not known, as the structure is too large for quantum mechanical treatment. We subtract the hydration energies from the vacuum adsorption energies of 3-amino acid peptide to get the effective adsorption energies of these peptides on various calcite surface locations.

As evident from the amino acid sequence in this 12-amino acid residue peptide chain, there is a range of side-chain structures. This allows studying the effect of side-chain functionality on the peptide-calcite surface interaction. Our objective is to determine how the steric hindrance and reactivity of these side chains can influence the parallel alignment of the peptide along mineral surface and thus, the attachment energy, and how side-chain geometries can influence the topography at the interface. For comparison, we have chosen to study the interaction of a 12-amino acid peptide residue with the calcite surface step with alternating glycine and alanine residues in the 12-amino-acid peptide chain. Glycine has H- and alanine has CH_3– side-chain residues in the amino acid. These are the two simplest side-chain residues and they exert minimum steric hindrance to the peptide-calcite interface. Again, the peptide-

calcite interface interactions at both acidic and alkaline conditions were studied, with the peptide residue being neutral or negatively charged. Glycine and alanine are the two most "fundamental" amino acids in biochemical pathways and in natural occurrences in prebiotic systems. Both are specified by guanine/cytosine base pairing at the first two positions, the strongest possible interaction. Figure 2.1 shows the structure of 3 different types of amino-acid chains (polypeptides) used in our study.

Results and Discussion

We will discuss the results of the interaction of small peptides on calcite surface in two different sections. First we will discuss the interaction of negatively charged peptide on various surface locations of calcite (104) surface, and then we will analyze the results for interactions with neutral/positively charged peptide on calcite surface. The reason to separate the results into these two categories is that they represent two different environment, alkaline pH and neutral pH respectively for negatively charged peptide and neutral/positively charged peptide. As we have mentioned in the methods section, we have first calculated the vacuum adsorption energy of the peptides on calcite surface, then we have calculated the hydration energy of the peptide to calculate the effect of hydration on adsorption of these peptides on mineral surface. Now onwards, the energy values represent the effective adsorption energy of the peptides on calcite surfaces. As mentioned earlier, we subtract the hydration energy of the peptides from the vacuum adsorption energies to obtain the effective adsorption energies.

Interaction of negatively charged peptides on calcite surface: 3-amino acid residue peptides

We studied interaction between negatively charged peptide residues with non-polar steps on calcite (104) surface, 2) negatively charged peptide residues with polar steps on calcite (104) surface, and 3) negatively charged peptide residues on flat calcite (104) surface. The calculations are done in alkaline pH condition.

1) Negatively charged peptide residues on non-polar steps:

For the non-polar surface step, there are two different situations. The carbonate on the surface step can form both an acute angle and an obtuse angle with the underlying surface. We have calculated adsorption of the peptides on both types of non-polar surface step (obtuse and acute). The Ca^{2+} - CO_3^{2-} distance is 3.301 Å and the Ca-Ca distance is 6.602 Å. Table 2.3 shows the corresponding adsorption energies. The average distance between the nitrogen atoms in the peptide bond of peptide residues are 3.458 Å in the investigated peptides. According to Langmuir-Blodgett film theory [Peterson et al, 1990; Buijnsters et al, 2001] if the distance between the repeating units residue in the adsorbent matches the distance between the repeating units in the adsorbate surface, the adsorbent long chain polymer or oligomeric organic compound can lie parallel to the surface step. We can see that the average distance between nitrogen atoms in peptide bond and the distance between Ca^{2+} - CO_3^{2-} ions in non-polar surface steps are comparable, within 0.15 Å. However, we have to consider another factor, which is steric hindrance presented by bulky side-chain groups in the amino acids.

Phe-leu-lys, lys-gln-tyr, gly-ser-trp – these 3 peptide residues have a benzene ring in there side chain. Benzene rings are fairly bulky functional groups which can cause steric hindrance with other functional groups that could potentially bind to the surface or step. That is why only the carboxylic groups of these peptides are electrostatically attracted and close to the calcite surface steps. Other side chain residues and —NH- and —N-C=O of the peptide bonds are hindered to bond by the benzene ring, and thus point away from the surface step. The electrostatic interaction between the oppositely charged species at the interface of the peptide and calcite surface step is still strong enough to adsorb these 3-amino acid residue peptides to a non-polar surface step. **(Lys-gln-tyr)$^{1-}$** has the most favorable adsorption energy (-2.87 eV/residue) on a non-polar step with carbonates forming an obtuse angle with the underlying terrace. The adsorption energies are significantly lower when the carbonates make an acute angle with the underlying terrace. The electron density on the oxygen in a carbonate ion is higher, and when it makes an acute angle, the oxygen atoms are exposed to the negatively charged peptides on a step direction (contrary to the obtuse angle case where the carbonate oxygens are on the "other" side of the peptides). For the acute angle case, **(phe-leu-lys)$^{1-}$** has the most favorable adsorption energy (-1.40 eV/residue).

2) Negatively charged peptide residues with polar steps parallel to [010] and [42-1]:

Polar steps on a calcite surface can be bounded by Ca^{2+} ions or CO_3^{2-} ions. Also the polar step can be parallel to both [010] and [42-1] direction on calcite surface. Out of these 4 possible scenarios, the interaction between negatively charged peptides

with CO_3^{2-} ions terminated polar step is not favorable. We get negative adsorption energies for the peptides in vacuum, but since the peptides are negatively charged, they have high hydration energy also, which eventually makes them unfavorable to get adsorbed. For the polar surface terminated by Ca^{2+}, the closest distance between two Ca^{2+} ions is 4.957 Å. In Table 2.4, we have listed the interface adsorption energies of each 3-amino acid peptide residue with the polar calcite surface step edge terminated by Ca^{2+} ions. Adsorption energies are little higher on step direction [010] compared to [42-1], although in both cases the adsorption of 3-amino acid residues are highly favorable. **(Leu-pro-cys)$^{2+}$** is most favorably adsorbed to steps parallel to [010] (-8.27 eV/residue). The presence of sulfur atom in the cysteine residue causes the strong electrostatic interaction with the step terminating Ca^{2+} ions. The energies of different peptides do not vary much when adsorbed to steps parallel to [42-1]. Here, **(gly-ser-trp)$^{1-}$** has the most favorable adsorption energy (-6.98 eV/residue).

3) Negatively charged peptide residues on flat-terraces

Table 2.5 lists the adsorption energies of different negatively charged 3-amino acid peptide residues on flat (104) terraces. Comparison of these adsorption energy values on a flat terrace with polar step edges helps us understand the preferred location of the peptides on a mineral surface, or in other words, what surface location is promoted by biological molecules during natural biomineralization of calcite. The adsorption energies of the peptides on flat terraces are significantly lower than the adsorption energies on steps. The most favorable adsorption energy on a flat terrace is -1.37 eV/residue for **(lys-gln-tyr)$^{1-}$**. The 3-

amino acid residue peptides in alkaline conditions favor the surface steps for adsorption on calcite surface, and they favor the step direction parallel to [010] terminated by Ca^{2+} for adsorption.

Figure 2.2 shows a sample picture of the adsorption site of all 3 amino-acid residues on the polar calcite surface step parallel to [010], and Figure 2.3 shows adsorption sites of all 3 amino-acid residues on the non-polar step parallel to [42-1].

Interaction of neutral/positively charged peptides on calcite surface: 3-amino acid residue peptides

We have also studied the interaction of neutral and positively charged peptides on calcite (104) surfaces. The peptides are either neutral or positively charged depending on their respective isoelectric points. We maintained a neutral biological pH throughout these set of calculations by adjusting the protonation/deprotonation state of the peptides. The neutral biological pH is reminiscent of the natural conditions under which most of the calcite biomineralization occur.

1) Neutral/positively charged peptide residues on non-polar steps

Here we describe the interaction of the neutral/positively charged peptide on two different types of non-polar calcite surface steps parallel to the [48-1] ([4-4-1]), a) the carbonates forming an obtuse angle with the underlying terrace, and b) the carbonates forming an acute angle with the underlying terrace. Table 2.6 lists the adsorption energies of the 3-amino acid residues peptide with the non-polar step. The results show that this scenario is less favorable compared to interaction of negatively

charged peptides on non-polar steps parallel to [48-1]. Although the most favorable adsorption energy (-2.72 eV/residue for the **(leu-pro-cys)** peptide) is close to the value we found as the most favorable energy with negatively charged peptide (-2.87 eV/residue), the other peptides have very low negative adsorption energy, and **(lys-gln-tyr)$^{2+}$** gets repelled from the step. The main reason for this weak adsorption to this non-polar surface step is the unfavorable attraction between the Ca^{2+} ion in the step and the neutral/positively charged peptide. For the acute angle case, the adsorption energies are less favorable compared to the obtuse angle case. **Leu-pro-cys** is most favorable to adsorb on non-polar step (-1.56eV/residue).

2) Neutral/positively charged peptide residues on polar steps parallel to [010] and [42-1]:

As in the case of negatively charged peptides, here we also have different types of polar steps: those terminated by either Ca^{2+} or CO_3^{2-} ions and step directions parallel to either the [010] or [42-1] direction. Unlike the case with negatively charged peptides, we get favorable adsorption energies in all 4 possible cases mentioned above. The adsorption energies are shown in Table 2.7. In case of Ca^{2+} terminated steps parallel to [010], **(lys-gln-tyr)$^{2+}$** has the most favorable adsorption energy (-4.34 eV/residue), and **(phe-leu-lys)$^{1+}$** (-5.87 eV/residue) in case of steps parallel to [42-1].

The adsorption energies are more negative with steps terminated by CO_3^{2-} compared to steps terminated by Ca^{2+}. Moreover, the adsorption energies are higher when CO_3^{2-} terminated steps are parallel to [42-1], than when they are parallel to [010].The distance between the consecutive carbonate ions on the step edge parallel

to [010] is 4.96 Å, and the distance is 4.36 Å between the carbonate ions at the step edge parallel to [42-1]. The later of these two distances (carbonates at the step edge parallel to [42-1]) are more comparable with the distances between the consecutive nitrogen atoms in the amide bonds in peptide, which are in the order of 3.9 – 4.2 Å. The most favorable adsorption energy is for **(lys-gln-tyr)**$^{2+}$ (-11.91 eV/residue) on steps terminated by CO_3^{2-} parallel to [42-1] , and **(phe-leu-lys)**$^{1+}$ (-5.79 eV/residue) on steps terminated by Ca^{2+} . The adsorption energies are higher when carbonate ions are terminating the step parallel to [42-1] because the O atoms of the carbonate groups interact with the neutral or positively charged peptide. The peptides with positive charge have higher adsorption energies than the neutral peptides, because of more electrostatic attraction between the negative carbonate ions at step and positive amide groups on the peptide. Though the effect of hydration shields the attraction of both neutral and positively charged groups (in amino acids) towards the carbonate ions on the step edge, the electrostatic attraction is higher in the case of positive amide groups (in the amino acid) than the neutral groups.

3) Neutral/positively charged peptide residues on flat terrace of calcite surface

The adsorption energies of neutral/positively charged peptides on flat surface are listed on Table 2.9. As with the negatively charged peptides, here also the adsorption energies are small negative values, as flat terrace locations are less favorable for adsorption of peptides compared to step directions on calcite surface. **(Leu-pro-cys)** has the most favorable adsorption energy among these peptides on a flat surface (-2.28 eV/residue).

Interaction of 12-amino acid residue peptides with calcite surface steps

The main motivation for using longer peptides is to find out how these align along surface steps on calcite surfaces, i.e., how periodicity and side-chain geometry influence alignment and, thus, adsorption energy. In this study, the chain length is increased from 3 amino-acid peptide residues to 12 amino-acid peptide residues. We used the protein GPA (glycophorin A, **pro-glu-val-pro-glu-gly-ala-val-asp-thr-ala-ile**) which is a calcium binding protein in the coccolithophorid *Emiliania Huxleyi*[12]**.** As described above, this 12-residue amino acid forms a Ca^{2+} binding loop (Figure 2.4). Like the 3-amino acid peptides, here we also studied all possible configurations of the peptide-calcite surface interactions. First we varied the pH conditions by considering both the negatively charged 12-amino acid residue peptide and the neutral 12 residue peptide. We studied the interaction of both these types on 1) non-polar steps parallel to step direction [48-1] (and the symmetry-equivalent [4-4-1]) with both obtuse and acute angles of carbonate ions with the underlying terrace, 2) polar steps terminated by Ca^{2+} ions and CO_3^{2-} ions parallel to step direction [010] and [42-1], and 3) flat (104) terraces. Adsorption energies are again corrected for the hydration energy of the peptide to obtain the effective adsorption energies of the 12-amino acid residue peptides. Hydration energies for the 12-amino acid residue peptide with complex side chain cannot be calculated due to extensive computational time required for its complex structure.

1) Interaction of a negatively charged 12-amino acid residue peptide chain with different surface locations of calcite (104) surface

The adsorption energies for the negatively charged peptide with complex and simple structure 12-amino acid residues are listed in Table 2.10.

As shown in Figure 2.5, the peptide bond backbone of this 12-amino acid residue is U shaped in its adsorbed state. As evident from the adsorption energy, the negatively charged side-chain residues of the 12-amino acid peptides are strongly attracted to the Ca^{2+} ion present at the step-edge. However the 12-amino acid residue peptide is terminated by a bulky side-chain containing amino acids. Proline and glutamine are present at one end, and isoleucine and threonine are present at the other end. These above mentioned amino acid contains alkane side chains or amide containing carboxylic acid side chains, which are long and cause steric hindrance to some part of the peptide chain. That is why the 12-residue peptide takes a U-shaped alignment along the polar step-edge, where the end members are pointing away from the polar steps (terminated by calcium ions and carbonate ions in two different cases) on two ends of the peptide, and the center part of the peptide aligns parallel to the step-edge. The proximity of the amino acid to the polar step largely depends on the R group of that particular amino acid. The smaller the R group, the closer can a particular amino acid get to the polar surface step edge.

The adsorption energies are most favorable (for both complex and simple structured peptides) on polar steps terminated by Ca^{2+} ions. The energies are more favorable on step direction parallel to [010] compared to [42-1]. The adsorption

energy of the complex structured peptide on a flat terrace of calcite surface is more favorable than some of the polar and non-polar step locations.

2) Interaction of a neutral 12-amino acid residue peptide chain with different surface locations of calcite (104) surface

The adsorption energies for the neutral peptide with complex and simple structure 12-amino acid residues are listed on Table 2.11.

The orientation of the peptides along surface steps, both polar and non-polar, are similar to what we have observed in the case of negatively charged 12-amino acid peptide residues. Expectedly, the most negative adsorption energy is found for the peptide on the polar surface step terminated by carbonate ions parallel to the step direction [010]. However, we also calculate substantial adsorption when these peptides adsorb on calcite surface step terminated by Ca^{2+} ions. The adsorption energies are less negative for simple structured peptides with alternating glycine and alanine, but as mentioned earlier, the complex structure peptide energies are vacuum energies, and if we are able to subtract the hydration energies for the complex structure peptides, the two types of adsorption energies for simple and complex amino acids will be comparable. The main difference between the two types (complex and simple structure 12 amino acid peptides) lie in their geometric orientation alongside calcite surface steps, where the simple structured peptide adopt more parallel alignment compared to its complex counterpart.

Conclusions

In our study involving peptide-calcite interactions, we have presented detailed interpretation and results of our earlier work involving 3-amino acid and 12-amino acid peptide residues. We have addressed questions regarding geometry, orientation, and adsorption energies of different peptides when they interact with calcite surface steps. The periodicity of the surface atoms on calcite surface steps, their relative positions with respect to step directions, and the chemistry of the side-chain of amino acids in a peptide play a major role in the adsorption of peptides on calcite surface steps. We have seen that under favorable conditions, peptides are more favorably adsorbed on a calcite (104) surface step parallel to [42-1] direction than [010] direction. The distance between consecutive calcium ions or carbonate ions are 4.36 Å in the step direction parallel to [42-1] compared to 4.96 Å in the step direction parallel to [010]. The smaller distance in [42-1] matches better with the separation of adsorbing functional groups in the peptides investigated. We also observe that on non-polar surface steps, the peptides are more favorably adsorbed when the carbonate ions forms an obtuse angle with the underlying terrace rather than an acute angle. The different side-chains of the amino-acids present in the peptide during peptide-calcite interaction play a significant role in peptide adsorption on the calcite surface. We initially studied the interaction of small 3-amino acid residue peptides with the step-edge of calcite surface to establish the role of functional groups while interacting with atoms on such a step-edge. The most favorable adsorption energy is calculated for **(lys-gln-tyr)$^{-1}$** to a non-polar step parallel to [48-1] ([4-4-1]), and to a polar step parallel to [010] terminated by Ca^{2+}. **(Phe-leu-lys)$^{1-}$** exhibits the most favorable

adsorption energy on a polar step edge parallel to [42-1] terminated by Ca^{2+} ions. (**Lys-gln-tyr)**$^{2+}$ and **(phe-leu-lys)**$^{1+}$ has the most favorable adsorption energies among the neutral or positively charged peptides on different surface step locations. We can conclude from the above results that if the amino acid side chain contains a benzene ring or a cloud of electrons (electron pairs or π-electrons) that can interact with the mineral surface atoms, it will be favorably adsorbed to that surface location, overcoming the counteracting effect or steric hindrance. Among the above-mentioned peptides that favorably get adsorbed to the calcite surface steps, lysine and glutamine contain amide groups that have electron pairs and tyrosine and phenyl-alanine contain benzene rings. The π-electrons of benzene rings interact with calcium ions at the surface steps.

We increased the complexity of the adsorbates by increasing the length of the peptide to mimic natural conditions more closely. Long-chain peptides are more common in naturally occurring biominerals. By comparing the adsorption energies of simple and complex structured 12-amino acid peptides, we have been able to establish that simple-structured peptides are more likely to have parallel alignment at the step-edge of calcite surface. That does not necessarily mean that simple-structured peptides are more common in nature. Actually our results show that the 12-amino acid residue peptides with complex structure side chains have comparable (more favorable in some cases) adsorption energies on calcite surface steps with simple structured peptides. We can conclude that the simple-structured peptides can provide structural matching with the growing calcite surface, and the complex structured peptides that have complex side chains are more likely to facilitate

adsorption on calcite surface steps. In addition, the latter are more capable to complex Ca^{2+} ions and may serve as a carrier of these ions to calcite surfaces. The complex side-chains in amino acids play a significant role in interaction with the calcite surface atoms on surface step locations.

These model set-ups described in this chapter can serve to further our overall understanding of the interaction between organic molecules and inorganic surfaces. The specific interactions of side-chain functional groups of amino acids with specific calcite surfaces has been discussed in this chapter. This analogy can be used to study several other combinations of peptide-calcite interface. One can deduce the structural information of peptides of an organism searching protein data bank, and experimental studies can provide insight into what kind of growth phases of calcite is occuring on the exoskeleton of that organism. Using these two types of informations, molecular models can be developed to study effects of functional groups present in the amino acid of the organism in biomineral formation. This can help to generate a database on different functional group's influence on biomineral formation. To mimic the natural environment for biominerals formation more closely, one would need to prepare a multi-dimensional model of organic networks and to observe the growth of calcite crystals under the influence of such an organic framework. Ultimately, the interplay of the organic, inorganic (mineral), and water phase in a three-dimensional network should be studied in a dynamic model using molecular dynamics to mimic more closely a natural biomineralization process.

Table 2.1: Determination of amino acids from DNA-codons

	1st amino acid	2nd amino acid	3rd amino acid
Codon	GCA	CAG	GGT
Anti-codon	CGU	GUC	CCA
Amino acid	Arginine	Valine	Proline
Codon	GAA	GGT	ACA
Anti-codon	CUU	CCA	UGU
Amino acid	Leucine	Proline	Cysteine
Codon	TTC	GTC	ATG
Anti-codon	AAG	CAG	UAC
Amino acid	Lysine	Glutamine	Tyrosine
Codon	AAG	AAT	TTC
Anti-codon	UUC	UUA	AAG
Amino acid	Phenyl alanine	Leucine	Lysine
Codon	GAA	CGG	GGC
Anti-codon	CUU	GCC	CCG
Amino acid	Leucine	Alanine	Proline
Codon	CCT	AGG	ACC
Anti-codon	GGA	UCC	UGG
Amino acid	Glycine	Serine	Tryptophan

Table 2.2: Potential parameters for CALCITE forcefield

O-O	Buckingham[1]	*inter*molecular; < 14 **Å**	A = 1477.95 eV	ρ = 0.2455 Å	C = 0 eV/ Å^6
Ca-O	Buckingham[1]	inter*molecular;* < 14 **Å**	A = 792.27	ρ = 0.2891 Å	C = 0 eV/ Å^6
O-C	Morse[2]	*intra*molecular	D = 4.9664	r_0 = 1.2025 Å	K_b = 63.233 eV/ Å^2
O-C-O angle	Three-body[3]	*intra*molecular	K_0= 1.785	θ_0=120°	
CO_3-plane	Umbrella[4]	*intra*molecular	$\omega_0 = 0°$	K_0 = 4336.47 eV	
charges	C = +1.345	O = -1.115	Ca = +2.000		

[1]Buckingham: $A \exp(-r/\rho) - C r^{-6}$ C in eV Å^6

[2]Morse: $D [(1 - \exp \{-a(r-r_o)\})^2 - 1]$ $a = (K_b/2D)^{1/2}$

[3]Three-body: $E = K_0 (\theta-\theta_0)^2$

[4]Umbrella: $E = K_0 (1 – \cos \omega)$ for $\omega_0 = 0°$ ω = Angle between the C-O bond and its projection on O-C-O plane.

Table 2.3. Adsorption energies of *negatively charged* 3-amino acid residue peptides on *non-polar* steps parallel to [48-1] ([4-4-1])

3-amino acid residue peptide	**$E_{adsorption\ per\ amino\ acid}$ (eV) (E_1)**	**$E_{hydration/amino\ acid}$ (eV) (E_2)**	**$E_{effective\ adsorption/amino\ acid}$ (eV) (E_1-E_2) (obtuse angle)**	**$E_{adsorption\ per\ amino\ acid}$ (eV) (E_1)**	**$E_{hydration/amino\ acid}$ (eV) (E_2)**	**$E_{effective\ adsorption/amino\ acid}$ (eV) (E_1-E_2) (acute angle)**
arg-val-pro (1-)	-2.59	-1.29	-1.30	-2.38	-1.29	-1.09
leu-pro-cys (2-)	-4.33	-3.05	-1.28	-2.69	-3.05	0.36
lys-gln-tyr (1-)	-4.42	-1.55	-2.87	-2.78	-1.55	-1.23
phe-leu-lys (1-)	-4.22	-1.47	-2.75	-2.87	-1.47	-1.40
leu-ala-pro (1-)	-3.84	-1.54	-2.30	-2.35	-1.54	-0.81
gly-ser-trp (1-)	-3.26	-1.43	-1.83	-2.44	-1.44	-1.01

Table 2.4. Adsorption energies of *negatively charged* 3-amino acid residue peptides on Ca^{2+} *polar* steps parallel to [010] and [42-1]

3-amino acid residue peptide	**$E_{adsorption}$ per amino acid (eV) (E_1)**	**$E_{hydration}$/ amino acid (eV) (E_2)**	**E effective adsorption/amino acid (eV) (E_1-E_2) (parallel to [010])**	**$E_{adsorption}$ per amino acid (eV) (E_1)**	**$E_{hydration}$/ amino acid (eV) (E_2)**	**E effective adsorption/amino acid (eV) (E_1-E_2) (parallel to [42-1])**
arg-val-pro (1-)	-6.46	-1.29	-5.17	-5.51	-1.29	-4.22
leu-pro-cys (2-)	-11.32	-3.05	-8.27	-8.89	-3.05	-5.84
lys-gln-tyr (1-)	-8.91	-1.55	-7.36	-7.81	-1.55	-6.26
phe-leu-lys (1-)	-7.36	-1.47	-5.89	-7.74	-1.47	-6.27
leu-ala-pro (1-)	-6.10	-1.54	-4.56	-7.54	-1.54	-6.00
gly-ser-trp (1-)	-7.94	-1.43	-6.51	-8.41	-1.43	-6.98

Table 2.5. Adsorption energies of *negatively charged* 3-amino acid residue peptides on *flat* (104) *terrace*

3-amino acid residue peptide	**$E_{adsorption\ per\ amino\ acid}$ (eV) (E_1)**	**$E_{hydration/amino\ acid}$ (eV) (E_2)**	**$E_{effective\ adsorption/amino\ acid}$ (eV) (E_1-E_2)**
arg-val-pro (1-)	-2.24	-1.29	-0.95
leu-pro-cys (2-)	-3.54	-3.05	-0.49
lys-gln-tyr (1-)	-2.92	-1.55	-1.37
phe-leu-lys (1-)	-2.50	-1.47	-1.03
leu-ala-pro (1-)	-2.36	-1.54	-0.82
gly-ser-trp (1-)	-2.57	-1.43	-1.14

Table 2.6. Adsorption energies of *neutral or positively charged* 3-amino acid residue peptides on *non-polar* steps parallel to [48-1] ([4-4-1])

3-amino acid residue peptide	$E_{adsorption\ per\ amino\ acid}$ (eV) (E_1)	$E_{hydration/\ amino\ acid}$ (eV) (E_2)	$E_{effective\ adsorption/amino\ acid}$ (eV) (E_1-E_2) (obtuse angle)	$E_{adsorption\ per\ amino\ acid}$ (eV) (E_1)	$E_{hydration/\ amino\ acid}$ (eV) (E_2)	$E_{effective\ adsorption/\ amino\ acid}$ (eV) (E_1-E_2) (acute angle)
arg-val-pro (1+)	-2.87	-2.41	-0.46	-2.50	-2.41	-0.09
leu-pro-cys	-3.74	-1.02	-2.72	-2.58	-1.02	-1.56
lys-gln-tyr (2+)	-2.63	-3.94	1.31	-2.81	-3.94	-1.13
phe-leu-lys (1+)	-2.87	-2.08	-0.79	-3.45	-2.08	-1.37
leu-ala-pro	-2.10	-1.94	-0.16	-2.01	-1.94	-0.07
gly-ser-trp	-3.07	-1.57	-1.50	-2.39	-1.57	-0.82

Table 2.7. Adsorption energies of *neutral or positively charged* 3-amino acid residue peptides on Ca^{2+} *polar* steps parallel to [010] and [42-1]

3-amino acid residue peptide	**$E_{adsorption\ per\ amino\ acid}$ (eV) (E_1)**	**$E_{hydration/amino\ acid}$ (eV) (E_2)**	**$E_{effective\ adsorption/amino\ acid}$ (eV) (E_1-E_2) (parallel to [010])**	**$E_{adsorption\ per\ amino\ acid}$ (eV) (E_1)**	**$E_{hydration/amino\ acid}$ (eV) (E_2)**	**$E_{effective\ adsorption/amino\ acid}$ (eV) (E_1-E_2) (parallel to [42-1])**
arg-val-pro (1+)	-4.64	-2.41	-2.23	-3.99	-2.41	-1.58
leu-pro-cys	-5.20	-1.02	-4.18	-4.37	-1.02	-3.35
lys-gln-tyr (2+)	-8.28	-3.94	-4.34	-5.85	-3.94	-1.91
phe-leu-lys (1+)	-4.19	-2.08	-2.11	-7.95	-2.08	-5.87
leu-ala-pro	-4.18	-1.94	-2.24	-4.99	-1.94	-3.05
gly-ser-trp	-3.91	-1.57	-2.34	-4.82	-1.57	-3.25

Table 2.8. Adsorption energies of *neutral or positively charged* 3-amino acid residue peptides on CO_3^{2-} *polar* steps parallel to [010] and [42-1] on calcite (104) face

3-amino acid residue peptide	**$E_{adsorption}$ per amino acid (eV) (E_1)**	**$E_{hydration/amino\ acid}$ (eV) (E_2)**	**$E_{effective\ adsorption/amino\ acid}$ (eV) (E_1-E_2) (parallel to [010])**	**$E_{adsorption}$ per amino acid (eV) (E_1)**	**$E_{hydration/amino\ acid}$ (eV) (E_2)**	**$E_{effective\ adsorption/amino\ acid}$ (eV) (E_1-E_2) (parallel to [42-1])**
arg-val-pro (1+)	-6.44	-2.41	-4.03	-8.26	-2.41	-5.85
leu-pro-cys	-3.17	-1.02	-2.15	-3.29	-1.02	-2.27
lys-gln-tyr (2+)	-9.56	-3.94	-5.62	-15.85	-3.94	-11.91
phe-leu-lys (1+)	-7.87	-2.08	-5.79	-10.43	-2.08	-8.35
leu-ala-pro	-2.70	-1.94	-0.76	-2.98	-1.94	-1.04
gly-ser-trp	-2.92	-1.57	-1.35	-3.77	-1.57	-2.20

Table 2.9. Adsorption energies of *negatively charged* 3-amino acid residue peptides on *flat terrace* of calcite (104) face

3-amino acid residue peptide	**$E_{adsorption\ per\ amino\ acid}$ (eV) (E_1)**	**$E_{hydration/amino\ acid}$ (eV) (E_2)**	**$E_{effective\ adsorption/amino\ acid}$ (eV) (E_1-E_2) (parallel to [010])**
arg-val-pro (1+)	-2.64	-2.41	-0.23
leu-pro-cys	-3.30	-1.02	-2.28
lys-gln-tyr (2+)	-3.59	-3.94	0.35
phe-leu-lys (1+)	-4.16	-2.08	-2.08
leu-ala-pro	-1.47	-1.94	0.47
gly-ser-trp	-2.01	-1.57	-0.44

Table 2.10. Adsorption energies of *negatively charged* 12-amino acid residue peptide with *complex structure* and *simple structure* on different calcite (104) surface locations

Calcite surface locations for complex-structured peptide	**Vacuum adsorption energy (eV/residue)**	**Calcite surface locations for simple structured peptide**	**Effective adsorption energy (eV/residue)**
non polar steps parallel to [48-1] with CO_3^{2-} making **obtuse angle**	-1.92	non polar steps parallel to [48-1] with CO_3^{2-} making **obtuse angle**	-1.26
non polar steps parallel to [48-1] with CO_3^{2-} making **acute angle**	-1.65	non polar steps parallel to [48-1] with CO_3^{2-} making **acute angle**	-0.78
polar steps terminated by Ca^{2+} parallel to [010]	-7.08	polar steps terminated by Ca^{2+} parallel to [010]	-2.19
polar steps terminated by Ca^{2+} parallel to [42-1]	-5.42	polar steps terminated by Ca^{2+} parallel to [42-1]	-1.94
polar steps terminated by CO_3^{2-} parallel to [010]	1.49	polar steps terminated by CO_3^{2-} parallel to [010]	-0.23
polar steps terminated by CO_3^{2-} parallel to [42-1]	-0.76	polar steps terminated by CO_3^{2-} parallel to [42-1]	-1.18
flat-terrace	-2.09	flat-terrace	-0.86

Table 2.11. Adsorption energies of *neutral* 12-amino acid residue peptide with *complex structure* and *simple structure* on different calcite (104) surface locations

Calcite surface locations for complex-structured peptide	**Vacuum adsorption energy (eV/residue)**	**Calcite surface locations for simple structured peptide**	**Effective adsorption energy (eV/residue)**
non polar steps parallel to [48-1] with CO_3^{2-} making **obtuse angle**	-2.49	non polar steps parallel to [48-1] with CO_3^{2-} making **obtuse angle**	-0.95
non polar steps parallel to [48-1] with CO_3^{2-} making **acute angle**	-1.79	non polar steps parallel to [48-1] with CO_3^{2-} making **acute angle**	-0.60
polar steps terminated by Ca^{2+} parallel to [010]	-3.79	polar steps terminated by Ca^{2+} parallel to [010]	-1.42
polar steps terminated by Ca^{2+} parallel to [42-1]	-2.96	polar steps terminated by Ca^{2+} parallel to [42-1]	-0.90
polar steps terminated by CO_3^{2-} parallel to [010]	-7.11	polar steps terminated by CO_3^{2-} parallel to [010]	-2.01
polar steps terminated by CO_3^{2-} parallel to [42-1]	-1.56	polar steps terminated by CO_3^{2-} parallel to [42-1]	-1.64
flat-terrace	-1.82	flat-terrace	-0.49

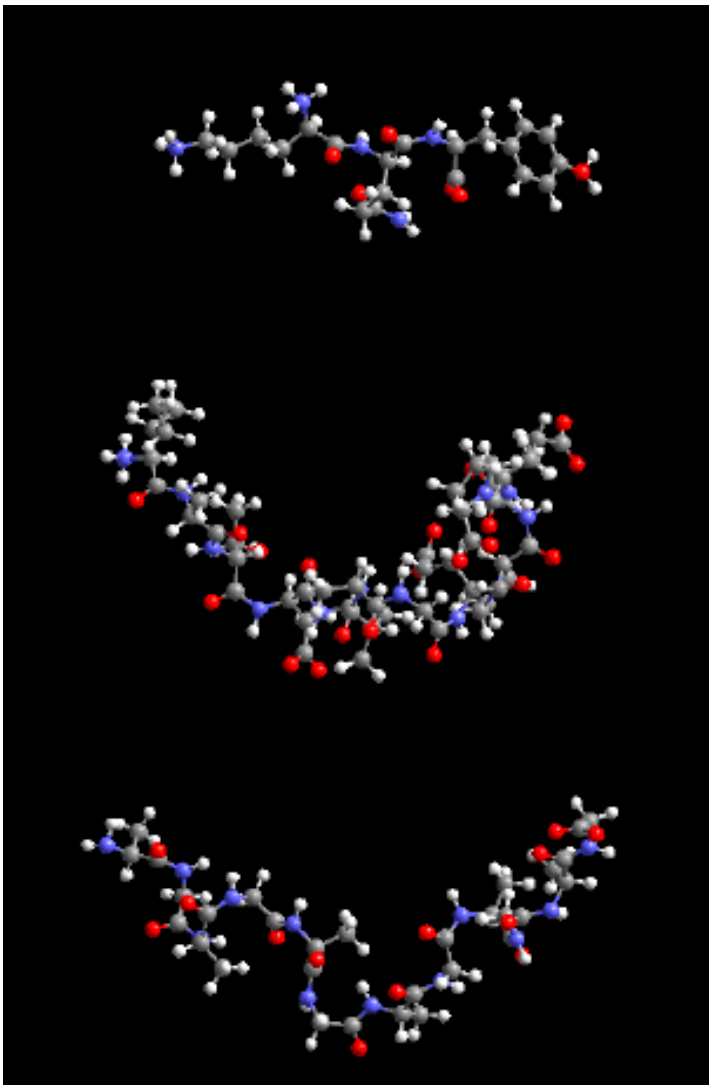

Figure 2.1. 3-amino acid and 12-amino acid peptide residues. The 12-amino acid peptide residues have complex and simple structure respectively.

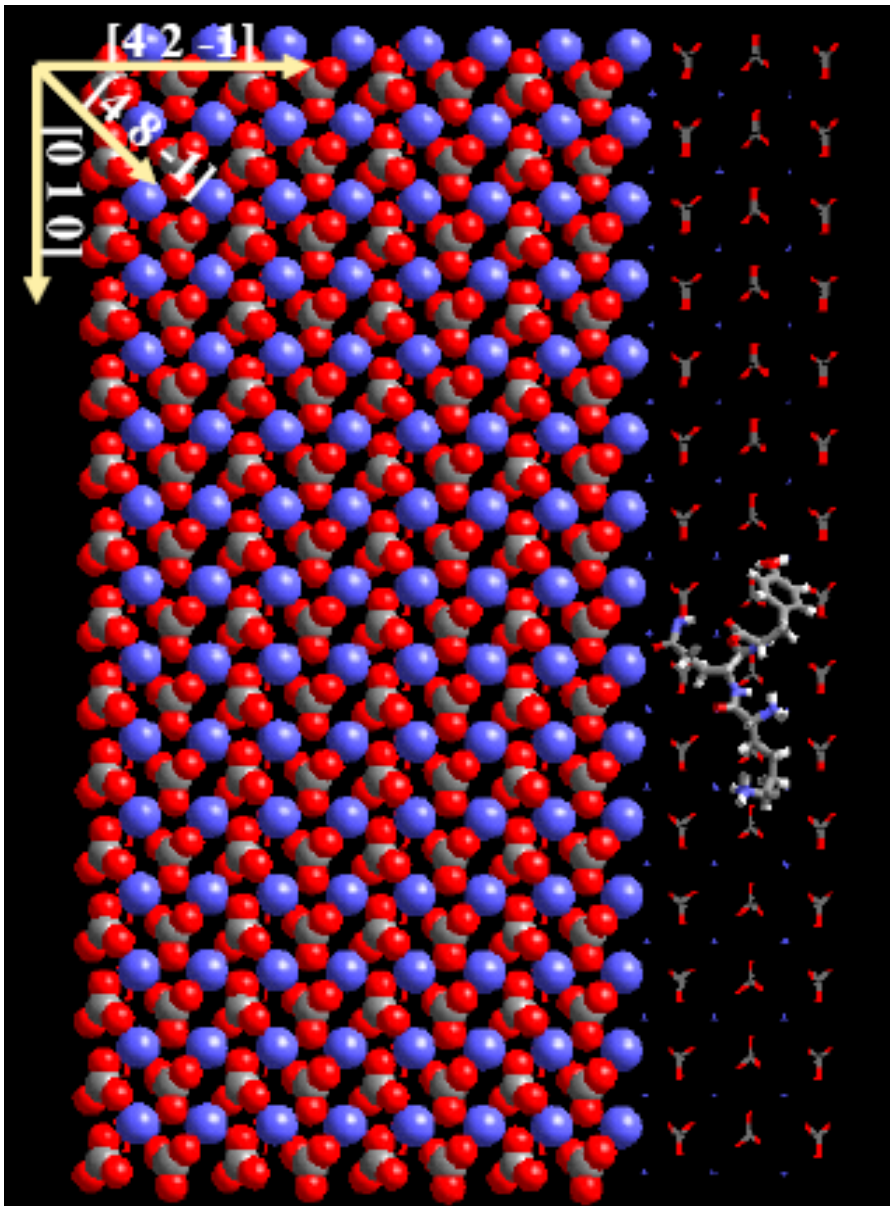

Figure 2.2 Adsorption site of 3 amino-acid residues on the polar calcite surface step parallel to [010]

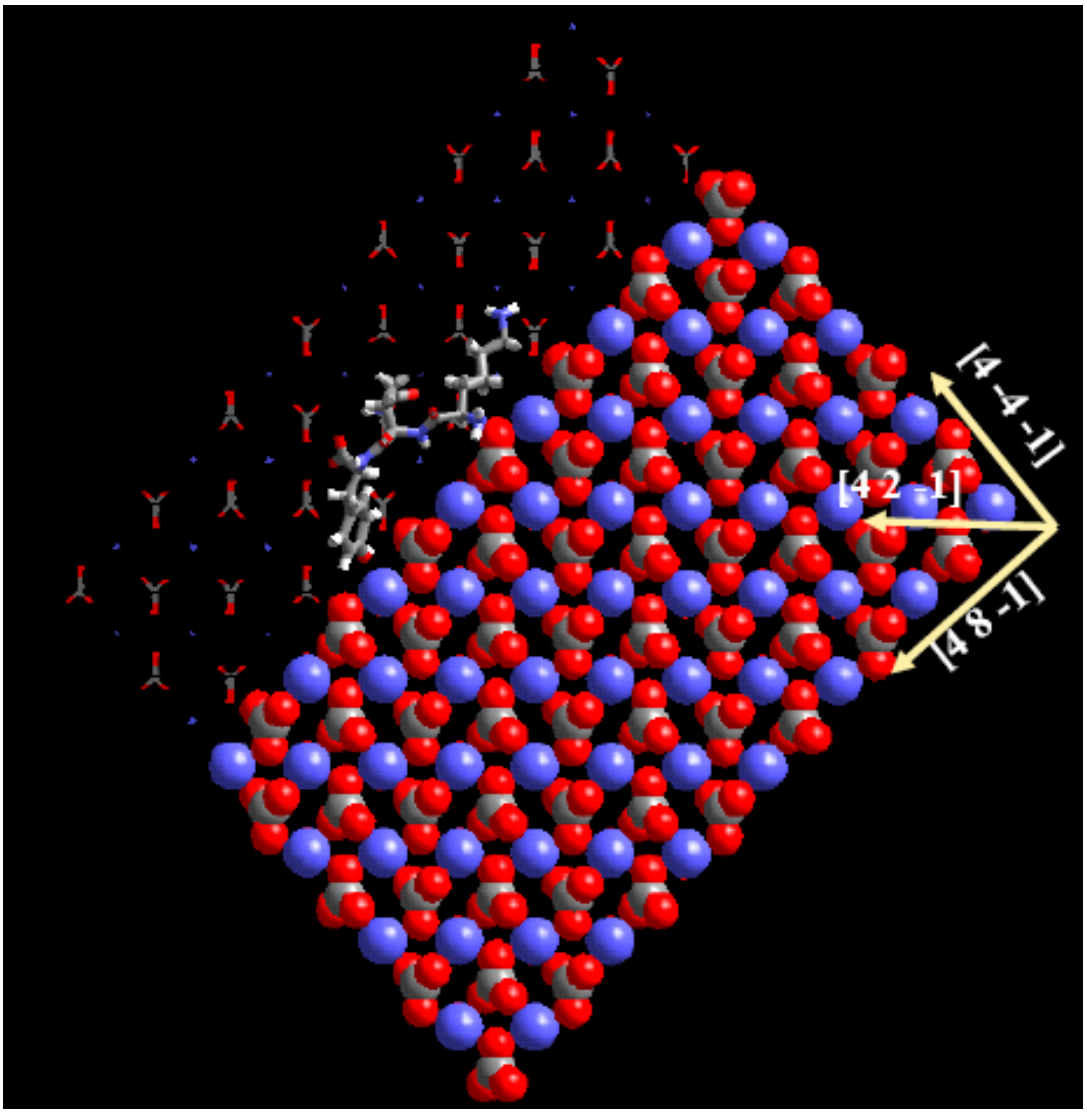

Figure 2.3. Adsorption site of 3 amino-acid residues on the polar calcite surface step parallel to [100]

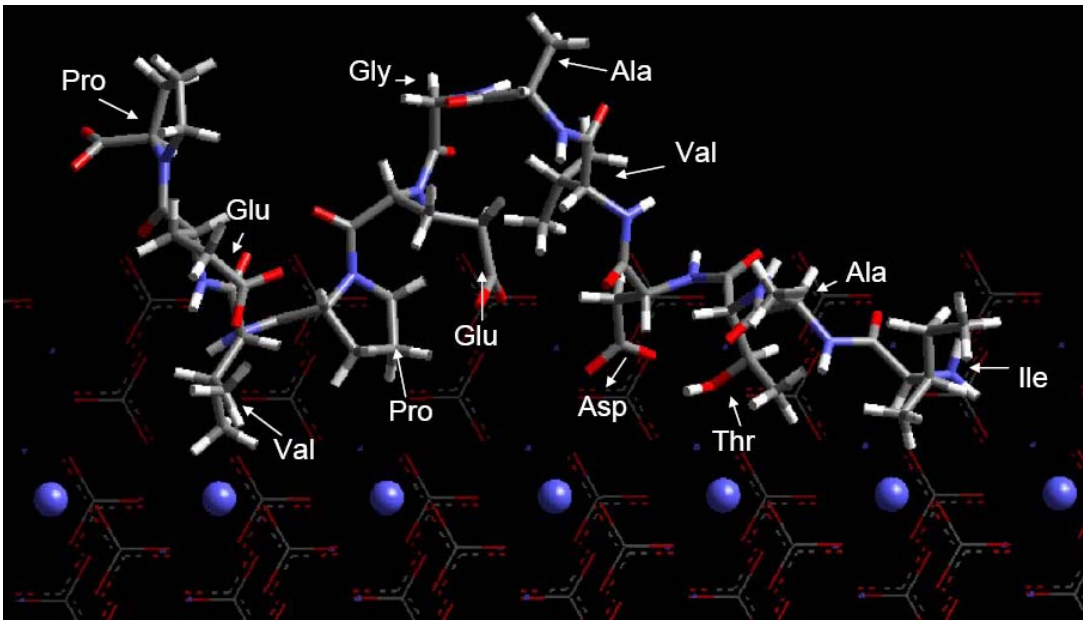

Figure 2.4. 12-amino acid residue peptide with complex structure

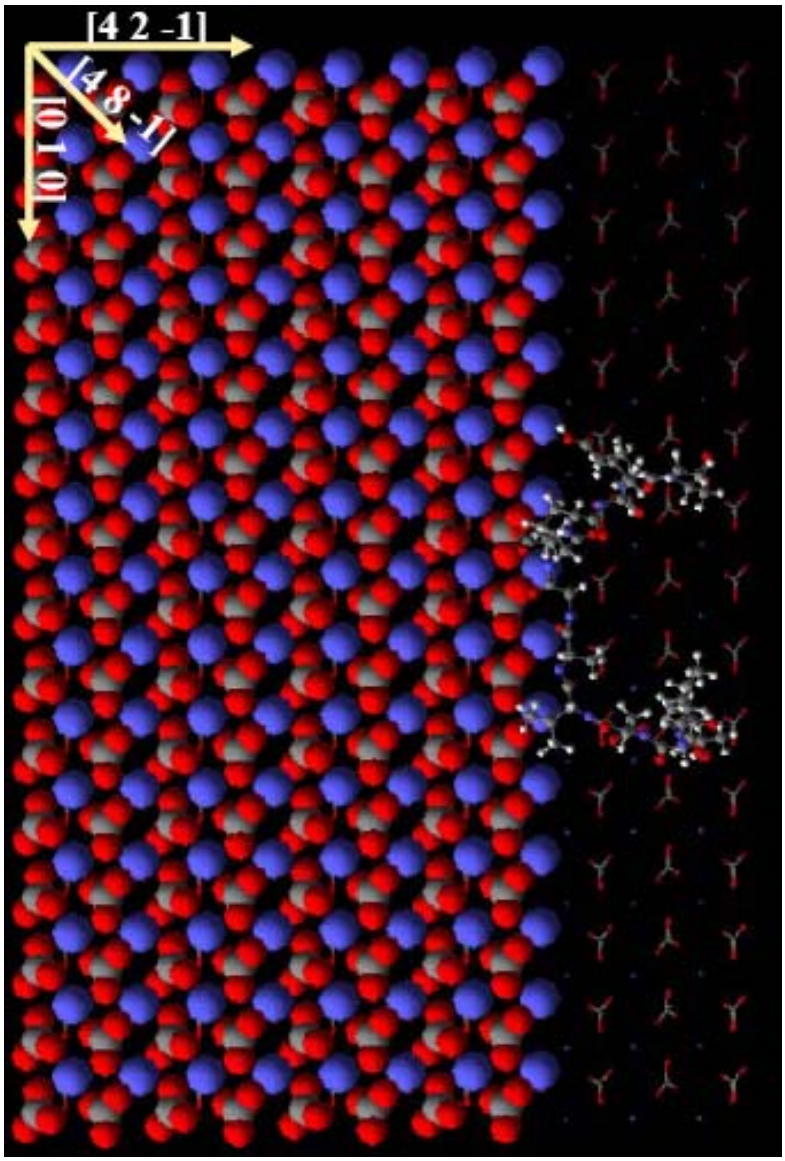

Figure 2.5. 12-amino acid residue peptide with complex structure aligned parallel to [010] surface step direction of calcite (104) surface

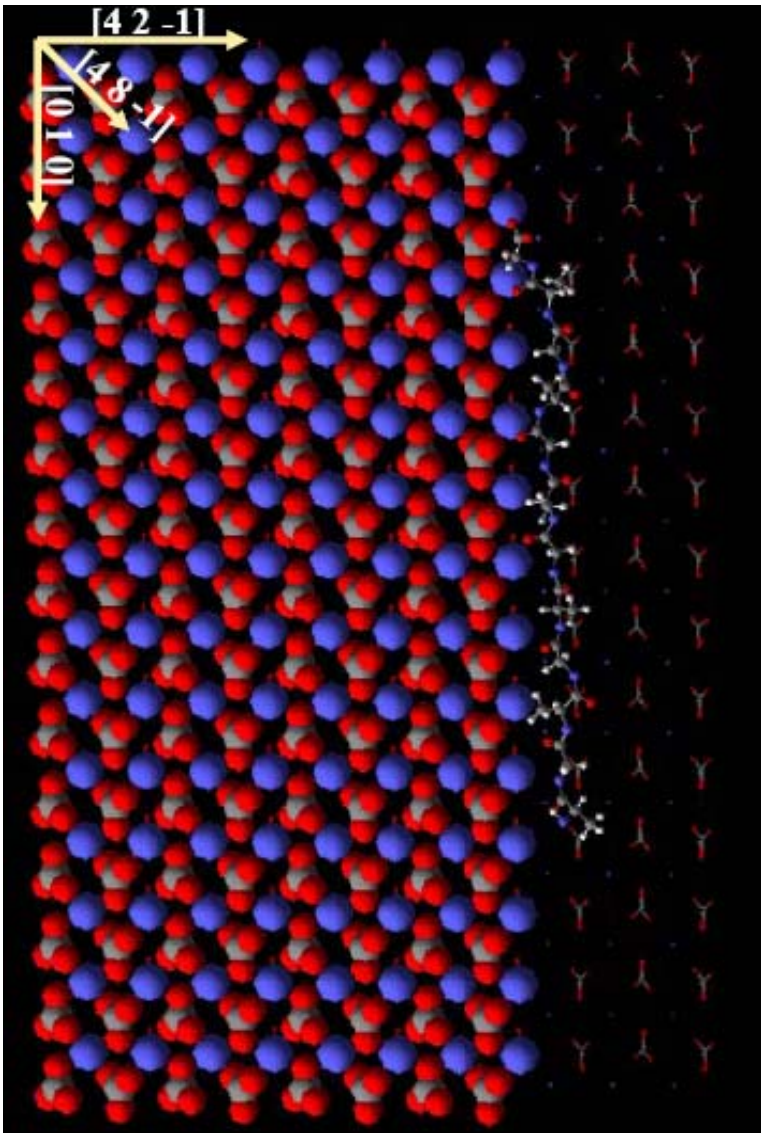

Figure 2.6. 12-amino acid residue peptide with simple structure aligned parallel to [010] surface step direction of calcite (104) surface

References

Becker U, Biswas S, Kendall T, Risthaus P, Putnis CV, Pina CM: **Interactions between mineral surfaces and dissolved species: From monovalent ions to complex organic molecules.** ***American Journal of Science*** 2005 **305**: 791-825

Buijnsters PJJA, Donners JJJM, Hill SJ, Heywood BR, Nolte RJM, Zwanenburg B, Sommerdijk NAJM: **Oriented Crystallization of Calcium Carbonate under Self-Organized Monolayers of Amide-Containing Phospholipids.** *Langmuir* **2001, 17**:3623-3628.

Cancés E, Mennucci B, Tomasi J: **A new integral equation formalism for the polarizable continuum model: Theoretical background and applications to isotropic and anisotropic dielectrics.** *Journal of Chemical Physics* 1997, **107:**3032-3041

Chargaff E, Vischer E: **The separation and quantitative estimation of purines and pyrimidines in minute amounts.** *Journal of Biological Chemistry* 1948, **176**:703-714.

Corstjens PLAM, van der Kooij A, Linschooten C, Brouwers G, Westbroek P, de Vrind-de Jong EW: **GPA, A calcium-binding protein in the coccolithophorid *Emiliania Huxleyi* (Prymnesiophyceae).** *Journal of Phycology* 1998, **34**:622-630.

Crick F, Burnett L, Brenner S, Watts-Tobin RJ: **General nature of the genetic code for proteins.** *Nature* 1961, **192:**1227-1232.

Crick F: **Central dogma of molecular biology.** *Nature* 1970, **227:**561-563.

de Leeuw NH, Parker, SC: **Atomistic simulation of the effect of molecular adsorption of water on the surface structure and energies of calcite surfaces.** ***Journal of the Chemical Society, Faraday Transaction*** 1997, **93**:467 - 475

Dickerson RE: **DNA structures from A to Z.** *Methods in Enzymology* 1992, **211:** 67-111.

Frisch MJ, Trucks GW, Schlegel HB, Scuseria GE, Robb MA, Cheeseman JR, Montgomery Jr JA, Vreven T, Kudin KN, Burant JC, Millam JM, Iyengar SS, Tomasi J, Barone V, Mennucci B, Cossi M, Scalmani G, Rega N, Petersson GA, Nakatsuji H, Hada M, Ehara M, Toyota K, Fukuda R, Hasegawa J, Ishida M, Nakajima T, Honda Y, Kitao O, Nakai H, Klene M, Li X, Knox JE, Hratchian, HP, Cross, JB, Bakken, V, Adamo, C, Jaramillo, J, Gomperts, R, Stratmann, RE, Yazyev, O, Austin, AJ, Cammi R, Pomelli C, Ochterski JW, Ayala PY,

Morokuma K, Voth GA, Salvador P, Dannenberg JJ, Zakrzewski VG, Dapprich S, Daniels AD, Strain MC, Farkas O, Malick DK, Rabuck AD, Raghavachari K, Foresman JB, Ortiz JV, Cui Q, Baboul AG, Clifford S, Cioslowski J, Stefanov BB, Liu G, Liashenko A, Piskorz P, Komaromi I, Martin RL, Fox DJ, Keith T, Al-Laham MA, Peng CY, Nanayakkara A, Challacombe M, Gill PMW, Johnson B, Chen W, Wong MW, Gonzalez C, Pople JA: **Gaussian 03, Revision C.02.** *Gaussian, Inc., Wallingford CT***,** 2004.

Henriksen K, Stipp SLS, Young JR, Marsh ME: **Biological control on calcite crystallization: AFM investigation of coccolith polysaccharide.** *American Mineralogist* 2004, **89:**1709-1716.

Kawasaki H, Kretsinger RH: **Calcium-binding proteins1: EF-hands.** *Protein Profile* 1995, **2**:297-490.

Kerisit S, Parker, SC, **Free energy of adsorption of water and calcium on the {10 - 14} calcite surface.** ***Chemical Communications*** **2004,** 52-53.

Kornberg R: **Molecular basis of eukaryotic transcription.** The Nobel Prize in Chemistry 2006.

Lim C, Bashford D, Karplus M: **Absolute pKa calculations with continuum dielectric methods.** *Journal of Physical Chemistry* 1991, **95:**5610-5620.

Mann S: **Molecular recognition in biomineralization.** *Nature* 1988, **332:**119-124.

Peterson IR: **Langmuir-Blodgett Films.** *Journal of Physics D: Applied Physics* 1990, **23:**379-395.

Rappe AK, Goddard III WA: **Charge equilibration for molecular dynamics simulation.** *Journal of Physical Chemistry* 1991, **95**:3358-3363.

Ringwood AE: **Chemical evolution of terrestrial planets.** *Geochimica et. Cosmochimica Acta* 1996, **30:**41-104.

Skinner HCW: **Biominerals.** *Mineralogical Magazine* 2005, **69:**621-641.

Teng HH, Dove PM, Orme CA, De Yoreo JJ: **Thermodynamics of Calcite Growth: Baseline for Understanding Biomineral Formation.** *Science* 1998, **282**:724-727

Chapter 3

Calcite seed formation by interaction with Langmuir films: two-dimensional interactions of biofilms with mineral surfaces

Introduction

In Chapter 2, we have discussed interactions of peptides with calcite surfaces in one dimension that is the adsorption of long-chain oligomers on surfaces and along steps. The peptides act as host organic molecules or organic complexes in the biomineralization process. Peptides act as complexing agents to inorganic ions present in the inorganic template and carry them over to the growth-site of mineral formation [Becker et al, 2005]. The transportation of inorganic ions to the growth site and the subsequent adsorption/crystal growth has to be controlled. Once the ions reach the growth site and the growth process starts, interactions between the initial growth nucleus and organic molecules control the shape and growth kinetics of the growth island of the mineral phase.

Organic molecules that adsorb to the growth nuclei in concert with ordered organic templates determine the morphology of the biominerals. These two-dimensional

growth island-organic template interactions are stronger, when the interface energy (per unit surface area) between the organic template and the growth island is more negative.

This scenario is obtained if, *e.g.*, the negative functional groups of the organic template have the same periodicity as the arrangement of the calcium ions on a particular calcite surface that is in contact with the template. Typically, we consider crystal faces to be stable if their charge is neutral and if their dipole moment perpendicular to the surface is zero as these conditions often lead to stable surfaces with low surface energies. The situation can be different in biomineralization processes: the organic template can expose an array of negative functional groups such as deprotonated carboxylic groups or alternating positive and negative functional groups as in amino acids. In the first case, the strongest interface will be formed if the calcite surface is positively charged. Thus, a calcite (001) surface with Ca^{2+} termination may be a good candidate for such an interface even though calcite (001) surfaces are usually not found in inorganically grown calcite crystals because their charged surface results in a high surface energy. Not only must the polarity of the organic template and a particular crystal surface match but so must the distance between them and the angle between chains of functional groups and the respective angles on the mineral surface. There are several laboratory methods that control this periodic relationship between the templating biomolecular substrate and the inorganic phase, which lies in the epitaxial matching of lattice spacing of specific crystal planes with some ordered arrangement of molecular units in the template [Mann, 1988, Buijnsters et al, 2001]. Such approaches include the use of synthetic templates such as polymers [Berman et al, 1995], macromolecular complexes [Donners et al, 2000], phospholipid vesicles [Mann et al, 1986], and Langmuir films [Landau et al, 1986,

Landau et al, 1989]. Langmuir films consist of an array of hydrophilic functional groups that are in contact with the water surface, and hydrophobic aliphatic chains above the water surface. The separation between these molecules is controlled by pistons [Landau et al, 1989]. In the case of Langmuir monolayers, the amphiphilic molecules can be designed in such a way that they act as artificial two-dimensional nuclei for the promotion of crystal nucleation. Such films have been used as templates to direct the crystal nucleation and growth of amino acids, proteins, and calcium carbonate. This chapter describes the simulation of the growth and crystallization of calcium carbonate seed crystals from supersaturated calcium carbonate solutions in contact with such Langmuir films. It is found that modification of the polar group and head group of the surfactant has a marked effect on the crystallization process [Heywood et al, 1994]. Mobility of the molecules in the monolayer has also significant effect on the crystallization. In the experimental study, researchers have worked with the Langmuir monolayer made-up of:

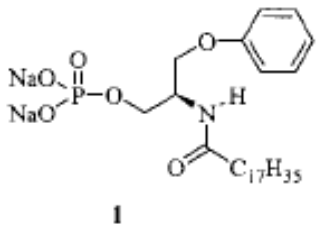

1

Benzyl(-)-(2*S*)-3-Phenoxy-2-octadecylaminopropan-1-ylmethylphosphate (compound 1) with a polar phosphonate group (on the left in the structure above) and an aliphatic chain ($C_{17}H_{35}$).

The effect of piston pressure on the surface area per surfactant molecule (compound 1) was studied by Buijnsters *et al.*, 2001. These results can be compared with the computational simulation of the Langmuir film composed of compound 1 by decreasing the area available for each surfactant molecule and calculating the resulting strain, which can be converted to pressure. Subsequently, the growth of calcite seed

nucleation under these Langmuir films at different pressure/ (surface area) conditions was evaluated. Compound 1**,** shown in figure 3.1, is an amide-containing phospholipid and was chosen in this study to evaluate organic matrix-mineral interfaces. The presence of a hydrophilic head group and a hydrophobic hydrocarbon chain closely depicts the physico-chemical properties of exopolymers of living organisms in nature.

Methods

Using the Cerius^2 software package, compound 1 is aligned in a two-dimensional array to create the Langmuir film. The elongated hydrocarbon chain is pointed upwards and the amide-containing phosphate head group points downwards in contact with the inorganic mineral surface. In an actual experiment, the organic film is initially in contact with a supersatured calcium carbonate solution and crystal nuclei form over time. However, this time scale is much longer than what is possible to simulate in molecular dynamics (MD) simulations (up to ≈ 1ns). Therefore, the crystal formation step has to be skipped and the stability of different organic-inorganic interfaces was evaluated in this study. First we have to determine the limiting force and unit area of the Langmuir film unto which it can withstand external pressure. We start with area of 46 Å^2 (per 8 phospholipid molecules in the Langmuir film) when the external force applied is 0 N/m. Then we slowly increase the pressure, and the virtual pistons placed on both sides of the Langmuir film move towards the center of the array. The entire Langmuir film is allowed to move during MD simulations at each particular force and surface area points. This way, the limiting area and force is found out to be 29.011 Å^2 and 25.4 N/m (Figure 3.2). When we increase the force to 25.5 N/m on both the pistons at the side of Langmuir film,

the whole film ruptures during the MD simulation. The force vs. limiting surface area data is listed on table 3.2.

In order to study the interaction of different calcite faces with such a film, the different calcite faces are placed under the Langmuir film at a particular force and surface area condition. Molecular dynamics and energy minimizations are performed for each face. Two-dimensional periodic boundary conditions are applied in each case, indicating that the surface is extended infinitely in both directions parallel to the interface. Three different calcite faces, (001), (100), and (104), were studied in such a way. In each of the interactions, both the organic compounds in the Langmuir film and the calcite lattice beneath it are free to relax to form the most stable interface during energy minimization and molecular dynamics simulation. It was observed that the the organic compounds do not affect the calcite structure beyond the fourth layer. The final interface energy per unit area provides an estimate on which face would be energetically favorable for the onset of calcite seed formation under a Langmuir film consisting of amide-containing phospholipids. Both the surface and interfacial energy in each case of organic-calcite interaction are calculated, and the sum of these energies is used as a criterion to decide on which would be the most likely interface.

We have used CALCITE-WATER force-field to the interactions within the organic molecules and for interactions between the organic molecule and the substrate. It is similar to the force-field we have used and described in chapter 2. We have included a three-body intramolecular potential term in the ANGLE BEND section to account for the interactions of water molecules with the calcite surface. We also included non bonding van der Waals interaction terms in the force-field to account for the interactions between

Ca^{2+} and CO_3^{2-} and water molecule. Interactions within the organic molecules and between the calcite and the organic molecules are based on the UNIVERSAL1.02 force field [Rappe et al, 1991]. The potentials and charges of atoms used in this force-field are listed in Table 3.1.

Results and Discussions

Of the three calcite faces under the Langmuir film, the (100) face yielded the lowest interfacial energy (-0.05 eV/Å^2) and the (104) face (this rhombohedral face is the most stable one if calcite is grown naturally, without the influence of organic matrix) the most unfavourable one (see Table 3.3). This suggests that a Langmuir film consisting of amide-containing phospholipids is not suitable to promote calcite seed formation with the (104) face forming the interface. For the phospholipid array used, the calcite (001) is also not likely to be formed.

The hydrophilic head group of the organic compounds present in the Langmuir film consists of phosphate group, benzene ring and amide bond. We chose a deprotonated phosphate group due to its low pKa values for the interaction with the calcite surface and these phosphonate groups are attracted to the Ca^{2+} ions at the crystal surface. The H atoms and the carbonate groups form weak van der Waals bonds, which cause minimal distortion of the calcite face, and helps promote the calcite seed formation. The hydrophobic benzene ring is pointing away from the calcite surface, and more tilted towards the long hydrophobic hydrocarbon chain of the next organic molecule present in Langmuir film. A close look at the orientation of the organic molecules in the Langmuir film rationalizes the favorable interaction between the organic lattice and Inorganic calcite. The hydrophobic part of each organic compound in the film, the long

hydrocarbon chain and the benzene ring, are aligned at an angle of 45^{o} with respect to the interfacial surface of organic and inorganic lattice. The hydrophilic part, the amide bond and the phosphate group are aligned almost perpendicular to the interface. This allows maximum interaction between the hydrophilic parts of the organic molecule and the calcium and carbonate ions on the calcite surface. The spacing, stoichiometry and the favorable chemical interaction between the hydrophilic end or the organic template and the calcite (100) face promote the calcite seed formation, as shown in figure 3.4. The water molecules around the calcite seeds represent hydration. Hydration counteracts the formation of seeds thermodynamically although it helps the Ca and carbonate ions to diffuse to their final adsorption sites. In this way, this computational setup mimics the natural process in an aqueous environment more closely, than, e.g., adsorption simulated in a vacuum.

Conclusions

The control of inorganic crystal growth is mainly mediated by an organic matrix or organic template. The principle is that the ions on the inorganic mineral surface align with functional groups of opposite charge in the biological matrix. Developing a suitable model for the mechanism of matrix-mediated crystal growth has been challenge to scientists over the years. As cited in this chapter, several experimental studies have been performed on growth of calcite nuclei in contact several organic matrices, mainly under compressed monolayers and Langmuir films. Our study in this chapter follows in the footsteps of the experimental conditions observed in these experimental studies of matrix-mediated calcite growth, and it gives additional insight into the molecular-scale mechanism of calcite seed nucleus formation. We have studied the calcite seed formation

in an aqueous system with several monolayers of water molecules around the Ca^{2+} and CO_3^{2-} ions. Water is an important factor in these studies, because the natural biomineralization process occurs in an aqueous environment. In the experimental studies performed, the compressed monolayers of organic molecules are generally prepared in aqueous solution [Buijnsters et al, 2001]. The crystallization of calcite and its polymorphs occurs in supersaturated calcium carbonate solutions [Rajam et al, 1991]. We use periodic boundary conditions during our study to avoid edge effects that may occur at the mineral cluster or in the organic film. Current work our research group investigates small peptide molecule interactions with water molecules simultaneously in contact with mineral surface. The initial results have shown that orientation of the peptide is dependent on calcite-water interaction. The same argument is followed in the study of this chapter 3, as the calcite seed nucleus formation in aqueous condition is governed by the compressed Langmuir monolayers present above the calcite-water system. Langmuir films are good candidates as model for biomembranes and biofilms, as Langmuir film contains amphiphilic molecules with polar head groups and non-polar tails like cell-membranes.

Work in this chapter has provided the insight into the theory specific mineral surfaces can grow or form under specific biological membrane. It has been shown in this chapter that calcite (100) surface nucleation occurs at the interface of Langmuir film-calcium carbonate solution, prevailing over calcite (104) face which is inorganically most stable. Spacing between Ca^{2+} ions in the top layer of calcite (100) plays an important role in calcite seed formation as it matches the distance between polar head-groups in Langmuir film. Work in this chapter is a stepping stone for future research in two-

dimensional molecular modeling studies of mineral growth and nucleation under organic matrix. Calcite's polymorph aragonite, vaterite will be suitable candidates for this study, along with various other organic matrices like polysaccharides, dendrimers and other macromolecules. These macromolecules have not been studied at a molecular scale in order to find out which functional groups are mainly responsible for triggering calcite nucleation. Computational modeling work with these set of matrix-mineral combination will give scientists a clear picture about the *in vitro* process occurring during natural biomineralization.

Even though the experiments described in this chapter and the simulations performed in our study help to rationalize how specific organic templates may trigger specific faces of different calcium carbonate polymorphs, little information is available at this point on the actual composition and structure of biofilms of different organisms in a natural system. It is equally unknown, how much of the crystal morphology is controlled by face and step-specific organic molecule adsorption (see chapter 2) and how much by well-ordered organic templates as described in this chapter.

Table 3.1. Potential parameters for CALCITE-WATER forcefield

O-O	Buckingham[1]	*inter*molecular; < 14 **Å**	A = 1477.95 eV	ρ = 0.2455 Å	C = 0 eV/ Å^6
Ca-O	Buckingham[1]	inter*molecular;* < 14 **Å**	A = 792.27 eV	ρ = 0.2891 Å	C = 0 eV/ Å^6
O-C	Morse[2]	*intra*molecular	D = 4.9664 eV	r_0 = 1.2025 Å	K_b = 63.233 eV/ Å^2
O-C-O angle	Three-body[3]	*intra*molecular	K_0= 1.785	θ_0=120°	
H-O-H angle	Three-body[3]	*intramolecular*	K_0 = 60	θ_0=109.47°	
CO_3-plane	Umbrella[4]	*intra*molecular	ω_0 = 0°	K_0 = 4336.47 eV	
charges	C = +1.345	O = -1.115	Ca = +2.000	H_w = +0.41	O_w = -0.82

[1]Buckingham: A exp (-r/ρ) - C r $^{-6}$ C in eV Å^6

[2]Morse: D [(1 - exp {-a(r-r_o)})^2 - 1] a = $(K_b/2D)^{1/2}$

[3]Three-body: E = K_0 (θ-θ_0)^2

[4]Umbrella: E = K_0 (1 – cos ω) for ω_0 = 0° ω = Angle between the C-O bond and its projection on O-C-O plane.

Table 3.2. **Force vs. Surface area for the Langmuir film made with amide containing phospholipid**

Force (N/m)	Surface Area ($Å^2$)
0	47.06
1	42.12
5	41.91
9	34.21
12	31.03
18	30.87
25.4	29.01
25.5	film ruptures

Table 3.3. **Interfacial energies between various calcite surface and Langmuir film**

Calcite surface	**$E_{surface}$** **(eV/Å^2)**	**$E_{interface}$** **(eV/Å^2)**	**E_{total} ($E_{surface}$+ $E_{interface}$)** **(eV/Å^2)**
Calcite (100)	0.06	-0.05	0.01
Calcite (104)	0.0	2.1	2.1
Calcite (001)	0.3	-0.02	0.28

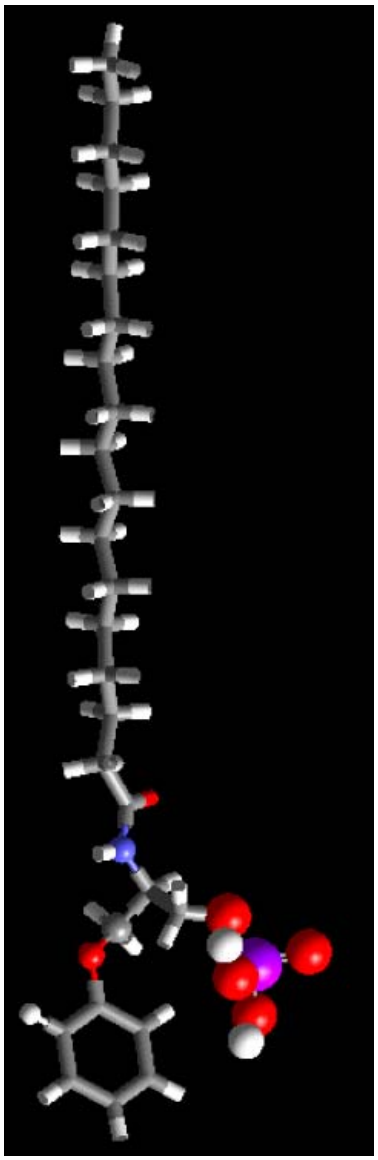

Figure 3.1 Building block of the Langmuir film: amphiphilic molecule consisting of an amide-containing phospholipid. The hydrophobic part contains a long hydrocarbon chain, and the hydrophilic part contains PO_4^{3-} ions and amide group.

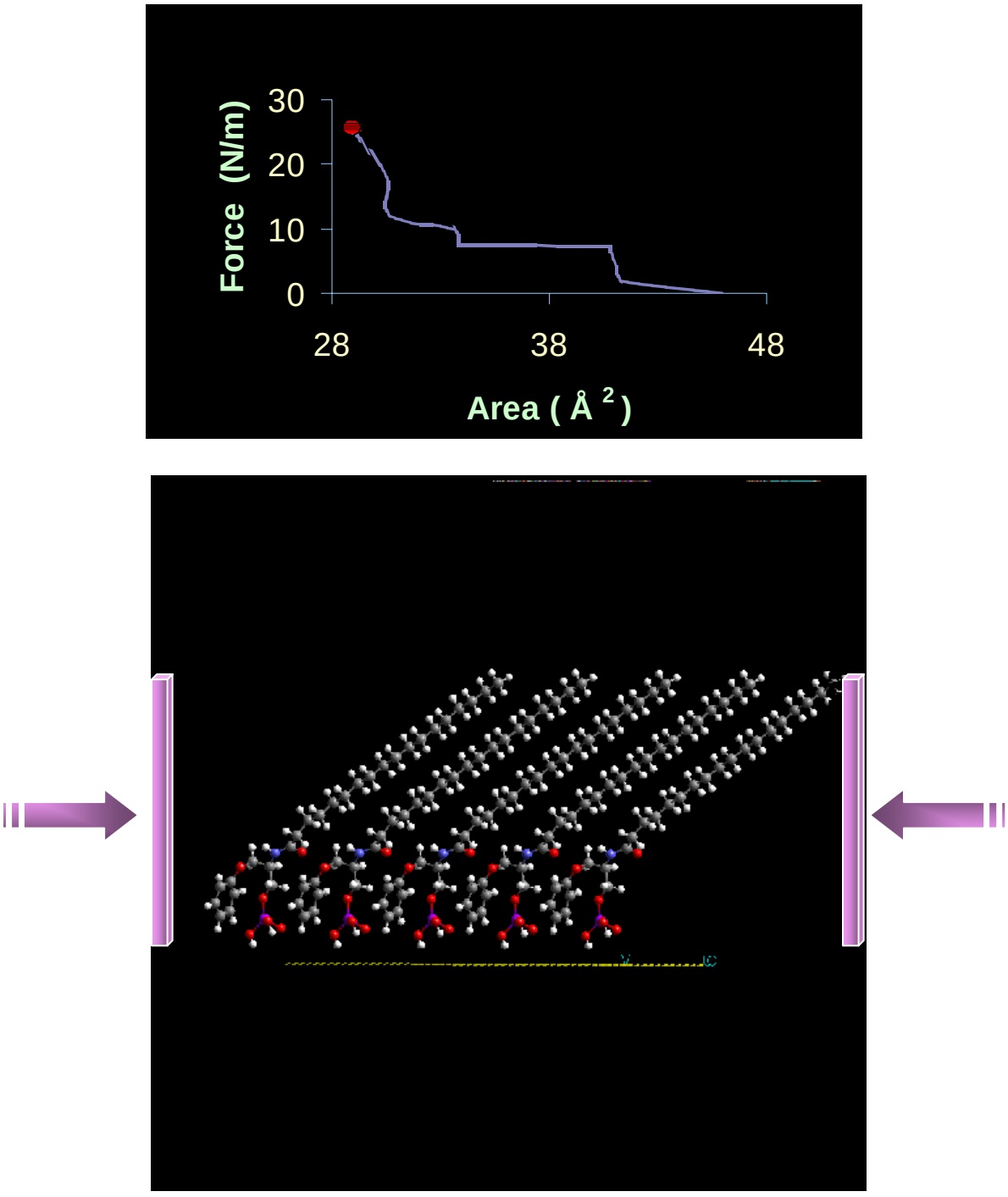

Figure 3.2. Force vs. surface area curve is shown in above picture, where the surface area of the Langmuir film decreased with increase of external force. Limiting force and surface area condition for Langmuir film made up of amide-containing phospholipid. The limiting area and force is found out to be 29.011 $Å^2$ and 25.4 N/m

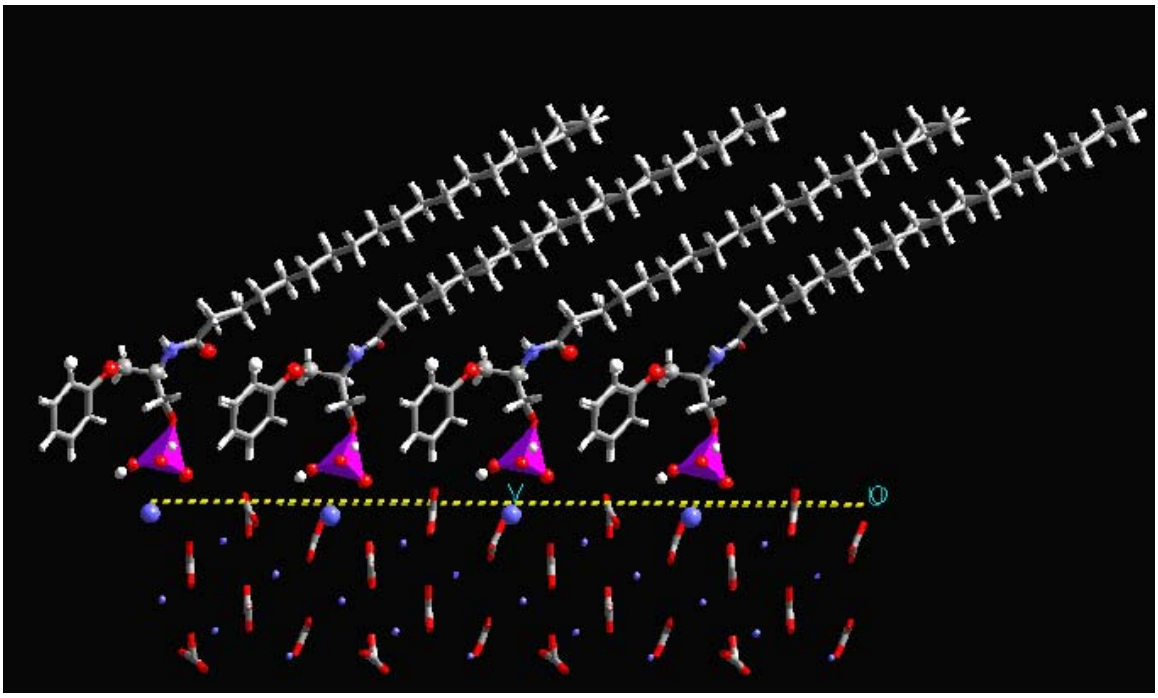

Figure 3.3. Calcite (100) surface under Langmuir film: this interface yields the most favorable interfacial energy among the faces studied ((100), (001), and (104)).

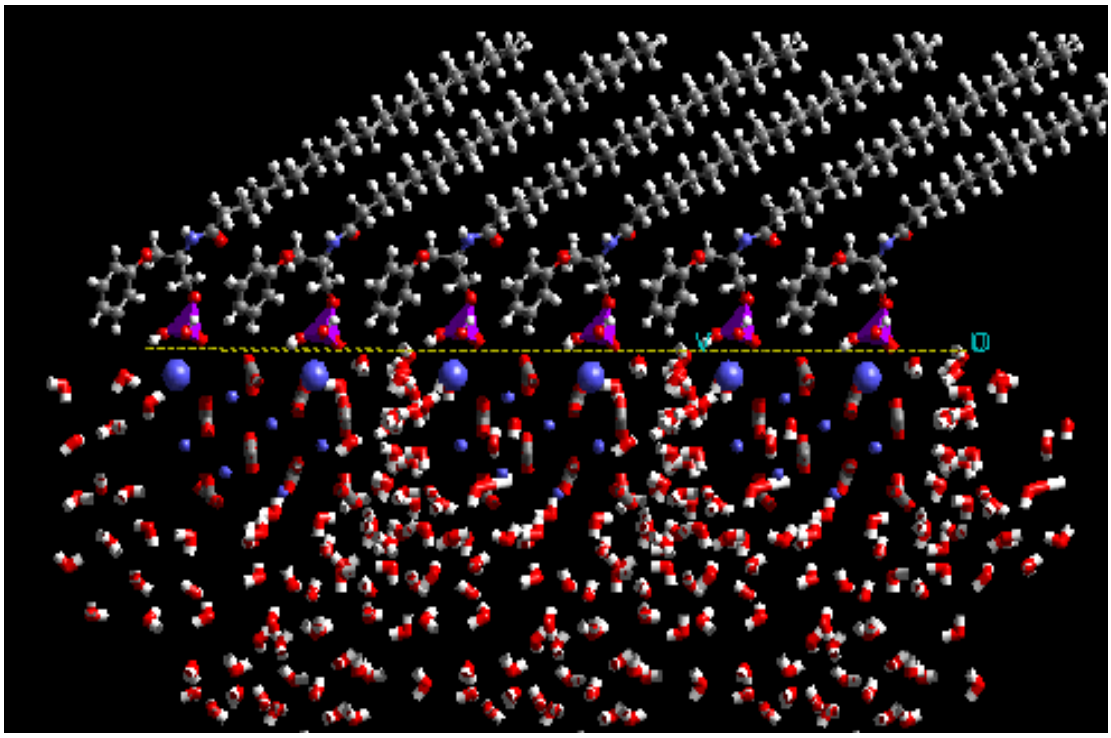

Figure 3.4. Onset of calcite seed formation at calcite (100) surface under Langmuir film in an aqueous environment.

References

Becker U, Biswas S, Kendall T, Risthaus P, Putnis CV, Pina CM: **Interactions between mineral surfaces and dissolved species: From monovalent ions to complex organic molecules.** ***American Journal of Science*** 2005 **305**: 791-825

Berman A, Ahn DJ, Lio A, Salmeron M, Reichert A, Charych D: **Total Alignment of Calcite at Acidic Polydiacetylene Films: Cooperativity at the Organic-Inorganic Interface**. *Science,* 1995, **269:**515-518

Buijnsters PJJA, Donners JJJM, Hill SJ, Heywood BR, Nolte RJM, Zwanenburg B, Sommerdijk NAJM: **Oriented crystallization of calcium carbonate under self-organized monolayers of amide-containing phospholipids**. *Langmuir*, 2001, **17**:3623-3628

Donners JJJM, Heywood BR, Meijer EW, Nolte RJM, Roman C, Schenning APHJ, Sommerdijk NAJM: **Amorphous calcium carbonate stabilized by poly (propylene imine) dendrimers**. *Chemical Communications*, 2000, **19**:1937-1938

Heywood BR, Mann S: **Molecular Construction of Oriented Inorganic Materials: Controlled Nucleation of Calcite and Aragonite under Compressed Langmuir Monolayers.** *Chemistry of Materials*, 1994, **6**:311-318

Landau EM, Levanon M, Leiserowitz L, Lahav M, Sagiv J: **Transfer of structural information from Langmuir monolayers to three-dimensional growing crystals.** *Nature*, 1985, **318**:353-356.

Landau EM, Wolf SG, Levanon M, Leiserowitz L, Lahav M, Sagiv J: **Stereochemical studies in crystal nucleation. Oriented crystal growth of glycine at interfaces covered with Langmuir and Langmuir-Blodgett films of resolved .alpha.-amino acids**. *Journal of American Chemical Society.* 1989, **111**:1436-1445

Mann S, Hannington JP, Williams RJP: **Phospholipid vesicles as a model system for biomineralization**. *Nature,* 1986, **324**:565-567.

Mann S: **Molecular recognition in biomineralization.** *Nature*1988, **332(6160):**119-124

Rajam S, Heywood BR, Walker JBA, Mann S, Davey RJ, Birchall JD: **Oriented crystallization of $CaCo_3$ under compressed monolayers. Part 1.—Morphological studies of mature crystals.** *Journal of Chemical Society, Faraday Transaction*, 1991, **87**:727-734

Rappe AK, Goddard III WA: **Charge equilibration for molecular dynamics simulation.** *Journal of Physical Chemistry* 1991, **95**:3358-3363.

Chapter 4

Molecular modeling of cell-adhesion peptides on hydroxyapatite surfaces and surface steps

Introduction

Understanding the interaction between organic molecules and inorganic surfaces is an important aspect in the development of functional bone-tissue engineered substitutes and in developing a general concept for bone and teeth growth. Specifically, the microenvironment on hydroxyapatite and carbonated apatite surfaces can influence cellular behavior positively by enhancing cell adhesion, spreading, and growth or negatively by promoting cell death (apoptosis, [Woo et al, 2007]). Through observation of nature's bone mineralization process, biomimetic techniques of precipitating bone-like mineral on polymeric scaffolding have been developed [Rezwan et al, 2006]. Soaking a biodegradable, 3D scaffold in a supersaturated solution that contains similar ion concentrations to that of human serum at body temperature (37 °C) will heterogeneously precipitate a carbonated apatite phase onto the scaffold [Linhart et al, 2000]. Such a

carbonated apatite layer can be used as a platform for biomolecular delivery of proteins, growth factors and peptides.

We looked at the interactions of bioactive surfaces with biomaterials that cause cell adhesion during bone-tissue regeneration. The main aspect of bone-tissue engineering is attaining original functionality of the damaged tissue. To achieve that, cell adhesion to synthetic support (e.g. biomaterials) via bioactive surfaces is required to happen. The bioactive surfaces can be extracellular proteins, cell-mediated synthetic proteins or bio-engineered motifs. All these 3 types of bioactive surfaces interact with the biomaterial (carbonated hydroxyapatite mineral present in bone). This biological molecule-inorganic mineral interaction leads to a series of cellular events including cell-adhesion that finally leads to bone-tissue regeneration. Thus it is important to understand the interaction between bioactive surfaces(proteins) and biomaterial(carbonated hydroxyapatite) in order to understand bone-tissue engineering, because these interactions are stepping stone of the bone tissue regeneration process. Thus it is important to understand the interaction of peptides and proteins with the mineral surface to engineer bone-growth and regeneration. Molecular modeling has been widely used [Becker et al, 2005, Boiziau et al, 1987] to investigate organic molecule-mineral surface interactions in various systems. We are applying this method to study interaction between cell-adhesion peptides and the hydroxyapatite system to understand bone-growth and regeneration. The main hypothesis that is tested in this chapter is the influence of peptide orientation on selective adsorption of peptides on mineral surface. Hydroxyapatite is chosen as biomaterials surface as relaxed hydroxyapatite surface represents the actual biomaterial component of bone, i.e., carbonated hydroxyapatite.

We have started our work with hydroxyapatite without any carbonate substitution. Hydroxyapatite (HA), $Ca_5(PO4)_3OH$, is not a major rock-forming mineral, but it can be an important phosphate source for plant growth [Rodriguez and Fraga, 1999] and is crucial as the main inorganic constituent of natural bone [Astala and Stott, 2005]. In addition, with silicon doping, it is the basis of bioactive ceramics, which show promise as bone-repair materials [Astala et al, 2005]. HA has a hexagonal structure with space group $P6_3/m$ and lattice parameters $a = b = 9.4225$ Å and $c = 6.8850$ Å [Astala et al, 2005]. There are two formula units per unit cell and the arrangement of calcium and phosphate ions can be viewed as consisting of isolated phosphate anion tetrahedra with Ca^{2+} in the space between and a chain of OH^- ions along the *c*-axis to balance the charge. Monoclinic structures with four formula units per unit cell have also been reported [Morgan et al, 2000, Eliott et al, 1973] where the monoclinic unit cell is obtained from the hexagonal one by doubling the *b* lattice parameter and by having different arrangements of the anion chains.

The focus of this work is to study the interaction of cell-adhesion peptides with the hydroxyapatite surface and surface steps using both a cluster approach and one with periodic boundary conditions. The cell-adhesion peptides that are used in this study are YIGSR (tyr-ile-gly-ser-arg) (derived from laminin protein) and RGD (arg-gly-asp) (a ubiquitous protein). The orientation of peptides on the surface, while interacting with the surface ions, is not definitively known. Orientation of the peptides dictates the morphology of the hydroxyapatite mineral surface, which facilitates bone growth and regeneration. Several experimental studies of hydroxyapatite surface morphology under the influence of the peptides have been performed. [Frayssinet et al, 1998] determined

cell-growth rate on a sintered disk at various temperatures. [Linhart et al, 2001] looked at biologically and chemically optimized composites that can be used as biodegradable bone-substitution material. [Okamoto et al, 1998] demonstrated that the regulation of cell adhesion to HA is different from that to titanium. RGD-containing serum proteins may play a major role in regulating the specific adhesion of osteoblasts to HA and in inducing enhanced cell growth and differentiation. In another experimental study with fusion peptide, [Gilbert et al, 2000] showed that the RGD portion of the hydrated fusion peptide is highly dynamic on the hydroxyapatite surface. But none of these studies focuses on the orientation of the peptide sequences when adsorbed on the hydroxyapatite surface. The molecular level details and the study of atomistic interactions between the peptide and hydroxyapatite may provide the insight into developing a more controlled design for immobilizing bioactive sequences on hydroxyapatite for biomaterials, tissue engineering, and vaccine applications.

A primary goal of this work was to determine the orientation of cell-adhesion peptides when adsorbed on hydroxyapatite surface. Another objective was to determine the effect of orientation of the peptide on the hydroxyapatite surface. Initial positions of the peptides on the mineral surface were varied before the empirical energetics calculations were performed. Empirical methods were used to study the adsorption of these peptides on hydroxyapatite surfaces using different approaches such as clusters and periodic surfaces. In order to calculate the specific interactions at the organic-inorganic interface, a force field for hydroxyapatite-BSP peptides interactions was developed in this study.

Molecular modeling has proven useful for investigating protein-substrate and peptide-substrate interactions in calcite, calcium oxalate, and apatite systems [Wierzbicki et al, 2000, de Leeuw, 2004, Mkhonto et al, 2000]. Insight pertaining to the interactions of oligopeptides with biominerals can be deduced from this type of modeling, such as adsorption conformation, adsorption energies, and stability of the organic-inorganic interface.

Developing bioactive bone tissue engineered constructs that can recruit and direct cell behavior towards an osteogenic lineage has been increasingly investigated [Petite et al, 2000, Rezwan et al, 2006, Sun et al, 1999]. Strategies of biomaterial-induced cell change include using calcium phosphate substrates and surface modification via peptides adsorption. Peptide sequences for bone tissue have been designed to mimic sections of proteins such as bone sialoprotein (BSP), osteopontin, laminin, fibronectin, statherin, collagen, and osteonectin. Some of the established BSP peptides are E_7PRGDT, RGD, RGE, and YIGSR. Main focus in this chapter is on the interaction of RGD and YIGSR on different surface locations of hydroxyapatite.

Methods

Hydroxyapatite is a naturally-occurring form of calcium apatite with the formula $Ca_5(PO_4)_3(OH)$, which is often written $Ca_{10}(PO_4)_6(OH)_2$ to denote that the unit cell comprises two formula units. Hydroxyapatite is the hydroxyl end member of the solid solution where the hydroxyl anion can be replaced by fluoride, chloride, or carbonate. Apatite crystallizes in the hexagonal bipyramidal crystal system. There are various prismatic faces along which hydroxyapatite can be cleaved, with the resulting cleavage surfaces providing locations for effective interaction with peptides during bone-tissue

engineering. The top and bottom of an apatite prism consist of a (001) surface, which is the naturally occurring surface where peptides interact with the mineral.

Using the Cerius^2 software, hydroxyapatite (001) surfaces and surface steps parallel to [010] are created. The HYDROXYAPATITE force field was developed and used to investigate the interactions within the organic molecules and for interactions between the organic molecule and the substrate. This HYDROXYAPATITE force field is derived from the UNIVERSAL1.02 force-field [Rappe et al, 1991] for the interactions within the peptides, but it is tailor-made to accommodate interactions relevant to hydroxyapatite surfaces and organic molecule. The potential parameters used to build this force field are listed in Table 4.1.

The force-field parameters control the interaction between phosphorus and oxygen molecules in the phosphate group and the O-P-O angle in the tetrahedral phosphate group. These parameters also account for the bond stretching action between the P and O atoms and interatomic van der Waals interaction. In order to find the absolute energy minimum with its corresponding structure of a molecule adsorbed to the surface, the molecules were brought close to the surface manually in different orientations. The position of the adsorbate was optimized for each starting position using Cerius^2.

The charge distribution within the peptide molecules was calculated using the QEq charge equilibration scheme for the neutral peptide molecule. Subsequently, the respective (according to the deprotonation state) number of protons was removed and the corresponding negative charge was adjusted by evenly distributing the charge difference due to deprotonation over the remaining charged molecule. The individual atomic charges from this initial charge distribution were not changed in subsequent adsorption

calculations. This is important because redistributing the charges within a calculation or in between adsorption energy calculations introduces arbitrary fluctuations in the calculated adsorption energies. This approach is justified because none of the reactions discussed in this study involve significant charge transfer. The charges of atoms in the hydroxyapatite are those listed in Table 4.1.

Molecular dynamics simulations at 300 K were performed to avoid trapping the adsorbate in a local energy minimum before and during optimization. These dynamics simulations were performed using a constant *NVE* ensemble. This is the most suitable ensemble for the setup that we used with constant number of atoms (constant *N*), non-periodic system (thus using *V* rather than *P*), and an adiabatic approach (constant E). The structure is allowed to evolve in time, by solving Newton's equation of motion. Every 100 simulation steps, velocities are rescaled if the averaged temperature goes outside a predefined window around the target temperature. The dynamic time step is 0.001 ps, and for each MD run, we run 500 steps (0.5 ps).

As mentioned earlier, RGD and YIGSR have been as cell-adhesion peptides. RGD has a hairpin-like structure in its unfolded state. It is an experimentally well-characterized cell-adhesion peptide [Okamoto et al, 1998]. In this chapter, study of the interaction of RGD and YIGSR on different surface locations on the (001) hydroxyapatite surface was the main objective. One of these surface features is a step in the [010] direction that was created in such a way that charge-neutrality was preserved and the dipole moment of the entire cluster or unit cell minimized.

Two different set-ups were used in calculations involving peptide-HA interactions; a slab with periodic boundary conditions parallel to the slab and a cluster

that is an atomic equivalent of a hexagonal apatite prism. A hexagonal cluster with 380 formula units of hydroxyapatite was created. Peptide interactions with apatite (001) surface steps parallel to [010] and on flat (001) surfaces are studied using both the periodic slab and cluster approach and the respective adsorption energies are compared. Cluster calculations have the advantage of being faster than those using periodic boundary conditions due to the use of a Ewald-summation scheme for the latter.

First, the cluster calculations involving different peptides are described. The hexagonal cluster is terminated by (001) surfaces at the top and bottom. Special care has to be taken to make the cluster stoichiometric, charge neutral, and to avoid a dipole moment perpendicular to any of its surfaces. The cluster is chosen in such a way that there are 76 formula units of $Ca_5(PO_4)_3(OH)$ in the cluster. Different initial positions of the peptide are applied some distance away from the flat terrace of the hexagonal cluster and rhombohedral cluster of the hydroxyapatite. Then, peptide geometry is optimized on the cluster with all atom positions within the cluster being fixed. Finally the calcium ions at the top of the hexagonal cluster are allowed to move during the energy minimization process. This allows us to study the relaxation and movement of calcium ions during the adsorption of peptides on the mineral surface, which mimics dynamic carbonated hydroxyapatite surface in bone.

Subsequently, a surface step parallel to [010] on the hydroxyapatite (001) surface is introduced. This particular step direction was chosen to keep the cluster stoichiometric and charge neutral. A small dipole moment perpendicular to the step is unavoidable in this setup. Peptide adsorption energies can vary with the starting position and orientation of the peptide along the surface steps. This variation in adsorption energy occurs because

each of the peptide has different functional groups at the side chain (of the amino acids present in them). These side chain functional groups interact with the mineral surface atoms differently at different orientation of the peptide alongside mineral surface, because different atoms of the functional groups are exposed to the hydroxyapatite surface atoms in different peptide orientations. Thus we get variable adsorption energies depending upon orientation of the peptide. We start with several different starting positions (described below) for the peptide, and observe their final orientation on the hydroxyapatite surface after energy minimization. For both step and flat surface on cluster, the different starting positions are as follows:

Orientation 1: Peptide backbone is parallel to the [010] direction for both RGD and YIGSR.

Orientation 2: Peptide bond backbone is perpendicular to [010] ([010] step direction) for both RGD and YIGSR.

Orientation 3: (Applicable only to RGD) D (aspartic acid) of RGD is pointing away from surface, parallel to z-axis. Open end of "hairpin" on the surface.

Orientation 4: Initial orientation of the peptide is on the edge of hexagonal cluster. This is applicable for both RGD and YIGSR. Peptides are present at the edge of the hexagonal and rhombohedral flat surface.

Orientation 5: Initial peptide orientation is at the step edge parallel to [010] on the hydroxyapatite (001) surface. This is applicable for both RGD and YIGSR, but the bulk structure is only hexagonal step-edge.

Cluster calculations are compared with periodic boundary condition calculations. The same hydroxyapatite (001) surface is created and periodic boundary conditions are applied during peptide-mineral surface interaction.

Calculation of hydration energies is necessary to estimate the effective adsorption energy of these peptides at different orientations on the hydroxyapatite surface. Both RGD and YIGSR have diverse side chains, and not all functional groups on the amino acid side chains are equally hydrated. MS Modeling 4.1 DMol^3 has been used to calculate the extent of hydration on different fragments of both RGD and YIGSR. Here in the hydration energy calculations, water is used as a homogeneous solvent with a dielectric constant of 78.54, and the contribution of the "Cosmo" hydration energy to the total energy is calculated. "Cosmo" describes the free energy between water molecules and functional groups in peptides. We subtract the hydration energy of the part of the peptides that are both hydrated and on the mineral surface, from its adsorption energy, which gives us the effective hydration energy of the peptide.

Results and Discussions

The results of RGD and YIGSR peptide interactions with hydroxyapatite (010) surface at different surface locations and conditions are discussed in this section. RGD is a small 3-amino-acid peptide residue having a hairpin-like structure at the beginning of calculation. YIGSR is a five amino-acid residue peptide with a more diverse side-chain composition (phenyl group in tyrosine, alkane chain in isoleucine, alcohol in serine, amide in arginine) of the amino-acid residues. This is the cause for different types of interactions with the surface atoms on the hydroxyapatite surface, and orientations of YIGSR vary substantially during adsorption onto the mineral surface. The variation in

final adsorption energies of YIGSR adsorption on hydroxyapatite surface in different surface locations shows the importance of orientation-dependence of peptide during adsorption on mineral surface.

RGD

1) Adsorption energies of RGD on a flat hydroxyapatite (001) face using periodic boundary condition

Here, results from the cluster calculations with periodic boundary conditions are compared. Adsorption of RGD to a flat infinite two-dimensional slab is less favorable compared to adsorption to a cluster. Adsorption energies are low negative values with orientation 2 (RGD perpendicular to [010]) being the most favorable (-2.26 eV). Adsorption energies are listed in Table 4.4.

2) Adsorption of RGD on terrace of hexagonal cluster of hydroxyapatite (001) face

Figure 4.1 shows the adsorption of RGD on the terrace of a hexagonal cluster of the hydroxyapatite (001) face. The adsorption energy is -2.64 eV when the atoms in the cluster are fixed. When the Ca^{2+} ions are allowed to move, they interact with the aspartic acid residue of RGD. The calcium ions are electrostatically attracted to the $–COO^-$ group in aspartic acid, which causes the RGD to move closer to the hexagonal cluster during energy minimization. The Ca^{2+} ions relax parallel to the [010] direction, and they do not distort the lateral symmetry of the cluster during relaxation.

When the cluster is kept fixed during the simulation, adsorption energies have low negative values when the RGD is at the step or near the step edge. However, adsorption energies become highly negative and more favorable for RGD near the step-edge (orientation 4), when the calcium ions at the top-layer of the cluster are allowed to move.

This adsorption site has the most favorable adsorption energy of all surface positions and interactions (-9.45 eV) (Figure 4.1). One important observation that has been made during the interaction of RGD on flat surfaces is that RGD maintains its "hairpin"-like structure during adsorption on the mineral surface.

3) Adsorption energies of RGD on the *step* of a hexagonal cluster of a hydroxyapatite (001) face

A step parallel to [010] direction on the hydroxyapatite (001) surface has been created, and the adsorption of RGD onto the step edge is studied. When the surface is fixed, adsorption is most favorable when the open end of the RGD "hairpin" loop is in contact with the surface. However, when the top layer Ca^{2+} ions are allowed to relax, RGD at the corner of the step edge (orientation 5) is the most favorable position for adsorption. The adsorption energy is then -5.79 eV. Adsorption to the step edge causes distortion of the RGD "hairpin" shape. The hairpin loop opens up during interaction with the hydroxyapatite surface step, and after adsorption, it assumes a vertical position, almost perpendicular to the mineral surface (Figure 4.2). Alteration of the hairpin shape could result in an altered effect on cell-adhesion. Once the hairpin shape is distorted, possibly the effectiveness of the RGD sequence is compromised. The adsorption energies for RGD adsorption to the step edge of a hydroxyapatite (001) surface are listed in table 4.3.

A general interpretation that can be drawn from the RGD-hydroxyapatite interaction are that the difference in energies in static and flexible condition is higher for orientation 3 than orientation 2. That means RGD in its "hairpin" loop position is more likely to become adsorbed onto the hydroxyapatite surface and surface steps. It can be

concluded that the interaction of aspartic acid with calcium ions during energy minimization process for orientation 3 is the reason behind more negative adsorption energies and larger energy differences between static and flexible conditions. In orientation 3, aspartic acid (D) moves closer to the surface whereas the arginine (R) residue moves away from the hydroxyapatite surface during energy minimization. Arginine does not have any strongly electronegative atoms in its side chain. It mostly contains amide groups and alkane carbon chains, which do not favorably interact with calcium ions on the hydroxyapatite surface.

The adsorption energies are more negative when RGD is in a parallel orientation to the [010] as compared with the perpendicular orientation. However, these are the final orientations of RGD along the surface step after adsorption. RGD changes its orientation during adsorption onto the hexagonal cluster surface step of apatite surface parallel to [010].

It can also be inferred that RGD would prefer to bind to the step-edge of the hexagonal cluster rather than flat-terrace. An edge-atom is less-coordinated than a flat terrace-atom which instigates better adsorption of the peptide by virtue of the peptide having more access to the surface atoms of the mineral and causing more electrostatic attraction. Favorable binding of RGD on the hydroxyapatite surface depends on the orientation of the peptide.

Effect of hydration on adsorption energies of RGD on hydroxyapatite: As described in the methods section, we have calculated the hydration energies of the RGD peptide sequentially, considering the extent of hydration on different functional groups. It has to be kept in mind that not all functional groups in the peptide take part in hydration, and

not all of the functional groups are bonded to the mineral surface. The final adsorbate structure on the mineral surface evaluates which functional groups of the peptide are bonded to the mineral surface, and hydration energies of these functional groups have been subtracted from the peptide vacuum adsorption energy to obtain their effective adsorption energies. The alkane side chains in the peptide do not affect the adsorption process substantially, and they are largely un-hydrated. The NH_2- with peptide bond elements are more strongly hydrated than other functional groups (-1.465 eV hydration energy), followed by the amide functional group ($C(NH)=NH\text{-}NH_2$) of arginine (R) (-1.106eV). The COO^- groups have hydration energies of ~ -0.2 eV to -0.5 eV. When the peptide is kept parallel or perpendicular to the [010] direction (orientation 1 and 2), the amide groups and carboxylic groups interact with the mineral surface, allowing the peptide to maintain its "hairpin" position. Only in the case of orientation 3, when the open end of the "hairpin" of RGD is facing away from the hydroxyapatite surface, the hydration effects of the COO^- groups on adsorption are considered and subtracted accordingly from the vacuum adsorption energies to obtain effective adsorption energies. Effective adsorption energies including hydration for RGD are given in table 4.2, 4.3, and 4.4 along with their respective vacuum calculation counterpart.

YIGSR

YIGSR is a longer peptide than RGD, and it has more diverse side-chain amino-acid residues than RGD. YIGSR contains isoleucine, which has an alkane-like carbon-chain side-chain residue, serine, which is a more electronegative side chain containing $–CH_2OH$, and tyrosine, which contains a phenol group. This diversity makes YIGSR an

interesting peptide to study because different functional groups of this peptide may have different interactions with the surface atoms of the hydroxyapatite surface. Calculation with YIGSR is performed using a similar set of starting positions of the peptide as with RGD.

1) Adsorption of YIGSR to a hydroxyapatite (001) face using 2-D periodic boundary conditions

Here also the cluster calculations are compared with calculations on a periodic surface. Adsorption energies vary from -0.88eV to -1.14 eV per residue in static conditions and -1.03 eV to -1.85 eV when Ca^{2+} ions are relaxed. The values are comparable with the flat-hexagonal cluster values, but are significantly less than adsorption energies at the step-edge of the hexagonal cluster. Both cluster and periodic slab has a dipole moment at [010] direction. The results are listed in table 4.7.

2) Adsorption energies of YIGSR to a terrace of a hexagonal cluster of hydroxyapatite (001) face

Figure 4.3 shows the alignment of YIGSR along the hexagonal cluster. The adsorption energies vary with the starting orientation of the peptide, and are more negative when the calcium ions of the top-layer of the hexagonal hydroxyapatite cluster are allowed to move during energy minimization. The Ca^{2+} ions are relaxed along the [010] direction by ~ 0.1 Å from their original position. While interacting with the various functional groups of the peptide, the Ca^{2+} does not disturb the lateral symmetry of the hexagonal cluster. YIGSR unfolds during its interaction with the hydroxyapatite surface

when it has its open end of the hairpin structure on the surface (orientation 3). The results are listed in table 4.5.

3) Adsorption of YIGSR to a [010] *step* of a hexagonal cluster of a hydroxyapatite (001) face

We observe that the adsorption energies are more negative when the orientation of the YIGSR peptide is along the step-edge or near the step-edge parallel to [010] on a hydroxyapatite (001) surface compared to adsorption of YIGSR to a flat terrace of the (010) surface of a hexagonal cluster. The adsorption is most favorable when YIGSR is at the corner of step-edge (orientation 5) (Figure 4.4). Adsorption energies are listed in table 4.6.

An interesting aspect of YIGSR interaction with the hydroxyapatite surface is the stretching of the YIGSR peptide during energy minimization and adsorption. The starting orientation of the 5-residue amino acid is in a folded state. When the peptide starts interacting with the hexagonal hydroxyapatite cluster, different functional groups ($-CH_2OH$, phenyl group, isopropyl group, and amide group) interact differently with the surface atoms. Phenyl groups interact through the sharing of the electron cloud, whereas alcohol and amide groups exert more direct electrostatic interactions. Isopropyl groups interact mainly through van-der-Waals interactions. This causes the stretching out of the peptide from folded state during adsorption.

As observed with RGD, the arginine residue moves away from the surface of hydroxyapatite. It is also observed that the calcium ions migrate up from the hydroxyapatite (001) surface of the hexagonal cluster when the top layer of the surface is

relaxed during interaction with YIGSR. The migration of the calcium ions are towards the functional groups with more electronegative atoms in the peptide sequence, namely serine (S), and tyrosine (Y).

Effect of hydration on adsorption energies of YIGSR on hydroxyapatite: At the end of the RGD section, the effect of hydration energies on the adsorption of that peptide on mineral surface has been mentioned. Similar approach has been taken determining the effect of hydration of various functional groups present in YIGSR, on its adsorption on hydroxyapatite surface. YIGSR is longer than RGD and it has more versatile functional groups in its side chain than RGD. YIGSR has an alkyl side chain in isoleucine, and H atom in glycine, which has minimal hydration effect during interaction with mineral surface. The phenol group of tyrosine (Y) has hydration energy of -0.46 eV, and the CH_2-OH group of serine (S) has hydration energy of -0.756 eV. These groups (phenol and alcohol) come close to the surface when YIGSR is at the edge of hydroxyapatite surface (orientation 5). NH_2- with peptide bond and amide group of arginine (R) has the most negative hydration energies (-1.23 eV and -0.86 eV respectively), and they also interact with the hydroxyapatite surface atoms more than the other functional groups on (especially for orientation 3). We subtract the amide group and amines hydration energies from the vacuum adsorption energies of YIGSR to obtain effective adsorption energies. The results are listed in table 4.5, 4.6, and 4.7.

Conclusions

From our molecular modeling study of cell-adhesion peptides on hydroxyapatite surface, we can infer that the adsorption of cell adhesion peptides on hydroxyapatite surfaces depends significantly on the orientation of the peptide with respect to the

hydroxyapatite surface. Understandably, the energy is higher when the peptide is at the step edge or edge of the surface, as compared with the flat terrace. Adsorption energies are higher when the top Ca^{2+} layer of hydroxyapatite cluster is allowed to move, and the initial position of the peptide is at the edge of the cluster. The effective electrostatic interaction between peptide and mineral surface atoms is higher near the edge. This can help us to decide that during bone regeneration, the BSP will facilitate adsorption on the mineral surface when the surface is relaxed, and will influence growth at step edge. This is relevant considering the fact that carbonated hydroxyapatite provides a dynamic system in bone-regeneration, and the mineral surface is likely to be at relaxed-state during interaction with proteins during bone-regeneration. Only the top Ca^{2+} layer of the hydroxyapatite surface is relaxed during the study, but one can testify the relaxation of the first 3-4 layers of the hydroxyapatite surface, though it will be computationally expensive. The relaxation of Ca^{2+} ions take place in longitudinal ([010]) direction. Due to the relaxation, the lateral symmetry of the hexagonal cluster or periodic slab is not distorted.

Similar trends have been observed in adsorption energies for both RGD and YIGSR on the hydroxyapatite cluster set-up. When we compare cluster results with periodic boundary conditions, it is found that the step edge energies are less favorable (less negative) for adsorption than flat surface initial position of the peptide in periodic boundary condition. This difference in adsorption energies between cluster and periodic boundary condition set up is more prominent when the mineral surface is relaxed, compared to the all static surface. This also helps us to conclude that the adsorption of

peptides on mineral surface during bone regeneration is favorable under dynamic and relaxed condition of the hydroxyapatite surface.

In this chapter, the RGD and YIGSR interactions with hydroxyapatite surface is studied as a model of bioactive surface interaction with biomaterials during cell-adhesion mechanism. This cell adhesion mechanism triggers cellular events which finally causes bone-tissue regeneration. That is why understanding the molecular level interaction between peptides on biomaterial (hydroxyapatite in this case) surface is the stepping stone for understanding cell adhesion mechanism in bone-tissue engineering. RGD and YIGSR are small peptides, which are representatives of the bioactive surfaces like cell-synthesized or extracellular proteins. One can look into other different set of bioactive surface peptides to have better understanding of basic mechanism required for tissue engineering.

Our current forcefield has interaction terms for various non-bonding van-der-Waals interactions, thus accommodating a wide range of interactions during our study. Universal Force Field was used to simulate interactions within the organic molecule. The interaction between organic molecules (peptide in this case) and the mineral surface is monitored by the HYDROXYAPATITE forcefield. The use of the HYDROXYAPATITE force field can be extended to future studies involving organic-apatite interaction. Human bone contains 4-6 wt% of carbonate ions in the hydroxyapatite, which is about 1 CO_3^{2-} ions per unit cell of hydroxyapatite. Carbonate ions have flat trigonal planar structure, unlike the tetrahedral phosphate ions, which they will replace in the hydroxyapatite structure in carbonated apatite. This means the peptides, as an adsorbate, will interact with larger surface area of the mineral, and facilitate more mobility in the mineral

surface. The modeling of carbonated hydroxyapatite and the adsorption energies of cell-adhesion peptides on carbonated hydroxyapatite surface in aqueous environment will give us additional understanding of the exact mechanism of bone growth involving mineral-peptide interactions. In this chapter we have seen that conditions for bioactive surface formation are favorable under relaxed hydroxyapatite surface with mobile-Ca^{2+} ions. Carbonated hydroxyapatite is also a dynamic and relaxed mineral surface, which will favor bioactive surface formation necessary for bone-tissue regeneration.

The major concern for building a carbonated hydroxyapatite model using Cerius^2 is proper positioning of the carbonate group in the unit cell of the hydroxyapatite crystal. There can be one CO_3^{2-} per unit cell in the carbonated hydroxyapatite which will break the 3-fold symmetry of the crystal, or there can be a spiral arrangement of hydroxyapatite units in c direction where one OH^- will be replaced by CO_3^{2-}. The charge balance has to be maintained in the hydroxyapatite crystal as well during carbonate substitution. One CO_3^{2-} ion can be inserted in the unit cell replacing OH^-, and to balance the charge a Ca^{2+} ion can be replaced with H^+. The replacement of PO_4^{3-} by CO_3^{2-} is also possible, and can generate most energetically favorable model. Modelling study with all these various types of structural possibilities will help us to determine the most stable configuration of the carbonated hydroxyapatite surface, on which we can study the interactions of cell-adhesion peptides, to better understand the bioactive-surface biomaterial interaction prior to bone-tissue engineering.

Table 4.1: Potential parameters for APATITE forcefield

O-O	Buckingham [1]	*inter*molecular; < 14 **Å**	A = 54459.74 eV	ρ = 0.213 Å	C = 3.47 eV/ Å^6
O-O(H)	Buckingham	intramolecular < 14 **Å**	A = 347464.33 eV	ρ = 0.213 Å	C = 3.47 eV/ Å^6
Ca-O(H)	Buckingham [1]	intra*molecular;* < 14 **Å**	A = 685.92 eV	ρ = 0.344 Å	C = 0 eV/ Å^6
Ca-O	Buckingham [1]	intra*molecular;* < 14 **Å**	A = 1544.03 eV	ρ = 0.297 Å	C = 0 eV/ Å^6
O-P	Morse[2]	*intra*molecular	D = 1.5799 eV	r_0 = 2.03 Å	K_b = 1.625 eV/ Å^2
O(H)-H	Morse[2]	*intra*molecular	D = 7.1757 eV	r_0 = 3.18 Å	K_b = 1.199 eV/ Å^2
O-P-O angle	Three-body[3]	*intra*molecular	K_0= 8.043 eV/rad^2	θ_0=109.47°	
charges	P = +1.6927	O(Phosphate) = -1.0448	Ca = +1.6647	O(Hydroxide) = -1.8647	H = + 1.0000

[1]Buckingham: A exp (-r/ρ) - C r $^{-6}$ C in eV Å^6

[2]Morse: D [(1 - exp {-a(r-r_o)})^2 - 1] a = (K_b/2D)$^{1/2}$

[3]Three-body: E = K_0 (θ-θ_0)^2

Table 4.2: Adsorption energies of RGD on terrace of hexagonal cluster of hydroxyapatite (001) face:

Peptide orientation on hydroxyapatite (001) surface	**static hydroxyapatite (001) surface $E_{adsorption}$ (eV) (E_1)**	**Hydration energy of the relevant functional group (eV) (E_2)**	**Effectie adsorption energy $E_{adsorption}$ (eV) (E_{-1}-E_2)**	**hydroxyapatite (001) surface with top Ca^{2+} layer flexible $E_{adsorption}$ (eV) (E_1)**	**Hydration energy of the relevant functional group (eV) (E_2)**	**Effectie adsorption energy $E_{adsorption}$ (eV) (E_{-1}-E_2)**
RGD parallel to Y-axis **(Orientation 1)**	-4.59	-1.95	-2.64	-6.15	-1.95	-4.20
RGD perpendicular to Y-axis **(Orientation 2)**	-5.01	-1.95	-3.06	-6.57	-1.95	-4.62
RGD with open end of "hairpin" on the surface **(Orientation 3)**	-4.2	-1.66	-2.54	-5.19	-1.66	-3.53
RGD at the edge of the cluster **(Orientation 4)**	-5.28	-1.62	-3.66	-11.07	-1.62	-9.45

Table 4.3: Adsorption energies of RGD on the *step* of hexagonal cluster of hydroxyapatite (001) face

Peptide orientation on hydroxyapatite (001) surface	**static hydroxyapatite (001) surface $E_{adsorption}$ (eV) (E_1)**	**Hydration energy of the relevant functional group (eV) (E_2)**	**Effectie adsorption energy $E_{adsorption}$ (eV) (E_1-E_2)**	**hydroxyapatite (001) surface with top Ca^{2+} layer flexible $E_{adsorption}$ (eV) (E_1)**	**Hydration energy of the relevant functional group (eV) (E_2)**	**Effectie adsorption energy $E_{adsorption}$ (eV) (E_1-E_2)**
RGD parallel to Y-axis **(Orientation 1)**	-6.36	-1.95	-4.41	-5.04	-1.95	-3.09
RGD perpendicular to Y-axis**(Orientation 1)**	-5.91	-1.95	-3.96	-3.84	-1.95	-1.89
RGD with open end of "hairpin" on the surface **(Orientation 3)**	-6.39	-1.66	-4.73	-5.97	-1.66	-4.31
RGD at the edge of the cluster **(Orientation 5)**	-5.04	-1.62	-3.42	-7.41	-1.62	-5.79

Table 4.4: Adsorption energies of RGD on hydroxyapatite (001) face under Periodic Boundary Condition

Peptide orientation on hydroxyapatite (001) surface	**static hydroxyapatite (001) surface $E_{adsorption}$ (eV) (E_1)**	**Hydration energy of the relevant functional group (eV) (E_2)**	**Effectie adsorption energy $E_{adsorption}$ (eV) (E_1-E_2)**	**hydroxyapatite (001) surface with top Ca^{2+} layer flexible $E_{adsorption}$ (eV) (E_1)**	**Hydration energy of the relevant functional group (eV) (E_2)**	**Effectie adsorption energy $E_{adsorption}$ (eV) (E_1-E_2)**
RGD parallel to Y-axis **(Orientation 1)**	-1.71	-1.44	-0.27	-3.27	-1.44	1.83
RGD perpendicular to Y-axis**(Orientation 2)**	-3.03	-1.44	-1.59	-3.66	-1.44	-2.22
RGD with open end of "hairpin" on the surface**(Orientation 3)**	-1.11	-0.85	-0.26	-1.11	-0.85	-0.26
RGD at the edge of the cluster**(Orientation 4)**	-2.04	-1.62	-0.42	-2.04	-1.62	-0.42

Table 4.5: Adsorption energies of YIGSR on terrace of hexagonal cluster hydroxyapatite (001) face:

Peptide orientation on fixed hydroxyapatite (001) surface	**static hydroxyapatite (001) surface $E_{adsorption}$ (eV) (E_1)**	**Hydration energy of the relevant functional group (eV) (E_2)**	**Effectie adsorption energy $E_{adsorption}$ (eV) (E_{-1}-E_2)**	**hydroxyapatite (001) surface with top Ca^{2+} layer flexible $E_{adsorption}$ (eV) (E_1)**	**Hydration energy of the relevant functional group (eV) (E_2)**	**Effectie adsorption energy $E_{adsorption}$ (eV) (E_{-1}-E_2)**
YIGSR parallel to Y-axis **(Orientation 1)**	-1.80	-1.69	-0.11	-3.4	-1.69	-1.71
YIGSR perpendicular to Y-axis**(Orientation 2)**	-6.85	-1.35	-5.5	-3.4	-1.35	-2.05
YIGSR with open end of "hairpin" on the surface **(Orientation 3)**	-7.3	-2.1	-5.2	-21.9	-2.96	-18.94
YIGSR at the edge of the cluster**(Orientation 4)**	-2.05	-1.63	-1.52	-2.35	-1.63	-0.72

Table 4.6: Adsorption energies of YIGSR on the *step* of hexagonal cluster of hydroxyapatite (001) face

Peptide orientation on fixed hydroxyapatite (001) surface	**static hydroxyapatite (001) surface $E_{adsorption}$ (eV) (E_1)**	**Hydration energy of the relevant functional group (eV) (E_2)**	**Effectie adsorption energy $E_{adsorption}$ (eV) (E_{-1}-E_2)**	**hydroxyapatite (001) surface with top Ca^{2+} layer flexible $E_{adsorption}$ (eV) (E_1)**	**Hydration energy of the relevant functional group (eV) (E_2)**	**Effectie adsorption energy $E_{adsorption}$ (eV) (E_{-1}-E_2)**
YIGSR parallel to Y-axis **(Orientation 1)**	-6.19	-1.69	-4.5	-7.8	-1.69	-6.11
YIGSR perpendicular to Y-axis**(Orientation 2)**	-5.00	-1.35	-3.65	-14.2	-1.35	-12.85
YIGSR with open end of "hairpin" on the surface **(Orientation 3)**	-6.65	-2.1	-4.55	-13.9	-2.96	-10.94
YIGSR at the edge of the cluster**(Orientation 4)**	-10.05	-1.63	-8.42	-18.15	-1.63	-16.52

4.7: Adsorption energies of YIGSR on hydroxyapatite (001) face using periodic boundary conditions

Peptide orientation on fixed hydroxyapatite (001) surface	**static hydroxy-apatite (001) surface $E_{adsorption}$ (eV) (E_1)**	**Hydration energy of the relevant functional group (eV) (E_2)**	**Effectie adsorption energy $E_{adsorption}$ (eV) (E_{-1}-E_2)**	**hydroxyapatite (001) surface with top Ca^{2+} layer flexible $E_{adsorption}$ (eV) (E_1)**	**Hydration energy of the relevant functional group (eV) (E_2)**	**Effective adsorption energy $E_{adsorption}$ (eV) (E_{-1}-E_2)**
YIGSR parallel to Y-axis **(Orientation 1)**	-4.4	-2.1	-2.30	-5.15	-2.1	-3.05
YIGSR perpendicular to Y-axis**(Orientation 2)**	-5.75	-.99	-4.76	-9.25	-0.99	-8.96
YIGSR with open end of "hairpin" on the surface **(Orientation 3)**	-5.70	-2.1	-3.60	-8.95	-2.1	-6.85
YIGSR at the edge of the cluster**(Orientation 4)**	-5.1	-1.23	-3.87	-5.15	-1.23	-3.92

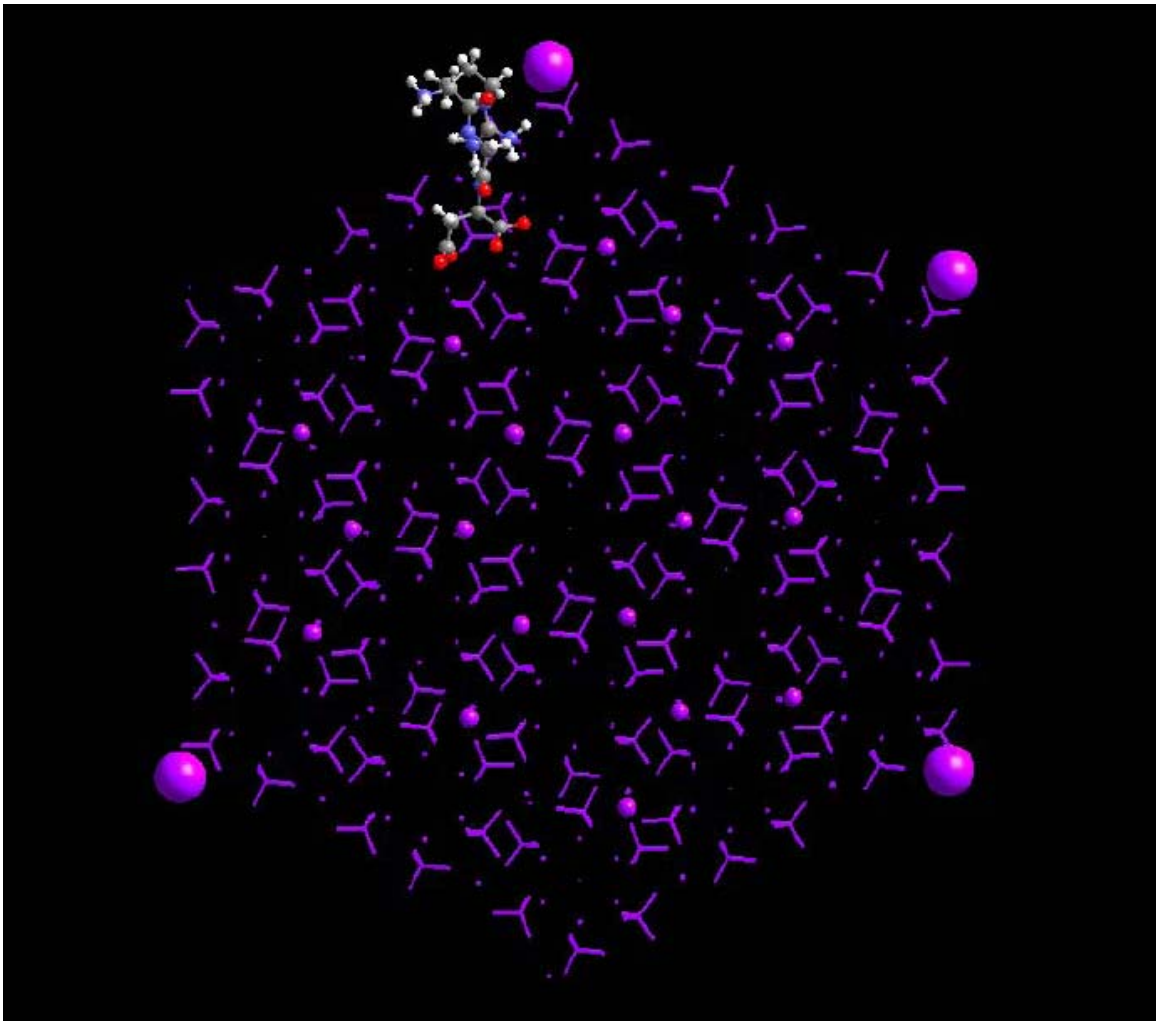

Figure 4.1. RGD at the edge of hexagonal cluster of hydroxyapatite (001) surface. The hydroxyapatite cluster is static.

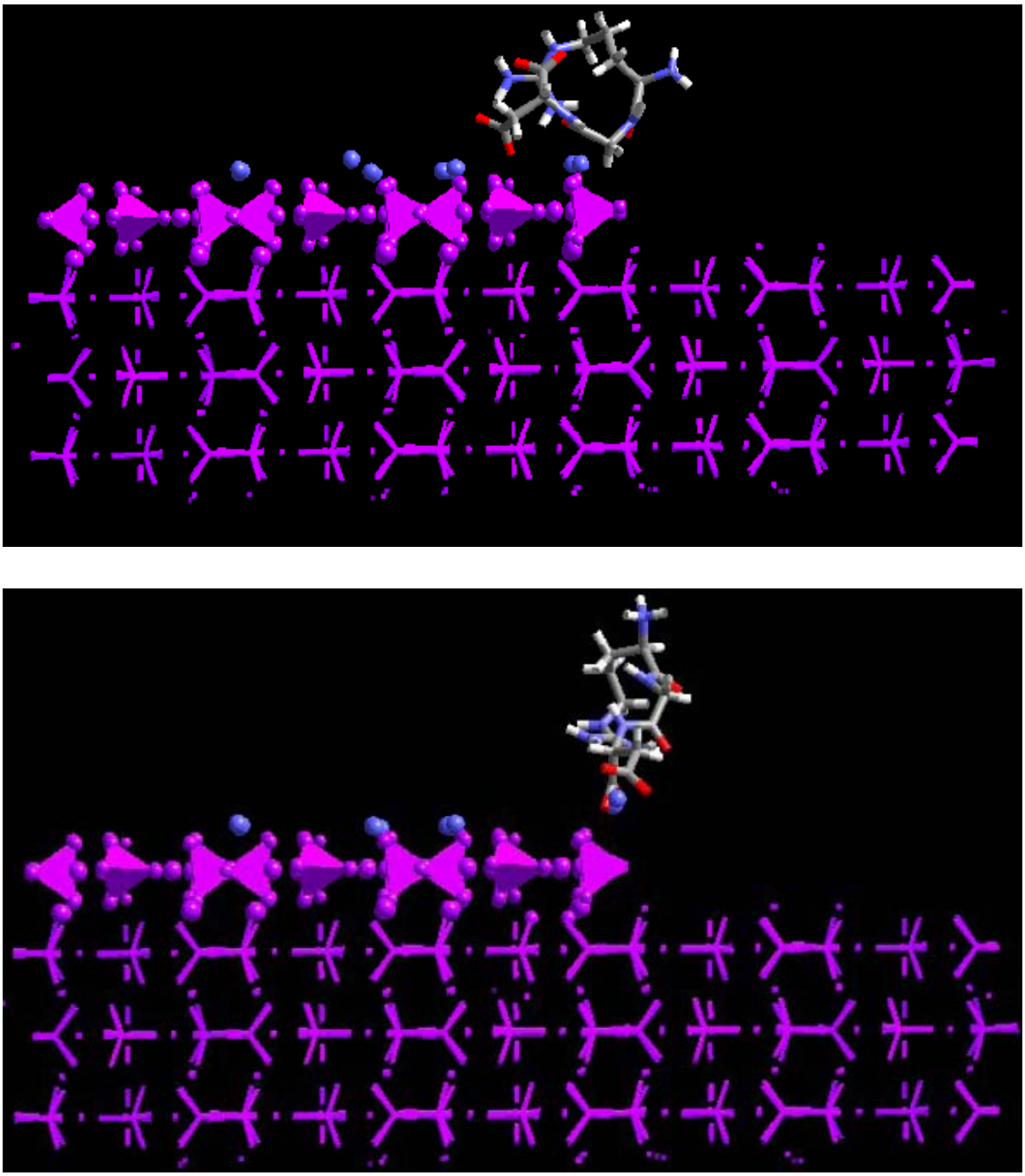

Figure 4.2. RGD at the step edge of the step direction parallel to [0 1 0] on hydroxyapatite (001) surface. The top Ca^{2+} layer is allowed to move during adsorption. RGD opens up its hairpin loop structure and takes a vertical position, almost perpendicular to the mineral surface. The top figure shows the initial starting position; the bottom figure shows final orientation after energy minimization.

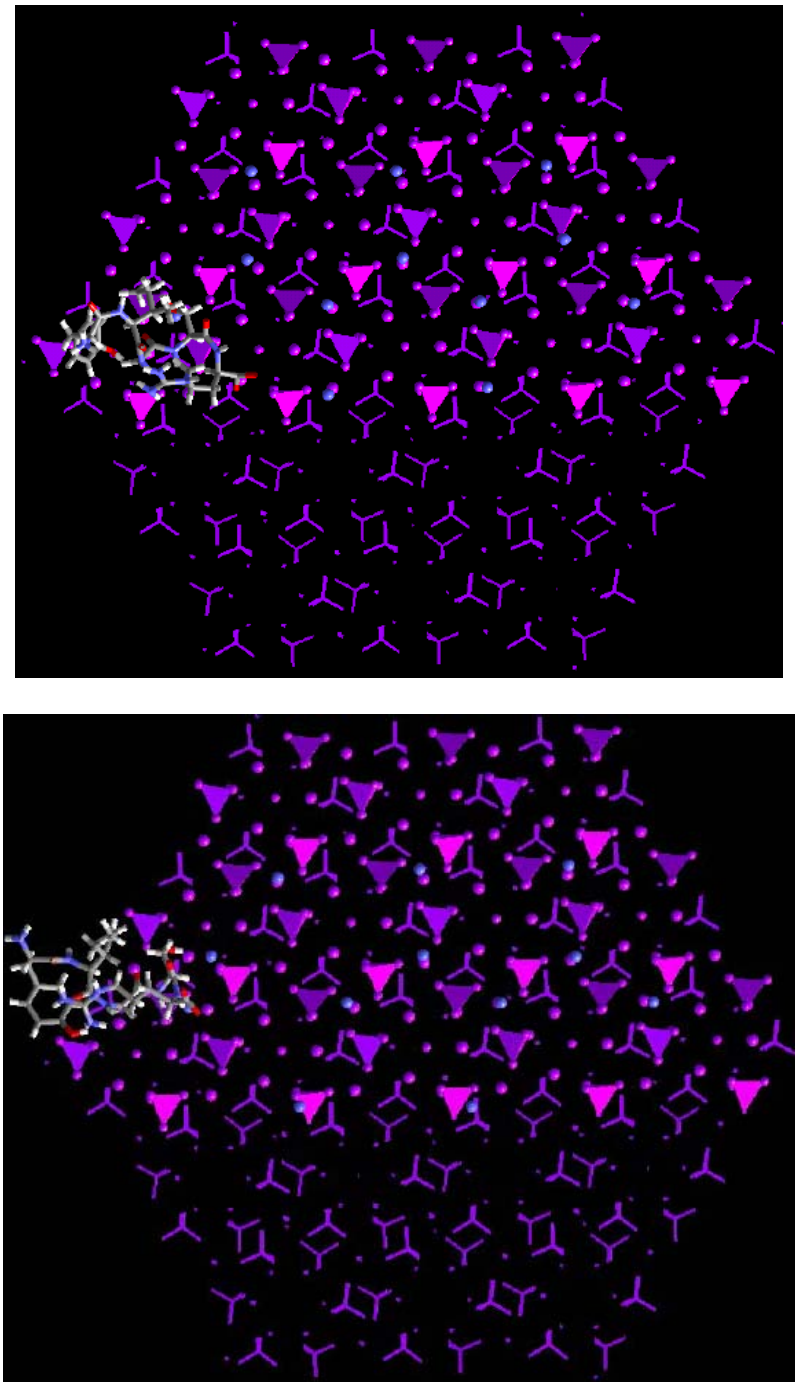

Figure 4.3. YIGSR on the step edge corner of step parallel to [0 1 0] on hydroxyapatite (001) surface. The adsorption condition is most favorable among all other interactions with YIGSR. YIGSR opens up its folded orientation during the interaction. The top layer of Ca^{2+} ion on the mineral surface is allowed to move. The top figure shows the initial starting position; the bottom figure shows final orientation after energy minimization

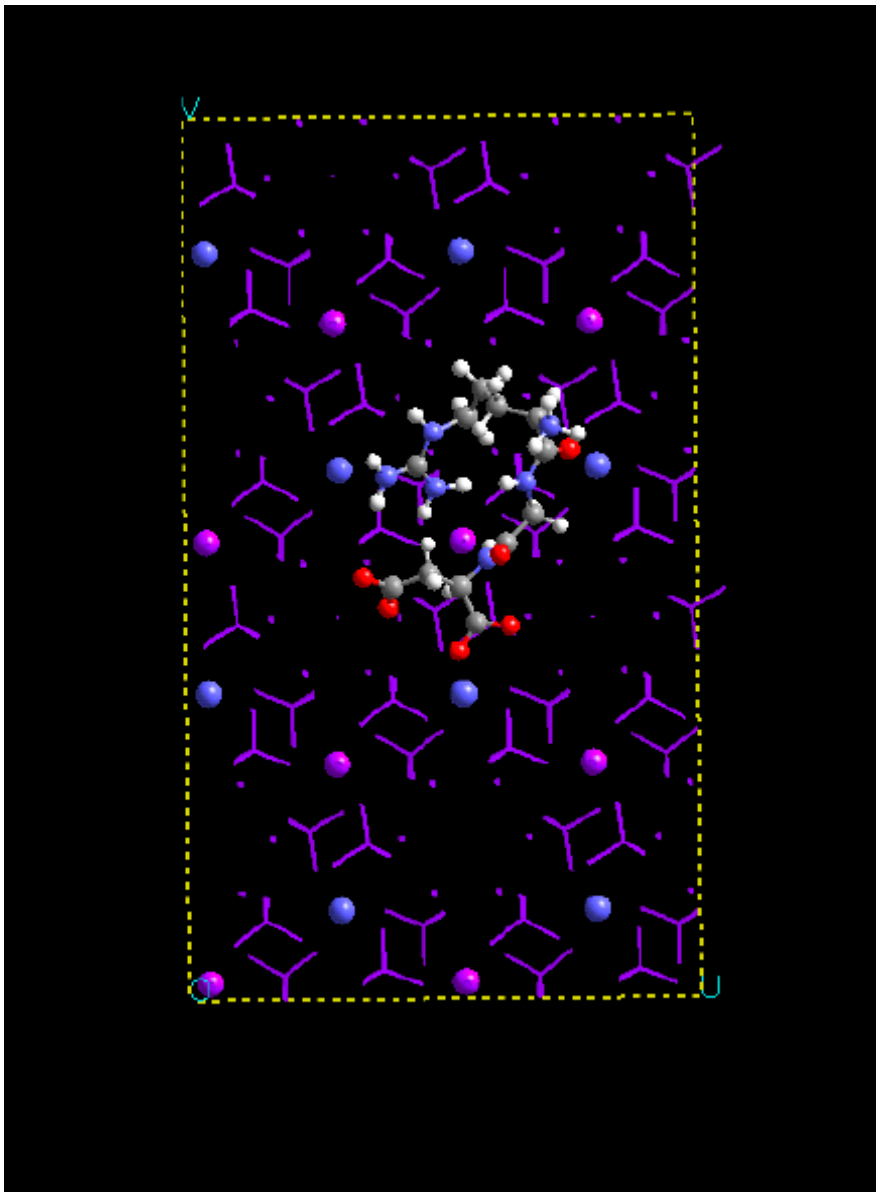

Figure 4.4. YIGSR adsorption on hydroxyapatite (001) surface under periodic boundary condition. The peptide is perpendicular to the Y axis, and the adsorption energy is most favorable among all the adsorption energies with PBC.

References

Astala R, Stott MJ: **First principle investigation of mineral component of bone: CO_3 substitution in hydroxyapatite.** *Chemistry of Materials* 2005, **17:**4125-4133

Becker U, Biswas S, Kendall T, Risthaus P, Putnis CV, Pina CM: **Interactions between mineral surfaces and dissolved species: From monovalent ions to complex organic molecules**. *American Journal of Science* 2005 **305**: 791-825

Boiziau C, Leroy S, Reynaud C, Lecayon G, Le Gressus C, Viel P: **Elementary Mechanisms in the Interaction of Organic Molecules with Mineral Surfaces**. *Journal of Adhesion* 1987 **23**:21-44

Burg KJ, Porter S, Kellam JF: **Biomaterial developments for bone tissue engineering.** *Biomaterials.* 2000 **21**:2347-2359

de Leeuw NH, Matter S: **A computer modeling study of the uptake and segregation of fluoride ions at the hydrated hydroxyapatite (0001) surface: introducing a $Ca_{10}(PO4)_6(OH)_2$ potential model**. *Physics of Chemistry and Chemistry of Physics* 2004 **6**:1860-1866.

Elliott JC, Mackie PE, Young RA: **Monoclinic Hydroxyapatite.** *Science* 1973, **180:** 1055-1057

Frayssinet P , Rouquet N , Fages J, Durand M , Vidalain PO , Bonel G: **The influence of sintering temperature on the proliferation of fibroblastic cells in contact with HA-bioceramics**. *Journal of Biomedical Materials Research* 1998, **35**: 337-347

Gilbert M, Shaw WJ, Long JR, Nelson K, Drobny GP, Giachelli CM, Stayton PS: **Chimeric Peptides of Statherin and Osteopontin That Bind Hydroxyapatite and Mediate Cell Adhesion**. *Journal of Biological Chemistry* 2000, **275**:16213-16218

Julien M, Khairoun I, LeGeros RZ, Delplace S, Pilet P, Weiss P, Daculsi G, Bouler JM, Guicheux J: **Physico-chemical–mechanical and in vitro biological properties of calcium phosphate cements with doped amorphous calcium phosphates.** *Biomaterials,* 2007, **28**: 956-965.

Linhart W, Peters F, Lehmann W, Schwarz K , Schilling AF , Amling M, Rueger JM, Epple M: **Biologically and chemically optimized composites of carbonated apatite and polyglycolide as bone substitution materials**. *Journal of Biomedical Materials Research* 2000, **54**: 162-171

Mkhonto D, de Leeuw N: **A computer modelling study of the effect of water on the surface structure and morphology of fluorapatite: introducing a $Ca_{10}(PO_4)_6F_2$ potential model**. *Journal of Material Chemistry* 2000, **12**:2633-2642

Morgan H, Wilson RM, Elliott JC, Dowker SEP, Anderson P: **Preparation and characterisation of monoclinic hydroxyapatite and its precipitated carbonate apatite intermediate.** *Biomaterials* 2000, **21:**617-627

Okamoto K, Matsuura T, Hosokawa R, Akagawa Y: **RGD peptides regulate the specific adhesion scheme of osteoblasts to hydroxyapatite but not to titanium**. *Journal of Dental Research* 1998, **77**:481-487.

Petite H, Viateau V, Bensaïd W, Meunier A, de Pollak C, Bourguignon M, Oudina K, Sedel L, Guillemin G: **Tissue-engineered bone regeneration**. *Nature Biotechnology* 2000, **18**, 959 – 963

Rappe AK, Goddard III WA: **Charge equilibration for molecular dynamics simulation.** *Journal of Physical Chemistry* 1991, **95**:3358-3363.

Rezwan K, Chen QZ, Blaker JJ, Boccaccini AR: **Biodegradable and bioactive porous polymer/inorganic composite scaffolds for bone tissue engineering.** *Biomaterials* 2006 **27:** 3413-3431

Rodriguez H, Fraga R: **Phosphate solubilizing bacteria and their role in plant growth promotion.** *Biotechnology Advances* 1999, **17**:319-339

Sun JS, Lin FH, Hung TY, Tsuang YH, Chang WSH, Liu HC: **The influence of hydroxyapatite particles on osteoclast cell activities**. *Journal of Biomedical Materials Research* 1999, **45**:311-321

Wierzbicki A, Cheung HS: **Molecular modeling of inhibition of hydroxyapatite by phosphocitrate**. *Journal of Molecular Structure (TheoChem)* 2000, **529**: 73-82

Woo KM, Seo J, Zhang R, Ma PX: **Suppression of apoptosis by enhanced protein adsorption on polymer/hydroxyapatite composite scaffolds.** *Biomaterials* 2007, **28:**2622-2630

Yarlagadda PKDV, Chandrasekharan M, Shyan JYM: **Recent advances and current developments in tissue scaffolding**. *Bio-Medical Materials and Engineering* 2005 **15**:159-177

Chapter 5

Co-adsorption of $As(OH)_3$ and different oxidation galena (100) surfaces

Introduction

Arsenic is being used for a variety of medicinal applications, such as in cancer therapy [Waxman et al, 2001], in dermatology [Schwartz, 1997], and in the treatment of acute leukemia [Perkins et al, 2000]. Arsenic is known for its carcinogenic effect [Thomas et al, 2001]. Arsenic mobility in groundwater spreads arsenic contamination in many areas in the world [Harvey et al, 2002]. This has made arsenic an important subject for research and exploration.

The worst arsenic catastrophe occurred in Bangladesh, where 35 million people were exposed to As levels above the US EPA standard [Harvey et al, 2002]. Arsenic mobilization from aquatic sediments is an environmental problem because waterborne arsenic can migrate into pristine areas, endangering aquatic organisms and people. As (III) is more soluble and mobile in solution than As (V). As (III) is also more toxic than its oxidized counterpart. The most common natural As (III) species in groundwater is As

$(OH)_3$. To minimize the concentration of As in groundwater, it is necessary that $As(OH)_3$ gets adsorbed on mineral surfaces and subsequently oxidized while oxidation in solution is often kinetically hindered. In this respect, it is important to know what the redox mechanisms are that transform arsenic from one oxidation state to another because these redox processes often control the mobility of this hazardous element. It has been found that the initial process of arsenic oxidation on niccolite (NiAs) may involve the reduction of adsorbed atomic oxygen radicals and the production of As $(OH)_3$ surface species [Nesbitt et al, 1999]. If co-adsorption of $As(OH)_3$ and oxidizing agents such as oxygen or ferric iron occurs on conducting or semiconducting mineral surfaces, long-range (atomic scale) electronic proximity effects may play a role [Becker et al., 2001; Rosso and Becker, 2003]. In such proximity effects, the chemical reaction of one surface site influences the electronic structure and reactivity of neighboring or nearby sites by spin polarization and electron/charge transfer over distances of up to tens of angstroms, thereby inducing the mobility or adsorption of another species on the surface some distance away. For the case of NiAs or FeAsS (arsenopyrite) oxidation, electron transfer may not only take place from As atoms that are directly bonded to the adsorbing atomic O. Electrons may travel over some distance through the arsenide to the oxidized As that gets hydrated. Bacteria can also be electron donating species, e.g., Shewanella alga BrY provides the electron for the reduction of Fe (III) to Fe (II) in As containing Fe (oxy-) hydroxides [Cummings et al, 1999]. Subsequently, the electron can be transferred to reduce As (V), and arsenic is released from the surface to solution.

Several studies have addressed the release of As (III) into solution [Nickson et al, 2000, Dixit et al, 2003] because As (III) is more soluble and mobile in solution than As

(V). As(III) is also more toxic than its oxidized counterpart. Thus, it may be helpful to understand the redox chemistry between As(III) and As(V), and how electron transfer may be mediated by different mineral surfaces. In this context, it is instructive to study the adsorption mechanism of $As(OH)_3$ to mineral surfaces. As(V) is adsorbed strongly in an oxidized environment to Fe and Al oxides and hydroxides [Waychunas et al, 1993]. As(III) is adsorbed weakly in anaerobic conditions by (a) reductive dissolution of iron minerals [Manning et al, 1998]; (b) weak retention of As(III) on Al–hydroxides and silicates [Anderson et al, 1976]

Adsorption of arsenite, As(III), has been studied on galena and sphalerite surfaces to address the problem of As release in solution by reductive dissolution [Bostick et al, 2003]. This study on the pH dependence showed that significant adsorption of As(III) takes place at neutral to alkaline pH (7-9) on both minerals, which may be due to the fact that $As(OH)_3$ has a pK_a value 9.3 .With increasing ionic strength, the adsorption of As(III) on both surfaces, PbS and ZnS, increases. Surfaces of these sulfides are negatively charged above pH 3, thus they do not form electrostatic bond with neutral or anionic As(III) species [Bostick et al, 2003].

The As-S bond distances of As(III) adsorbed to PbS and ZnS are longer than bond distances in orpiment (As_2S_3). The proposed mechanism suggests the formation of small As-S polymers with $As_3S_3(SH)_3$ structure. Here, the As-S bond length is 2.25 Å [Bostick et al, 2003].

These previous studies show that As(III) gets adsorbed to PbS and ZnS surfaces and physical properties like pH, ionic strength, and the addition of sulfide play a major role in its adsorption behavior. This study [Bostick et al, 2003] also shows that the

adsorption of As(III) species on PbS surface is a complex process. It does not happen through conventional ligand exchange mechanism or chemical bond formations. The formal oxidation state of the As(III) remains unchanged during adsorption. The adsorption of As(III) on galena surface increase with pH , but any inner-sphere complex formed on surface is relatively labile. Thus the question arises about the exact phenomenon/mechanism of As(III) adsorption on sulfide mineral surfaces, PbS in this case. One approach through which the surface complexation or adsorption of As(III) on PbS can takes place is surface proximity effects. Hematite, pyrite, and galena surfaces are investigated by researchers through STM, ab-initio calculations [Becker et al, 1996, Becker et al, 1997]. The findings of those studies evaluate how to combine surface complexation theory and proximity effect theory for the case of oxidation of PbS by Fe(III) and water [Becker et al, 2001]. Influenced by these studies, a quantum-mechanical approach was chosen to study electron transfer between redox couples through a mineral surface to investigate the long-range interaction of As $(OH)_3$ through a galena (100) surface with different oxidants.

The Proximity Effect: When the chemical reaction of one surface site influences the electronic structure and reactivity of neighboring or nearby sites by spin polarization and electron /charge exchange, and induces mobility or adsorption of another species on the surface in another surface site, it is called the proximity effect. The surface proximity effect can be manifested in different ways, although the principle is the same. For example, electron transfer in redox reactions on galena surfaces can electrically connect spatially separated adsorption sites or adsorption sites with specific surface sites (vacancies, kinks etc.) some distance away from the adsorption site. One such example is

described for pyrite where the oxidation of one site on a terrace influences next-nearest neighbor sites, making them far more susceptible to oxidative attack than sites further away [Becker et al, 2001].

Examples of proximity effect: Naturally-occurring and relatively abundant minerals such as hematite (Fe_2O_3), pyrite (FeS_2), and galena (PbS), are good candidates for studying proximity effects due to their semiconducting nature. Hematite influences transition metal mobility in many soils and pyrite and pyrrhotite often act as key components in acid mine runoff.

In the oxidation of galena via interaction with ferric iron and water, Fe^{3+} acts as the oxidizing agent (electron acceptor); water promotes this reaction and supplies the oxygen necessary to produce sulfate. It has been shown that ferric iron and the water molecule do not have to be bonded to the same surface atom [Becker et al, 2001]. The same analogy has been followed in the study of co-adsorption of $As(OH)_3$ and oxidizing species on galena surface. As mentioned earlier, finding a suitable mechanism for As(III) adsorption on galena surface is the main purpose of the study in this chapter. Though the exact adsorption mechanism of As(III) on galena surface is not known, the knowledge for possible mechanisms of As(III)-species adsorption on galena surface is known. [Becker et al, 2001] has shown the mechanistic approach for oxidation of a semiconducting mineral surface like galena via proximity effect. Similar path is followed in this study to address possible $As(OH)_3$ adsorption on galena.

The main purpose of this proximity effect study is to analyze the influence of different oxidizing species on the adsorption and potential oxidation of $As(OH)_3$ on a galena surface. Hereby, the oxidants do not react directly with $As(OH)_3$ but electron

transfer takes place over some distance. An interesting side effect of this system is that PbS is a reducing mineral by itself; however, with an oxidant adsorbed, it acts more like an electron shuttling compound, and thus, the system oxidant-galena may act as an oxidizing system. The oxidants used in this study are oxygen (elemental and molecular) and Fe(III). Fe can be low-spin or high-spin with 5 or 1 unpaired spins, respectively. Both cases were investigated to see how spin multiplicity affects the proximity effect. The starting position of the oxidizing species and adsorbate around the cluster have been varied : (i) both oxidant and $As(OH)_3$ on the same terrace of the cluster, (ii) Fe(III) at the corner and $As(OH)_3$ on the terrace of the cluster and (iii) both Fe(III) and $As(OH)_3$ on opposite corners of the cluster.

Methods:

Inorganic redox processes discussed in this chapter occurs via electron transfer. So all the calculations done in this study involves ab-initio or quantum mechanical approach. All calculations on galena were performed on a 4×4×2-atom Pb cluster (16 Pb and 16 S atoms) using both Hartree-Fock and a hybrid HF-DFT (B3LYP) approach incorporated in the computer program package Gaussian03. Hartree-Fock (HF) is an approximate method for the determination of the ground-state wave-function and ground-state energy of a quantum many-body system. It is typically used to solve the time-independent Schrödinger equation for a multi-electron atom or molecule as described in the Born-Oppenheimer approximation. Hartree Fock neglects electron correlation, which is important to include in order to evaluate proximity effects quantitatively, because the electron transfer between the redox couple through the mineral surface is strongly influenced by electron correlation. That is why correlation functionals are included in our

calculations using a hybrid functional such as B3LYP [(Becke 3-Parameter (Exchange), Lee, Yang and Parr (correlation; density functional theory)]. A hybrid functional is an exchange-correlation functional used in density functional theory (DFT) that incorporates a portion of exact exchange from Hartree-Fock theory with exchange and correlation from other sources (ab initio, such as LDA-local density approximation, or empirical)[Hertwig et al, 1997]. This gives a more realistic picture of the electron exchange and charge transfer occurring in a multi-electron system such as PbS(100) cluster along with oxidizing species and adsorbates.

A cluster was chosen due to the use of charged adsorbates and to avoid interactions with adsorbates in neighboring unit cells. This cluster size of galena was chosen as a compromise of computational expense and tolerable edge effects. The latter are described in Becker et al. 2001.

In each calculation, the adsorption energy of As(OH)3 on PbS cluster in the presence and absence of an oxidizing species are determined. In order to obtain individual adsorption energies for the individual adsorbates and the co-adsorption process, the following equations were used:

$$\Delta E_1 = E_{surface+ads.1+ads.2} - [E_{surface} + E_{ads.1} + E_{ads.2}] \quad \ldots\ldots\ldots\ldots \quad (1)$$

$$\Delta E_2 = E_{surface+ads.1} - [E_{surface} + E_{ads.1}] \quad \ldots\ldots\ldots\ldots\ldots\ldots\ldots\ldots \quad (2)$$

$$\Delta E_3 = E_{surface+ads.2.} - [E_{surface} + E_{ads.2}] \quad \ldots\ldots\ldots\ldots\ldots\ldots\ldots\ldots\ldots\ldots \quad (3)$$

$$E_{proximity} = \Delta E_1 - (\Delta E_2 + \Delta E_3) = E_{surface+ads.1+ads.2} - E_{surface+ads.1} - E_{surface+ads.2.} + E_{surface} \quad (4)$$

In the equations above, ads.1 is e.g., $As(OH)_3$, ads.2 can be atomic or molecular oxygen or Fe(III), and in this study, $Pb_{16}S_{16}$ serves as a model for "surface".

The initial position of the oxidizing species on one side of the cluster is also important in the ultimate outcome of proximity effect.

Results and Discussion

The results of our ab-initio calculations on the co-adsorption of As(OH)3 to galena (100) surfaces along with different oxidizing species are discussed in this section. Equations 2 and 3 calculate the adsorption energy of one particular species to a galena (100) surface in the absence of any other oxidizing or reducing species. Equation 1 calculates the co-adsorption energy of both reducing and oxidizing species together on the mineral surface. By combining these equations, proximity effect energies are obtained, whether adsorption of one species is promoted ($E_{proximity} < 0$) or hindered ($E_{proximity} > 0$) in the presence of the respective other. Moreover, if there is a significant change from individual adsorption energies (positive value) to overall co-adsorption energy (negative value) for a particular redox couple, then we can infer that that particular redox couple can facilitate co-adsorption on galena (100) surface.

Proximity effect of $As(OH)_3$ adsorption on galena (100) under the influence of co-adsorption of atomic oxygen

a) Hartree-Fock approach: First the effect of the co-adsorption of atomic oxygen on As(OH)3 adsorption on galena was studied. The total energies of each cluster, individual species and adsorption energies of As(OH)3 to galena in the presence and absence of an oxidizing species are listed in table 5.1. The chemical equations and subsequent proximity energies are listed as follows.

ΔE_1= $E_{Pb16S16.O.As(OH)3} - [E_{PbS} + E_O + E_{As(OH)3}]$ = 19.05 eV
ΔE_2 = $E_{Pb16S16..As(OH)3} - [E_{PbS} + E_{As(OH)3}]$ = 27.76 eV
ΔE_3= $E_{Pb16S16.O.} - [E_{PbS} + E_O]$ = 3.54 eV
$E_{proximity}$ = $\Delta E_1 - (\Delta E_2 + \Delta E_3)$ = -12.25 eV

b) B3LYP approach: The individual energies of species and cluster for B3LYP HF-DFT hybrid approach are listed in table 5.1.

ΔE_1= $E_{Pb16S16.O.As(OH)3} - [E_{PbS} + E_O + E_{As(OH)3}]$ = -40.0 eV
ΔE_2 = $E_{Pb16S16..As(OH)3} - [E_{PbS} + E_{As(OH)3}]$ = -20.14 eV
ΔE_3= $E_{Pb16S16.O.} - [E_{PbS} + E_O]$ = -3.27 eV
$E_{proximity}$ = $\Delta E_1 - (\Delta E_2 + \Delta E_3)$ = -16.6 eV

The negative values for the proximity energies for both HF and B3LYP mean that oxygen promotes the adsorption of $As(OH)_3$ on galena. Interestingly, the HF approach would suggest that individual adsorption of $As(OH)_3$ or atomic oxygen to PbS would not be possible. The B3LYP values for $E_{proximity}$ are more negative than the HF values. As we have discussed earlier, HF simplifies the calculation by not taking electron correlation into account. Thus the interaction of the redox couple through mineral surface during co-adsorption is limited to the direct combination of one-electron wave functions. In the hybrid functional scenario, the behavior of electrons in the redox couple and the galena surface is not independent of each other, as it incorporates electron correlation. Thus the proximity energies are usually more negative in B3LYP calculations. This trend is observed in the rest of the calculations involving other redox couples studied in this chapter. O atoms have two unpaired electrons, and in their atomic state, are very reactive due to their radical character. In nature, oxygen atom will accept electrons from galena and thus enhance $As(OH)_3$ adsorption (Figure 5.1).

Proximity effects on $As(OH)_3$ adsorption on galena (100) under the influence of molecular oxygen

Triplet oxygen is the ground state of the oxygen molecule. The electron configuration of the molecule has two unpaired electrons occupying two degenerate molecular orbitals. These orbitals are classified as a8ntibonding. **Singlet oxygen** is the common name used for the two metastable states of molecular oxygen (O_2) with higher energy than the ground state triplet oxygen. Singlet oxygen, where the electron spins are opposed in a higher energy state, is many times more reactive than triplet oxygen. When the oxygen molecule is away from the galena (100) surface, it is in its triplet state. During the co-adsorption of $As(OH)_3$ and oxygen onto the galena surface, the oxygen molecule approaches closer to the surface. The oxygen molecule moves ~ 1.5 Å towards the galena surface during the co-adsorption process The oxygen molecule is more reactive in its singlet state, and it crosses over the activation energy barrier as it approaches the surface (Figure 5.2). Oxygen adsorbed to the galena surface prefers to be in its singlet spin state. Electron exchange with the galena surface is more favorable with the singlet oxygen near the surface.

Singlet oxygen energies:

a) Hartree Fock:

$\Delta E_1 =$	$E_{Pb16S16.O2(s).As(OH)3} - [E_{PbS} + E_{O2(s)} + E_{As(OH)3}]$	= 30.75 eV
$\Delta E_2 =$	$E_{Pb16S16..As(OH)3} - [E_{PbS} + E_{As(OH)3}]$	= 27.76 eV
$\Delta E_3 =$	$E_{Pb16S16.O2.(t)} - [E_{PbS} + E_{O(t)}]$	= 4.90 eV
$E_{proximity} =$	$\Delta E1 - (\Delta E2 + \Delta E3)$	= -1.91 eV

b) B3LYP:

ΔE_1= $E_{Pb16S16.O2(s).As(OH)3} - [E_{PbS} + E_{O2(s)} + E_{As(OH)3}]$ = -14.42 eV
ΔE_2 = $E_{Pb16S16..As(OH)3} - [E_{PbS} + E_{As(OH)3}]$ = -20.14 eV
ΔE_3= $E_{Pb16S16.O2.(t)} - [E_{PbS} + E_{O(t)}]$ = 14.97 eV
$E_{proximity}$ = $\Delta E1 - (\Delta E2 + \Delta E3)$ = -9.25 eV

Triplet oxygen energies

a) Hartree Fock:

ΔE_1= $E_{Pb16S16.O2(t).As(OH)3} - [E_{PbS} + E_{O2(t)} + E_{As(OH)3}]$ = 27.76 eV
ΔE_2 = $E_{Pb16S16..As(OH)3} - [E_{PbS} + E_{As(OH)3}]$ = 27.76 eV
ΔE_3= $E_{Pb16S16.O2.(t)} - [E_{PbS} + E_{O(t)}]$ = 2.72 eV
$E_{proximity}$ = $\Delta E_1 - (\Delta E_2 + \Delta E_3)$ = -2.72 eV

b) B3LYP:

ΔE_1= $E_{Pb16S16.O2(t).As(OH)3} - [E_{PbS} + E_{O2(t)} + E_{As(OH)3}]$ = -13.61 eV
ΔE_2 = $E_{Pb16S16..As(OH)3} - [E_{PbS} + E_{As(OH)3}]$ = -20.14 eV
ΔE_3= $E_{Pb16S16.O2.(s)} - [E_{PbS} + E_{O(s)}]$ = 6.75 eV
$E_{proximity}$ = $\Delta E_1 - (\Delta E_2 + \Delta E_3)$ = -0.22 eV

We have obtained less negative proximity energy with triplet oxygen co-adsorption with $As(OH)_3$ using B3LYP (-0.22 eV) than singlet oxygen co-adsorbed with $As(OH)_3$ on galena surface. This shows that oxygen (at triplet state) adsorption with $As(OH)_3$ on galena cluster is not favored. When oxygen in the singlet state is co-adsorbed to the galena surface, the proximity energy using B3LYP is -9.25 eV, which is more favorable than HF calculations. In the earlier section we have discussed the reason of this trend (electron correlation). The results in this section show that atomic oxygen is a better candidate to facilitate co-adsorption of $As(OH)_3$ on a galena (100) surface than molecular oxygen.

The oxygen molecule moves only slightly (~0.5 Å) during the adsorption of $As(OH)_3$, while the distance between the cluster and the $As(OH)_3$ molecule changes by

~1.2 Å. The closest S-As distance is 2.25 Å in presence of oxygen molecule, and ~3.47 Å in absence of oxygen molecule.

Proximity effect in the presence of Fe (III) as oxidizing agent

As an alternative oxidant, the oxidation and proximity effect of Fe(III) with $As(OH)_3$ on galena is studied. Fe(III) has 5 unpaired 3d-electrons, which gives rise to a spin multiplicity of 6 (2×5/2+1), whereas in the low-spin case, there is only one unpaired electron giving rise to a spin multiplicity of 2 (2×1/2+1). This difference in spin-multiplicity due to high-spin or low-spin is true for both octahedral and tetrahedral field splitting. The proximity effect in the presence of both high-spin and low-spin Fe(III) is studied. The initial positions of Fe(III) to be on the same and opposite side of the cluster, and at a corner site are also considered.

Proximity effect on $As(OH)_3$ adsorption on galena (100) with Fe(III) high-spin

The individual energies and cluster energies are listed in table 5.1 for both HF and B3LYP calculations. The calculation for the proximity effect in the presence of Fe(III) as high-spin is as follows :

a) Hartree-Fock:

$\Delta E_1 =$ $E_{Pb16S16.Fe(hs).As(OH)3} - [E_{PbS} + E_{Fe(hs)} + E_{As(OH)3}]$ = 10.61 eV
$\Delta E_2 =$ $E_{Pb16S16..As(OH)3} - [E_{PbS} + E_{As(OH)3}]$ = 27.76 eV
$\Delta E_3 =$ $E_{Pb16S16.Fe.(ls)} - [E_{PbS} + E_{Fe(ls)}]$ = -11.16 eV
$E_{proximity} =$ $\Delta E_1 - (\Delta E_2 + \Delta E_3)$ = -5.91 eV

b) B3LYP:

ΔE_1= $E_{Pb16S16.Fe(hs).As(OH)3} - [E_{PbS} + E_{Fe(hs)} + E_{As(OH)3}]$ = -51.97 eV
ΔE_2 = $E_{Pb16S16..As(OH)3} - [E_{PbS} + E_{As(OH)3}]$ = -20.14 eV
ΔE_3= $E_{Pb16S16.Fe.(ls)} - [E_{PbS} + E_{Fe(ls)}]$ = -31.65 eV
$E_{proximity}$ = $\Delta E_1 - (\Delta E_2 + \Delta E_3)$ = -0.18 eV

Proximity effect on $As(OH)_3$ adsorption on galena (100) with Fe(III) low spin

The calculation for the proximity effect in the presence of Fe(III) as low-spin is as follows :

a) Hartree-Fock:

ΔE_1= $E_{Pb16S16.Fe(ls).As(OH)3} - [E_{PbS} + E_{Fe(ls)} + E_{As(OH)3}]$ = -0.27 eV
ΔE_2 = $E_{Pb16S16..As(OH)3} - [E_{PbS} + E_{As(OH)3}]$ = 27.76 eV
ΔE_3= $E_{Pb16S16.Fe.(hs)} - [E_{PbS} + E_{Fe(hs)}]$ = -6.53 eV
$E_{proximity}$ = $\Delta E_1 - (\Delta E_2 + \Delta E_3)$ = -21.5 eV

b) B3LYP:

ΔE_1= $E_{Pb16S16.Fe(ls).As(OH)3} - [E_{PbS} + E_{Fe(ls)} + E_{As(OH)3}]$ = -63.67 eV
ΔE_2 = $E_{Pb16S16..As(OH)3} - [E_{PbS} + E_{As(OH)3}]$ = -20.14 eV
ΔE_3= $E_{Pb16S16.Fe.(hs)} - [E_{PbS} + E_{Fe(hs)}]$ = -26.39 eV
$E_{proximity}$ = $\Delta E_1 - (\Delta E_2 + \Delta E_3)$ = - 17.14 eV

The calculated proximity energies are more negative when Fe(III) is at low-spin when co-adsorbed to galena surface with $As(OH)_3$ compared to Fe(III) at high spin. Fe(III) has 5 unpaired 3d-electrons in high-spin. When the Fe(III) gets closer to the surface during adsorption, it interacts with the electrons from closest S atom in galena cluster. According to ligand field theory, S atom electrons split the t2g and eg orbitals of 3d electron level of Fe(III). This causes the Fe(III) to transfer from high-spin to low-spin when getting close to the surface, and Fe(III) in low-spin state in co-adsorbed state on

galena (100) surface.. The initial and final distance of the oxidizing species and $As(OH)_3$ on either side of the cluster did not change significantly during the process of adsorption.

Significant differences between HF and B3LYP energies

In the results above, the HF and B3LYP energies are significantly different. This shows that the electron correlation effect for Fe(III) as oxidizing agent is substantial during co-adsorption of $As(OH)_3$ on galena (100) surface. Fe(III) has a higher number of atomic orbitals than oxygen. Thus HF approximation which follows the LCAO (linear combination of atomic orbitals) method, causes significant deviation from the actual electronic interaction taking place between redox couple and mineral surface. B3LYP takes into account of all electron correlations in Fe(III) atomic orbitals. Since Fe(III) has d-orbitals, it has more complicated electron correlation and electron exchange with its neighbors (the mineral surface electrons in this case) compared to oxygen atom/molecule [Friesner et al, 2001]. Thus the difference between HF and B3LYP is more significant in adsorption energies involving Fe(III). This trend is also found in other calculations involving Fe(III) (different spin states and positions of the Fe(III)) as oxidizing agent in this chapter. The relative influence of Fe(III) high-spin/low-spin on $As(OH)_3$ adsorption in galena surface is discussed after the calculations with Fe(III) low-spin as oxidizing agent.

It is observed that Fe (III) as an oxidizing species influences the $As(OH)_3$ adsorption on galena, in both high-spin and low-spin cases (Figure 5.3), though the proximity energy in low-spin case is more negative, i.e., adsorption is more favorable when Fe(III) is present in low-spin state as oxidizing agent. Fe(III) in low-spin state has 1 unpaired spin 3d electron (considering octahedral ligand field, and also considering

emission of 4s electron before 3d electrons during ionization). In high-spin case, Fe(III) has one electron each in five 3d energy levels(d_{xy}, d_{yz}, d_{zx}, d_{z2}, d_{x2-y2}) and the electron exchange with the galena cluster and arsenic hydroxide is delocalized, which may be the reason of less favorable proximity influence compared to the case of Fe(III) low-spin. Fe(III) low-spin has only one unpaired spin in 3d energy level, and the electron exchange and interaction with galena cluster is much more localized, which in turn has more proximity influence on $As(OH)_3$ adsorption on galena (100) cluster.

Proximity effect in the presence of Fe (III) as oxidizing agent in the corner of galena cluster

If the initial position of Fe(III) (both high-spin and low-spin) is located near the corner of the cluster (Figure 5.4) and $As(OH)_3$ is on the other side of the cluster, the electron sharing and charge density distribution is different from the two earlier cases where Fe is on the same side of the cluster. Cluster corners are more reactive than other positions of the cluster. Charge transfer and spin polarizations in the cluster corner facilitates mobility of the Fe(III) as oxidizing species, which in turn makes the $As(OH)_3$ species mobile on the other side of the cluster. In an earlier study, it was shown that adsorbed species on a mineral surface modify the corner sites of a mineral surface through proximity effects [Becker et al, 2001]. It is also shown that surface complexes may find a new energetic minimum at the surface that can be located at the corner. STM-STS images have confirmed the importance of proximity effect, and have also shown the oxidation of pyrite surface via O_2 in vacuum, where initial position of O_2 is at the corner of the mineral surface cluster [Becker et al, 2001]. It is expected that the Fe(III) at the

corner of the galena (100) cluster will facilitate the co-adsorption of $As(OH)_3$ through proximity effect .

Proximity effect on $As(OH)_3$ adsorption on galena (100) with Fe(III) high-spin at the corner of galena cluster

Here the effect with initial Fe(III) (high-spin) position at the corner of the galena cluster is studied.

a) Hartree Fock:

$\Delta E_1 =$ $E_{Pb16S16.Fecorner(hs).As(OH)3} - [E_{PbS} + E_{Fecorner(hs)} + E_{As(OH)3}$ = 7.07 eV

$\Delta E_2 =$ $E_{Pb16S16..As(OH)3} - [E_{PbS} + E_{As(OH)3}]$ = 27.76 eV

$\Delta E_3 =$ $E_{Pb16S16.Fe.corner(ls)} - [E_{PbS} + E_{Fecorner(ls)}]$ = 12.52 eV

$E_{proximity} =$ $\Delta E_1 - (\Delta E_2 + \Delta E_3)$ = - 8.17 eV

b) B3LYP:

$\Delta E_1 =$ $E_{Pb16S16.Fecorner(hs).As(OH)3} - [E_{PbS} + E_{Fecorner(hs)} + E_{As(OH)3}$ = -58.23 eV

$\Delta E_2 =$ $E_{Pb16S16..As(OH)3} - [E_{PbS} + E_{As(OH)3}]$ = -20.14 eV

$\Delta E_3 =$ $E_{Pb16S16.Fe.corner(ls)} - [E_{PbS} + E_{Fecorner(ls)}]$ = - 34.56eV

$E_{proximity} =$ $\Delta E_1 - (\Delta E_2 + \Delta E_3)$ = - 3.53 eV

Proximity effect on $As(OH)_3$ adsorption on galena (100) with Fe(III) low spin at the corner of galena cluster

The calculation for the proximity effect in the presence of Fe(III) in the corner as low-spin is as follows :

a) Hartree-Fock:

ΔE_1= $E_{Pb16S16.Fecorner(ls).As(OH)3} - [E_{PbS} + E_{Fecorner(hs)} + E_{As(OH)3}]$ = -2.72 eV
ΔE_2 = $E_{Pb16S16..As(OH)3} - [E_{PbS} + E_{As(OH)3}]$ = 27.76 eV
ΔE_3= $E_{Pb16S16.Fe.corner(ls)} - [E_{PbS} + E_{Fecorner(ls)}]$ = -5.71eV
$E_{proximity}$ = $\Delta E_1 - (\Delta E_2 + \Delta E_3)$ = -24.77 eV

b) B3LYP:

ΔE_1= $E_{Pb16S16.Fecorner(hs).As(OH)3} - [E_{PbS} + E_{Fecorner(hs)} + E_{As(OH)3}]$ = -70.47 eV
ΔE_2 = $E_{Pb16S16..As(OH)3} - [E_{PbS} + E_{As(OH)3}]$ = -20.14 eV
ΔE_3= $E_{Pb16S16.Fe.corner(hs)} - [E_{PbS} + E_{Fecorner(hs)}]$ = - 24.49 eV
$E_{proximity}$ = $\Delta E_1 - (\Delta E_2 + \Delta E_3)$ = - 25.84 eV

The adsorption energies in both HF and B3LYP case are comparable, though the energies are lower (more negative) compared to the previous case, when the oxidizing species Fe(III) is present at the side of galena cluster.

These results follow a similar trend in proximity energies with Fe(III) in the corner of the cluster, as we have observed when Fe(III) at the side of the galena cluster during co-adsorption. The adsorption energies are more negative when Fe(III) is at the corner of the cluster compared to the side of the cluster. The energies again show that Fe(III) is high-spin away from the surface, and switches to low-spin when it gets close to the surface and co-adsorbs to the galena (100) cluster along with $As(OH)_3$. The other scenario, where Fe(III) at high spin state is co-adsorbed with $As(OH)_3$ on galena surface has less favorable energy. In the earlier section it was shown that the ligand field splitting was responsible for Fe(III) transferring from high-spin to low-spin when it approached near the surface.

When The Fe ion as oxidizing species is present at the side of the cluster, it interacts more with atoms at the galena cluster, which facilitates electronic interactions with S atoms at the galena cluster through exchange of electron density and spin density, which

in turn influences $As(OH)_3$ adsorption on the other side of the cluster. But this interaction with S atoms delocalizes the electron exchange and charge transfer. This is not the case when the Fe atom is present at the corner of the cluster. In that case it is interacting with one S atom present at the corner of the cluster, and thus the electron exchange and charge transfer to the galena cluster is much more localized than the previous scenario (Fe at the side). This causes more negative adsorption energy and favorable condition for $As(OH)_3$ adsorption on galena cluster.

When both $As(OH)_3$ and Fe(III) are placed on two different corners of galena cluster, the adsorption energies become much lower for both the high-spin and low-spin case. The comparison of proximity energies for Fe(III) as oxidizing agent in different starting positions and spin configuration is given in table 5.2. When both the oxidizing species and adsorbate are on two separate and opposite corners of a cluster(Figure 5.5), the electron exchange and charge transfer is minimized, resulting in the adsorption and proximity energies lower than the case when only oxidizing species are present at the corner of the cluster.

The effect of low-spin Fe(III) is similar to the previous case where the initial position of Fe(III) was at the middle of the cluster. Low-spin Fe(III) at corner of the cluster favors the proximity effect more than the high-spin case, thus providing more negative proximity energy.

Conclusions

Through this study, we investigated the effect of oxidizing species on the adsorption of toxic elements such as As onto the mineral galena (100) surface. Using both Hartree-Fock theory and the hybrid functional B3LYP in the program Gaussian 03, different

starting positions of the oxidizing species with respect to the galena cluster has been compared. The effect of oxidizing species with different spin configuration has also been studied, as spin configuration has definitive influence on proximity effect energy. An oxygen atom or an oxygen molecule are the two most likely candidates in nature that can influence adsorption of a species on a mineral surface. Oxygen atoms can be present as oxides in different natural minerals. It is observed that oxygen atoms, most likely to be present as oxides, influence arsenic hydroxide adsorption to galena surface favorable. The energies are fairly negative (~ -13 eV), which suggests that As(III) species can be adsorbed on to galena in oxidizing natural environment. The adsorption energies are less negative in presence of oxygen molecule.

Fe(III) as an oxidizing species is also considered. Fe-oxides and hydroxides are common and abundant as mineral on earth's surface, and can substantially influence the concentration of As(III) speciation in ground-water. Calculations show us that Fe(III) in low-spin state is more likely to favor As(III) species adsorption on galena (100) cluster. Fe(III) is likely to be at a high-spin state when away from the galena surface, but it transfers to the low-spin state during co-adsorption process of $As(OH)_3$ onto the galena (100) surface. It is known that in presence of a strong ligand, which induces large crystal field splitting, Fe(III) forms low-spin configuration. Thus Fe(III) complexes with large organic ligands have low-spin in Fe(III). These types of complexes are common in bacterial and microbial cells. Thus these types of organisms can increase the concentration of low-spin Fe(III) species in nature, in locations where mobile As(III) concentration is high, and can facilitate As-adsorption on mineral surfaces, thus reducing

the concentration of As in ground water. Some of the well known low-spin Fe(III) complexes are alkyl-peroxo complexes or iron-porphyrin complexes [Rovira et al, 1997]..

The calculations show us that one can favorably adsorb As (III) into mineral surfaces in presence of natural oxidants and thus reduce the mobility of As (III) species in the groundwater. Adsorption of $As(OH)_3$ can lead to oxidation of As(III) species to As(V), which may cause favorable adsorption energy. Though the electron density on As(III) species increases at adsorbed state on galena surface, it is still unknown whether As(III) oxidizes to As(V) during the co-adsorption process to galena. Oxidation of As(III) to As(V) and subsequently reducing mobility and concentration of As (III) in groundwater will considerably reduce the As-poisoning and help us to solve a major environmental problem which is affecting a substantial amount of human population in today's world.

In the study of co-adsorption of $Fe(III)/O_2$ with $As(OH)_3$ on PbS(100) surface, one of the main objectives is to oxidize As(III). Here sulfide is present in the system as electron transporter medium between the redox couples present on either side of the cluster. Sulfide ions do not act as donor of electron, or reducing agent. To study the effect of sulfide as electron-supplier in the semiconducting mineral surface during co-adsorption, one can study the co-adsorption of $As(OH)_3$ with Fe(III) on arsenopyrite (FeAsS). Arsenopyrite has As(III) in its structure. Experiments and computational calculations can be set up to test whether the Fe(III) species oxidizes the As(III) on the other side of the cluster directly, or it oxidizes As(III) via the interaction with arsenic present in arsenopyrite. Galena surface was chosen for the study in chapter 5 mainly because of the simplicity of the structure aside from galena's abundance in the nature. Studying co-adsorption on galena surface helped us to separately study the influence of

Fe(III) on As(III) species adsorption without having any common-ion effect. But effect of common-ions in the co-adsorptions can be studied with the help of experiments and computational calculations. A series of experiments and computational calculations (similar to the calculations performed in chapter 5) can be set up to compare co-adsorption of redox couples on various mineral surfaces like pyrite (FeS_2), mackinawite (Fe, Ni)S. We can compare these results with galena to see the influence of cations, and structures on co-adsorption of redox couples on mineral surfaces through proximity effect.

Table 5.1: Adsorption energies of individual species and their adsorption on galena (100) cluster in presence and absence of oxidizing agent (Hartree- Fock and B3LYP theory calculations)

Cluster	energy (eV) HF	energy (eV) B3LYP
$Pb_{16}S_{16}$	-5806.56	-5955.67
$As(OH)_3$	-6320.57	-6315.13
Oxygen atom	-2032.12	-2043.00
Oxygen molecule (O_2) singlet	-4064.51	-4088.45
Oxygen molecule (O_2) triplet	-4068.04	-4090.09
Fe(III) high-spin	-3285.73	-3300.15
Fe(III) low-spin	-3277.29	-3294.44
$Pb_{16}S_{16}$ + $As(OH)_3$+ O	-14140.20	-14353.80
$Pb_{16}S_{16}$ + $As(OH)_3$+ O_2 singlet	-16160.89	-16373.68
$Pb_{16}S_{16}$ + $As(OH)_3$+ O_2 triplet	-16167.42	-16374.49
$Pb_{16}S_{16}$ + $As(OH)_3$	-12099.37	-12290.94
$Pb_{16}S_{16}$ + $As(OH)_3$ corner	-12093.11	-12285.49
$Pb_{16}S_{16}$ + O	-7835.14	-8001.94
$Pb_{16}S_{16}$ + O_2 singlet	-9870.79	-10037.87
$Pb_{16}S_{16}$ + O_2 triplet	-9869.70	-10030.79
$Pb_{16}S_{16}$ + $As(OH)_3$+ Fe(III) high-spin	-15402.24	-15622.92
$Pb_{16}S_{16}$ + $As(OH)_3$+ Fe(III) high-spin (corner)	-15405.78	-15629.18
$Pb_{16}S_{16}$ + $As(OH)_3$ (corner)+ Fe(III) high-spin (corner)	-15386.46	-15611.49
$Pb_{16}S_{16}$ + $As(OH)_3$+ Fe(III) low-spin	-15404.69	-15628.91
$Pb_{16}S_{16}$ + $As(OH)_3$+ Fe(III) low-spin (corner)	-15407.14	-15635.71
$Pb_{16}S_{16}$ + $As(OH)_3$ (corner)+ Fe(III) low-spin (corner)	-15414.22	-15621.56
$Pb_{16}S_{16}$ + Fe(III) high-spin	-9098.00	-9282.22
$Pb_{16}S_{16}$ + Fe(III) high-spin (corner)	-9096.37	-9280.31
$Pb_{16}S_{16}$ + Fe(III) low-spin	-9282.22	-9282.76
$Pb_{16}S_{16}$ + Fe(III) low-spin (corner)	-9280.31	-9284.67

Table 5.2: Comparison between proximity effect energies of $As(OH)_3$ on PbS(100) cluster for different starting positions and spin orientation of Fe(III)

Initial position of oxidizing species and adsorbate with respect to PbS(100) cluster	**Both Fe(III) and $As(OH)_3$ is at opposite sides of PbS(100) cluster** **Proximity Energy (eV)**	**Fe(III) is on one corner of PbS(100) cluster, $As(OH)_3$ is at the side of the cluster** **Proximity Energy (eV)**
Fe (III) high-spin (HF)	-5.91	-8.17
Fe (III) high-spin (B3LYP)	-0.18	-3.53
Fe(III)low-spin (HF)	-21.15	-24.77
Fe (III) low-spin (B3LYP)	-17.14	-25.84

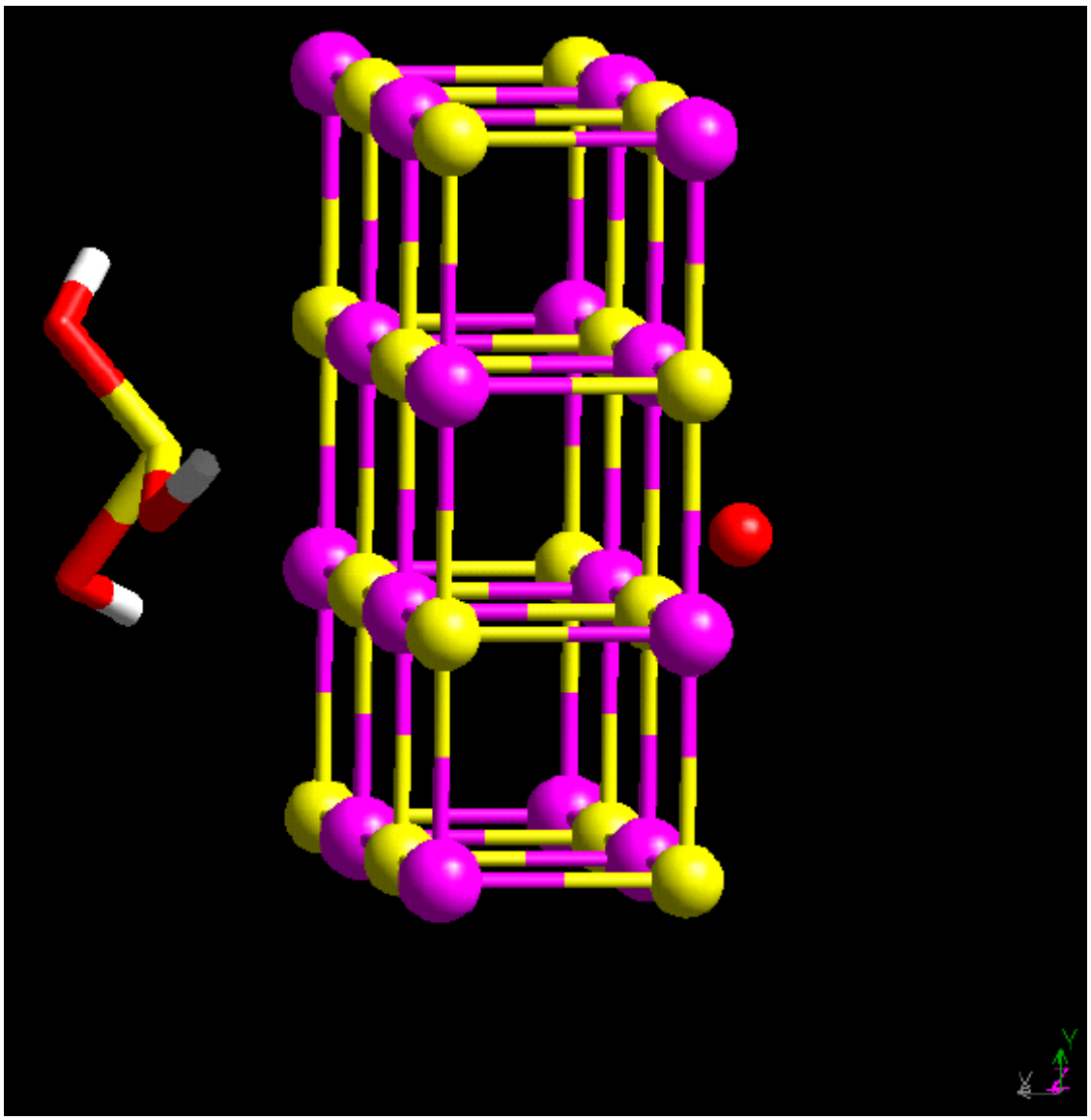

Figure 5.1. Oxygen atom at the side of the PbS(100) cluster as oxidizing agent, influencing the adsorption of $As(OH)_3$ on the other side of the cluster, through proximity effect. The distance of Oxygen atom from the nearest Pb atom in the cluster is 1.717 Å. Distance of As(III) in $As(OH)_3$ from nearest S atom in the cluster is 3.58 Å.

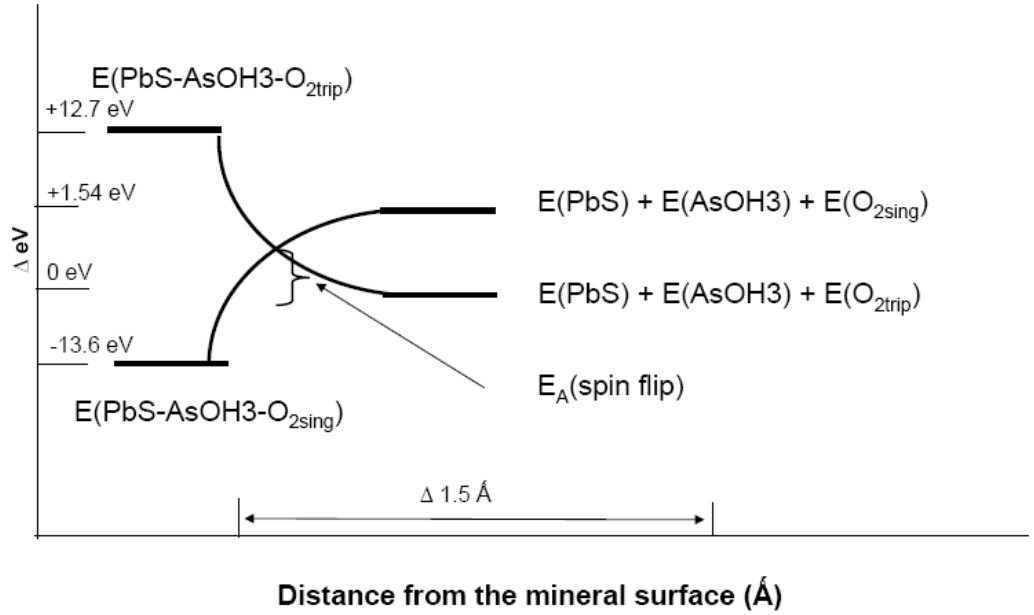

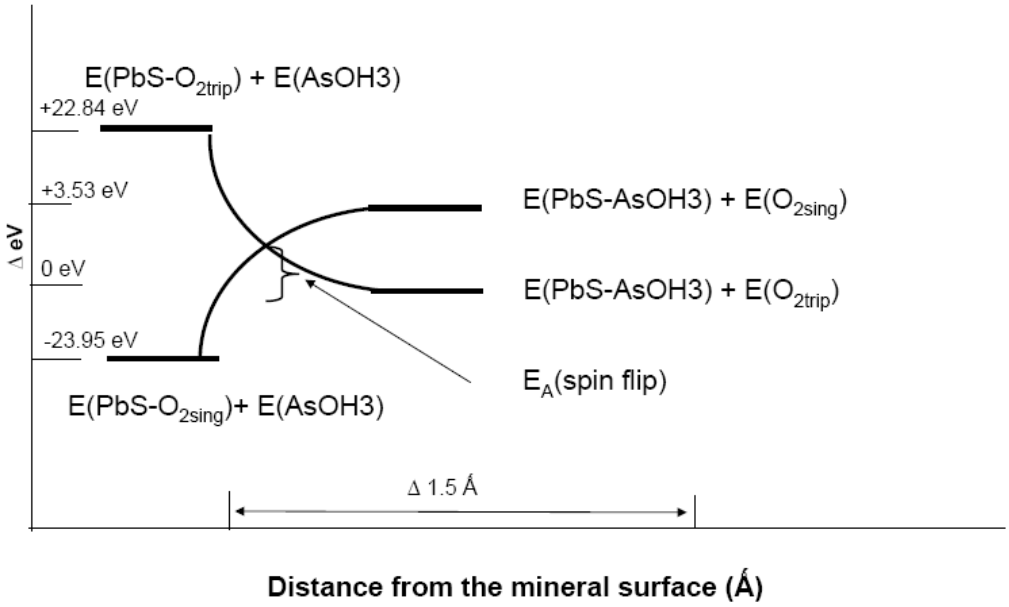

Figure 5.2. The spin flips between oxygen molecule triplet and singlet spin states during its co-adsorption on galena (100) surface along with $As(OH)_3$. Triplet state is more stable away from the surface, but as O_2 gets closer to the surface during adsorption, it crosses activation energy barrier and singlet spin state of O_2 becomes more stable close to the surface. The bottom picture shows that the spin transition from triplet to singlet takes place as well when O_2 exchanges place with $As(OH)_3$ on the galena (100) surface.

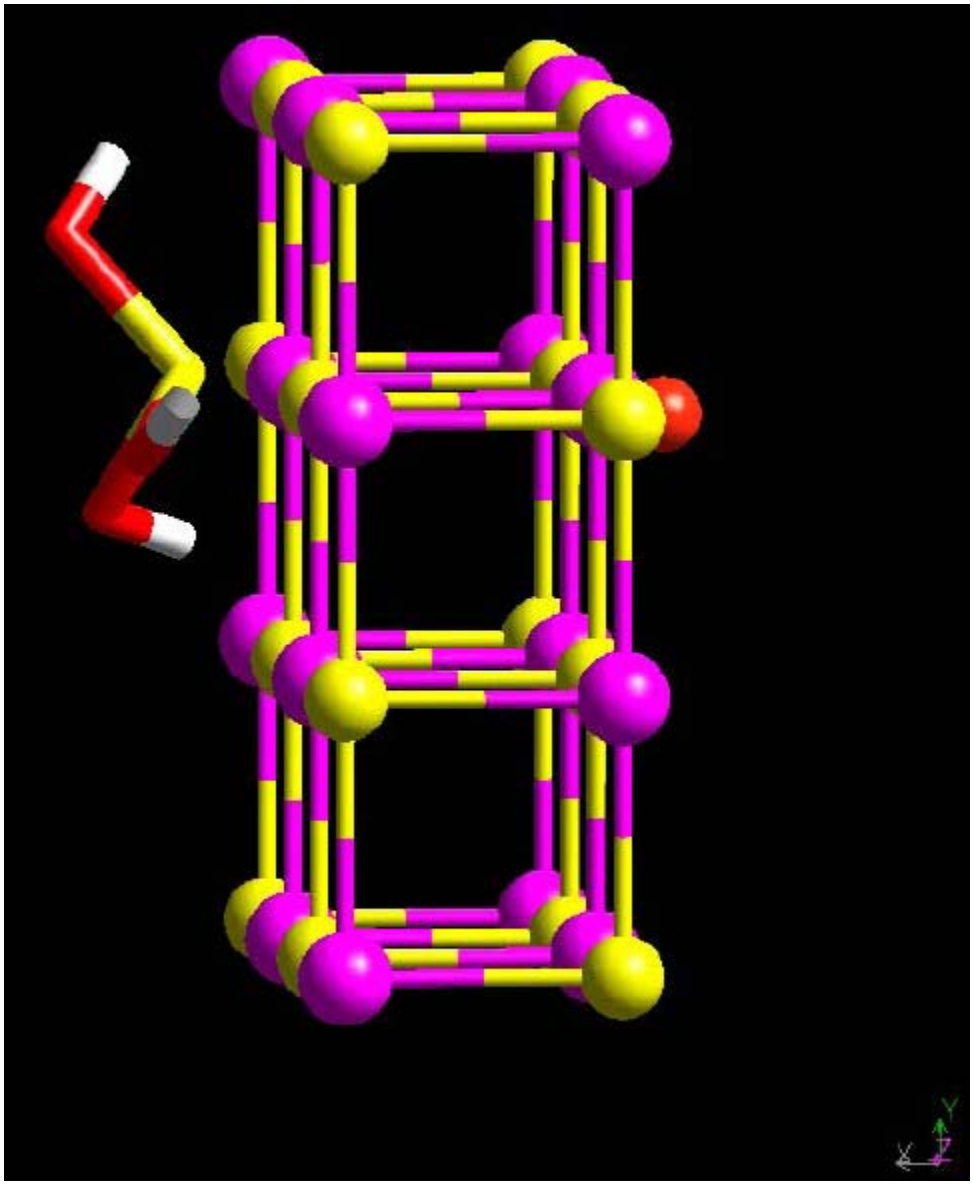

Figure 5.3. Fe(III) atom at the one side of the PbS(100) cluster as oxidizing agent, influencing the adsorption of $As(OH)_3$ on the other side of the cluster, through proximity effect. Both Fe(III) high-spin and low-spin case is studied . Fe(III) comes closer to the PbS cluster during the simulation by ~1.5 Å from its initial position.

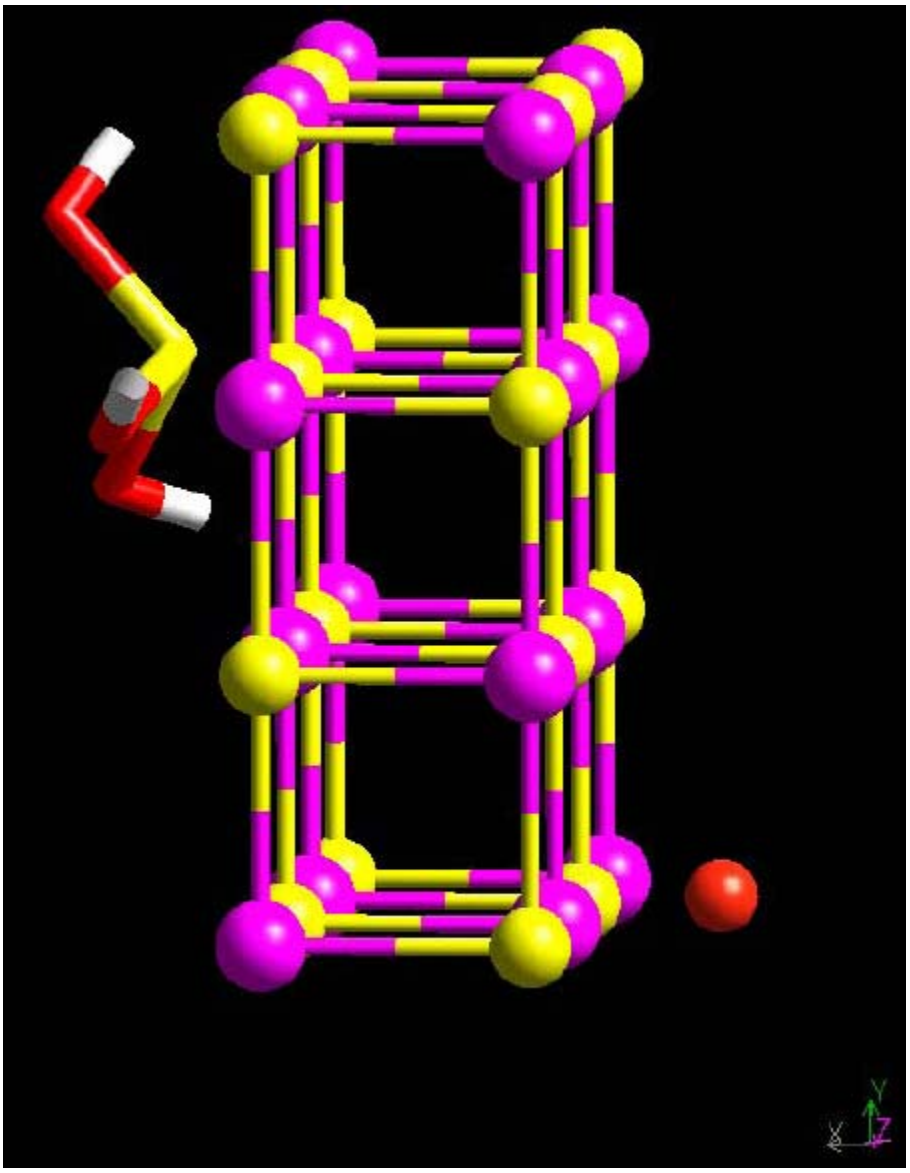

Figure 5.4. Fe(III) is present at the corner of PbS(100) cluster, and $As(OH)_3$ is in the opposite side of the cluster to Fe(III). The initial distance of Fe(III) to corner S-atom is 3.017 Å, which reduces to 1.89 Å during adsorption process through proximity effect.

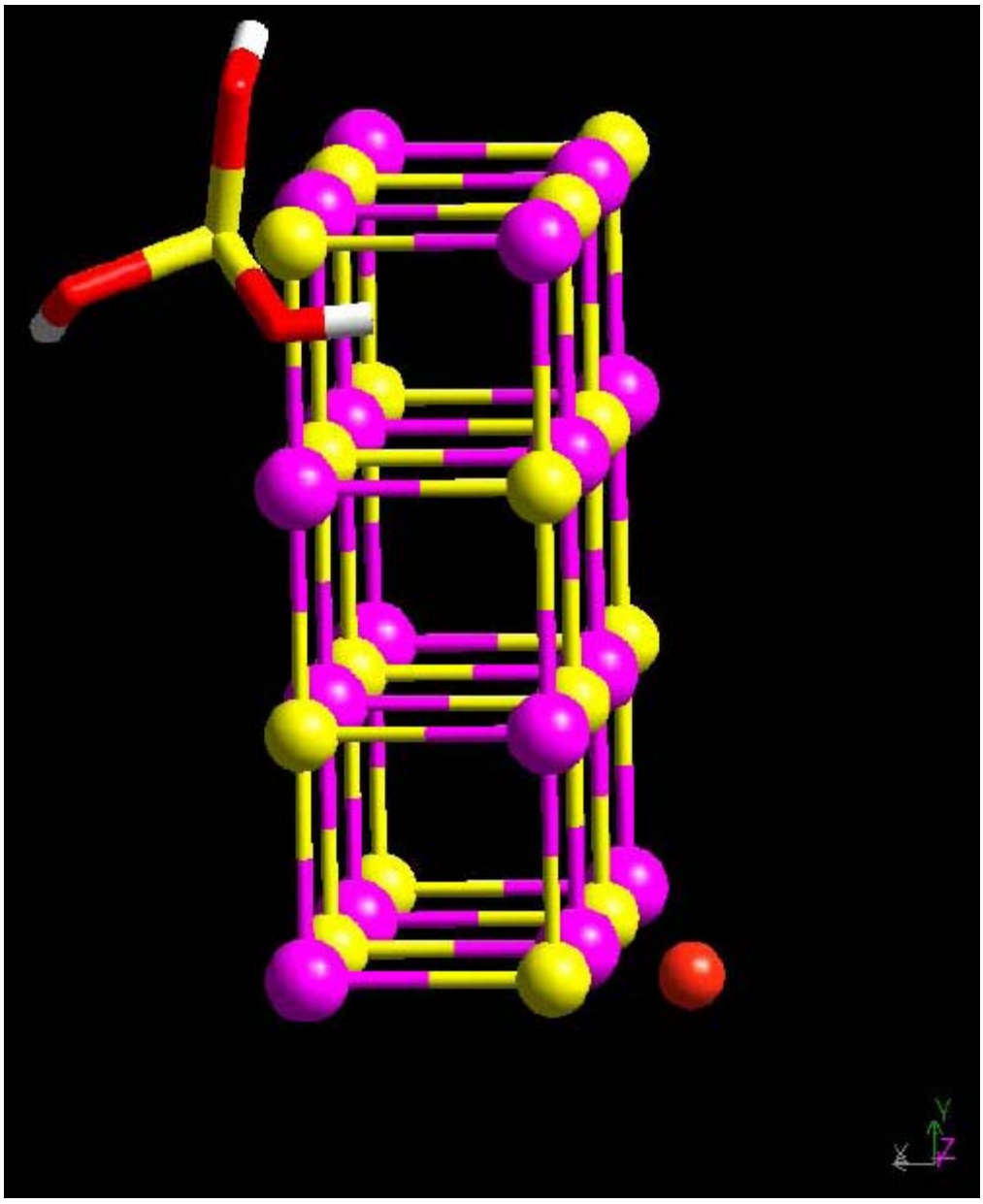

Figure 5.5. Both Fe(III) and $As(OH)_3$ are in the opposite corners of PbS(100) cluster. During the adsorption process, Fe (III) comes closer to the nearest S atoms from its initial position during the simulation

References

Anderson MA, Ferguson JF, Gavis J: **Arsenate adsorption on amorphous aluminum hydroxide.** *Journal of Colloid and Interface Science* 1976, **54:** 391–399

Becker U, Greatbanks SP, Rosso KM, Hillier IH, Vaughan DJ: **An embedding approach for the calculation of STM images: Method development and application to galena (PbS)** *Journal of Chemical Physics* 1997, **107:**7537–7542

Becker U, Hochella MF: **The calculation of STM images, STS spectra, and XPS peak shifts for galena: New tools forunderstanding mineral surface chemistry.** *Geochimica Cosmochimica Acta* 1996,**60:**2413–2426

Becker U, Rosso KM, Hochella MF**: The proximity effect on semiconducting mineral surfaces: a new aspect of mineral surface reactivity and surface complexation theory?** *Geochimica Cosmochimica Acta* 2001,**65:** 2641-2649

Bostick BC, Fendorf S, Manning BA: **Arsenite adsorption on galena (PbS) and sphalerite (ZnS).** *Geochimica et Cosmochimica Acta* 2003, **67:**895-907

Cummings DE, Caccavo F, Fendorf S, Rosenzweig RF: **Arsenic mobilization by the dissimilatory Fe(III)-reducing bacterium Shewanella alga BrY.** *Environmental Science & Technology* 1999, **33:**723-729

Dixit S, Hering JG: **Comparison of Arsenic(V) and Arsenic(III) Sorption onto Iron Oxide Minerals: Implications for Arsenic Mobility.** *Environmental Science & Technology* 2003, **37:**4182-4189

Friesner RA, Dunietz BD: **Large-Scale ab Initio Quantum Chemical Calculations on Biological Systems.** *Accounts of Chemical Research* 2001, **34:**351-358

Harvey CF, *et al.* **Arsenic Mobility and Groundwater Extraction in Bangladesh**. *Science* 2002, 298:1602-1606

Hertwig RH, Koch W: **On the parameterization of the local correlation functional. What is Becke-3-LYP?** *Chemical Physics Letters* 1997, **268**: 345-351

Manning BA, Fendorf SE, Goldberg S: **Surface structures and stability of arsenic(III) on goethite: Spectroscopic evidence for inner-sphere complexes.** *Environmental Science & Technology* 1998, **32:** 2383–2388

Nesbitt HW, Reinke M: **Properties of As and S at NiAs, NiS, and $Fe_{(1-x)}S$ surfaces, and reactivity of niccolite in air and water:** *American Mineralogist* 1999, **4:**639-649

Nickson RT, McArthur JM, Ravenscroft P, Burgess WG, Ahmed KM: Mechanism of arsenic release to groundwater, Bangladesh and West Bengal. *Applied Geochemistry* 2000, 15:403-413

Perkins C, Kim CN, Fang G, Bhalla KN: **Arsenic induces apoptosis of multidrug-resistant human myeloid leukemia cells that express Bcr-Abl or overexpress MDR, MRP, Bcl-2, or Bcl-x_L**. *Blood* 2000, 95:1014-1022

Rovira C, Kunc K, Hutter J, Ballone P, Parrinello M: **Equilibrium Geometries and Electronic Structure of Iron-Porphyrin Complexes:A Density Functional Study.** *Journal of Physical Chemistry A* 1997, **101:**8914-8925

Scwartz RA: **Arsenic and the Skin.** *International Journal of Dermatology* 1997, **36:**241-250

Thomas DJ, Styblo M, Lin S: **The Cellular Metabolism and Systemic Toxicity of Arsenic.** *Toxicology and Applied Pharmacology* 2001, **176:**127–144

Waxman S, Anderson KC: **History of the Development of Arsenic Derivatives in Cancer Therapy**. *Oncologist* 2001, 6:3-10

Waychunas GA, Rea BA, Fuller CC, Davis JA: **Surface chemistry of ferrihydrite. 1. EXAFS studies of the geometry of coprecipitated and adsorbed arsenate.** *Geochimica et Cosmochimica Acta* 1993, **57:**2251-2269

Chapter 6

Conclusions

Molecular modeling of mineral-surface adsorbates has given a new dimension to the research in surface science. The results presented in this thesis are examples on how to apply molecular simulations to molecular-level alterations in the formation and control of mineral surface deposition and growth.

Principle objective in studying interactions between mineral surface and organic adsorbates is to understand the mechanism of biomineral formation. When biominerals are formed, the mineral-organic interfaces form a hard-body exoskeleton on the outer surface of the organism that is exposed to the environment. The question arises whether the mineral surface is shaping the organic matrix by virtue of structural matching. To answer this question, organic template-inorganic mineral interaction at a molecular level is needed to be studied. We chose to work with calcite biomineralization because calcite is the most abundant biomineral found in nature.

In the study involving peptide-calcite interactions, first we have studied the influence of mineral surface on organic molecule organization at the water-mineral interface. The detailed interpretation and results of our work involving 3-amino acid and 12-amino peptide residues are presented in chapter 2. Questions regarding geometry,

orientation, and adsorption energies of different peptides when they interact with calcite surface steps have been addressed. It has been shown that under favorable conditions, peptides are more favorably adsorbed on a calcite (104) surface step parallel to the [42-1] direction rather than the [010] direction. The distance between consecutive calcium ions or carbonate ions are 4.36 Å in the step direction parallel to [42-1] compared to 4.96 Å in the step direction parallel to [010]. The smaller distance in [42-1] matches better with the separation of adsorbing functional groups in the peptides investigated. It is also observed that on non-polar surface steps, the peptides are more favorably adsorbed when the carbonate ions forms an obtuse angle with the underlying terrace rather than an acute angle. $(Phe\text{-}leu\text{-}lys)^{1-}$ exhibits the most favorable adsorption energy on a polar step edge parallel to [42-1] terminated by Ca^{2+} ions. $(Lys\text{-}gln\text{-}tyr)^{2+}$ and $(phe\text{-}leu\text{-}lys)^{1+}$ have the most favorable adsorption energies among the neutral or positively charged peptides on different surface step locations. We can conclude from the above results that if the amino acid side chain contains a benzene ring or a cloud of electrons (electron pairs or π-electrons) that can interact with the mineral surface atoms, it will be favorably adsorbed to that surface location, overcoming the counteracting effect or steric hindrance. Among the above-mentioned peptides that favorably get adsorbed to the calcite surface steps, lysine and glutamine contain amide groups that have electron pairs and tyrosine and phenyl-alanine contain benzene rings. The π-electrons of benzene rings interact with calcium ions at the surface steps.

Long-chain peptides are more common in naturally-occurring biominerals. By comparing the adsorption energies of simple and complex structured 12-amino acid peptides, it is shown that peptides without complex sidechains are more likely to have

parallel alignment to the step-edge of calcite surface. That does not necessarily mean that simple-structured peptides are more common in nature. We can conclude that the simple-structured peptides can provide structural matching with the growing calcite surface, and the peptides that have complex side chains are more likely to facilitate adsorption on calcite surface steps. In addition, the latter are more capable to complex Ca^{2+} ions and may serve as a carrier of these ions to calcite surfaces. The complex side chains in amino acids play a significant role in the interaction with the calcite surface atoms on surface step locations.

The model set-ups described in chapter 2 can serve to further our overall understanding of the interaction between organic molecules and inorganic surfaces. Different amino acids with various functional groups have been studied in chapter 2. Thus the selectivity of the calcite surfaces during biomineralization as a function of structure of the amino acid can be understood from the results presented in chapter 2. This will also help researchers to further investigate effect of structure and orientation of amino acids on other calcite surfaces (other than calcite (104)) during biomineral formation. To mimic the natural environment for biominerals formation more closely, one would need to prepare a multi-dimensional model of organic networks and to observe the growth of calcite crystals under the influence of such an organic framework. Ultimately, the interplay of the organic, inorganic (mineral), and water phase in a three-dimensional network should be studied in a dynamic model using molecular dynamics to mimic more closely a natural biomineralization process.

In chapter 2, it is addressed how small organic molecules interact with the mineral surface, and align themselves along terrace and surface steps. The different properties of

peptides add to the selectivity of mineral surface. The work in chapter two has helped to answer questions on different functional groups of a peptide and their role during biomineral formation, which was missing in previous AFM and other spectroscopic experiments showing various growth and step-direction stabilization of calcite. Though only a handful of peptides have been studied in the work in chapter 2, this work can be extended to various other peptide structures of various organisms. Different peptides will have different amino acid sequence, which will stabilize specific calcite surfaces.

In chapter 3, growth and formation of calcite nucleus under Langmuir films consisting of an amide-containing phospholipid, in aqueous condition has been studied. This study shows how the organic molecules themselves shape the formation of particular calcite surfaces, and govern their growth. Langmuir films were studied as the representative of biofilms, made up with phospholipids. Phospholipid bilayers are present in cell-membrane which often controls the formation of inorganic-nucleating surface from supersaturated solution. In the study in chapter 3, it is shown that the spacing between the phospholipid molecules in the Langmuir film influences the nucleation of calcite (100) surface in an aqueous environment. This study also emphasizes the importance of proper organic template during biomineralization. Organic templates like Langmuir film can be made up of several other amphiphilic molecules which are present as component of cell-walls of various biomineral-forming organism.

The results in chapter 2 and 3 give an indication of what set of organic molecule-mineral surface we have to choose when doing modeling studies on biomineralization. Various other calcite surfaces like (012) can be studied under biological systems to determine their presence as biominerals in nature. This modeling study will also enable

scientists to characterize the protein sequence of an organism in nature that forms calcite biominerals.

Interaction between mineral surface and adsorbates takes place inside our body as well as in natural environments. In chapter 4, interaction of cell-adhesion peptides with hydroxyapatite surfaces have been studied. This is another example of biomineral formation, but here the interaction between organic molecule and the mineral surface takes place inside the body, opposed to the exoskeleton formation in case of calcite. Hydroxyapatite is the major biomineral in our bones, and it acts as biomaterial surface during cell-adhesion and cellular response. Cellular response triggers a series of cellular events that finally cause bone-tissue regeneration. Interaction of the cell-adhesion peptides (functioning as bioactive surfaces) with the hydroxyapatite surface is the stepping stone for bone-tissue engineering. The research in this area of cell-adhesion peptide hydroxyapatite interaction mainly focuses on finding the right combination and sequence of peptides that can influence the bone-regeneration process by proper interaction with and formation of hydroxyapatite surface. The peptides studied in chapter 4 are RGD **(arg-gly-asp)** and YIGSR **(tyr-ile-gly-ser-arg)**. We can infer from the results in this chapter that the adsorption of cell-adhesion peptides on hydroxyapatite surface depends significantly on the orientation of the peptide with respect to the hydroxyapatite surface. Understandably, the energy is higher when the peptide is at the step edge or edge of the surface, compared to the flat terrace. Adsorption energies are significantly more favorable when we allow movement in the top Ca^{2+} layer of hydroxyapatite cluster, and the initial position of the peptide is at the edge of the cluster. The reason for relaxing the top Ca^{2+} layer is to make the hydroxyapatite-model more realistic, as relaxed

hydroxyapatite closely resembles the dynamic carbonated hydroxyapatite present in our bone. Thus it can be inferred that during bone regeneration, the proteins will facilitate adsorption on the mineral surface when the surface is relaxed, and will influence growth at the step edge. Only the top Ca^{2+} layer is relaxed during the study. Relaxation of Ca^{2+} ions takes place in the longitudinal ([010]) direction. Due to the relaxation, the lateral symmetry of the hexagonal cluster or periodic slab is not distorted. The surface remains (001) during the peptide-mineral interaction. The work on this chapter (4) answered questions on peptide orientation dependence during interaction with mineral surface. The experimental studies done so far on cell-adhesion peptides on hydroxyapatite surface [Gilbert et al, 2000, Okamoto et al, 1998] elucidated structural formations of peptides during interaction with hydroxyapatite surface. This study has progressed the understanding of peptide-mineral interactions prior to cellular response further, by focusing on the selectivity of the surface locations of the peptides and also on peptides orientation during interaction with biomaterial (hydroxyapatite) surface.

The work on chapter 2, 3, and 4 are molecular modeling studies based on empirical potential parameters. As mentioned earlier in several parts of the thesis, our main effort is to mimic the natural process of organic inorganic interactions and study the various mechanisms at molecular level. Cerius^2 software is used to create various mineral surfaces, and organic molecules such as peptides, Langmuir films. The empirical potentials are incorporated in the force field that we use for our study, most of which are derived from UNIVERSAL1.02 force field. A good force field with potential parameters matching experimental values provides a good model for computational studies such as molecular dynamics and energy minimization. Potential parameters present in the force-

field describe various interactions occurring during energy minimization process when organic-matrix and inorganic nucleating surfaces are allowed to interact. The arrangement of the organic matrix can be varied during the set-up of the model. But a force-field with accurate set of potential parameters will help the organic matrix to find a minimum energy configuration irrespective of its staring position alongside the mineral surface. The error in potential parameters will cause deviation from this absolute minimum energy for the organic matrix, as well as the interfacial energy between the organic matrix and inorganic nucleating surface.

In chapter 5, the interaction of a sulfide surface with inorganic adsorbates is discussed. Adsorption of a reduced As species on a galena surface is chosen for study, because As mobility and concentration in groundwater is a major problem worldwide due to the toxic nature of As. It has been observed that congruent oxygen adsorption promotes arsenic hydroxide adsorption to the galena surface. The adsorption energies are highly negative (~ -13 eV), which suggests that As(III) species can be adsorbed on to galena in an oxidizing environment. The adsorption energies are less negative in presence of oxygen molecule.

Fe (III) is also used as an oxidizing species. Our calculations show that Fe(III) in a low-spin state is more likely to favor As(III) species adsorption on galena (100). Fe(III)-complexes with large organic ligands chelate low-spin Fe(III). These types of complexes are common in bacterial and microbial cells. Thus, these types of organisms can increase the concentration of low-spin Fe(III) species in nature, in locations where mobile As(III) concentration is high, and can facilitate As-adsorption on mineral surfaces, thus reducing the concentration of As in ground water. Some of the well-known

low-spin Fe(III) complexes are alkyl-peroxo complexes [Lehnert et al, 2001] or iron-porphyrin complexes. This information may open a new area of research and collaboration between environmentalists, geologists, and biologists. This also gives rise to a question whether there are microbial species in nature that have Fe-complexes in their body which can shuttle/transport electrons that can ultimately facilitate proximity effect-like reactions in minerals?

Apart from galena, there are other possible mineral surfaces that can facilitate proximity effect-type adsorption. These surfaces can be hematite (Fe_2O_3), pyrite (FeS_2), which are naturally-occurring and relatively abundant semiconducting materials. Hematite influences transition metal mobility in many soils [Cornell and Schwertmann, 1996], and pyrite [Jambor and Blowes, 1994] and galena [Rimstidt et al., 1994] often act as key components in acid mine runoff. Reactions that occur on the surfaces of these minerals largely dictate the properties and importance that they display in nature.

In the study of co-adsorption of Fe(III)/O_2 with $As(OH)_3$ on PbS(100) surface, one of the main objectives is to oxidize As(III). Here sulfide is present in the system as electron transporter medium between the redox couples present on either side of the cluster. Sulfide ions do not act as donor of electron, or reducing agent. To study the effect of sulfide as electron-supplier in the semiconducting mineral surface during co-adsorption, one can study the co-adsorption of $As(OH)_3$ with Fe(III) on arsenopyrite (FeAsS). Arsenopyrite has As(III) in its structure. Experiments and computational calculations can be set up to test whether the Fe(III) species oxidizes the As(III) on the other side of the cluster directly, or it oxidizes As(III) via the interaction with arsenic present in arsenopyrite. Galena surface was chosen for the study in chapter 5 mainly

because of the simplicity of the structure aside from galena's abundance in the nature. Studying co-adsorption on galena surface helped us to separately study the influence of Fe(III) on As(III) species adsorption without having any common-ion effect. But effect of common-ions in the co-adsorptions can be studied with the help of experiments and computational calculations. A series of experiments and computational calculations (similar to the calculations performed in chapter 5) can be set up to compare co-adsorption of redox couples on various mineral surfaces like pyrite (FeS_2), mackinawite (Fe, Ni)S. We can compare these results with galena to see the influence of cations, and structures on co-adsorption of redox couples on mineral surfaces through proximity effect.

Various other redox couples, such as Fe^{III}/Fe^{II}, Cu^{II}/Cu^{I}, and Au^{III}/Au^{0}, can be studied on these semiconducting mineral surfaces using the theory of proximity effects. The co-adsorption of various redox couples on mineral surfaces does not only have an effect on the thermodynamics of the adsorption, but also, and probably more importantly, on their kinetics. The rate of adsorption of these species can be determined in the presence and absence of the respective other species, and it is possible to determine the activation energy barrier for the proximity effect.

Molecular modeling approaches in surface science, as well as in interdisciplinary science, are a major pathway in future scientific research. The possibility of answering "out-of-reach" questions for experiments is enormous. A scientist can control various aspects of a molecular modeling study, which provides more in-depth analysis of reaction mechanisms, of their thermodynamics and kinetics, of electron transfer mechanisms, and of structure changes during adsorption.

References

Lehnert N, Ho RYN, Que L, Jr., Solomon EI**: Spectroscopic Properties and Electronic Structure of Low-Spin Fe(III)-Alkylperoxo Complexes: Homolytic Cleavage of theO-O Bond.** *Journal of American Chemical Society* 2001**, 123**:8271-8290

Cornell RM, Schwertmann U**: The Iron Oxides.***VCH*.

Gilbert M, Shaw WJ, Long JR, Nelson K, Drobny GP, Giachelli CM, Stayton PS: **Chimeric Peptides of Statherin and Osteopontin That Bind Hydroxyapatite and Mediate Cell Adhesion**. *Journal of Biological Chemistry* 2000 **275**:16213-16218

Jambor JL, Blowes DW (eds.)**:Short Course Handbook on Environmental Geochemistry of Sulfide Mine-Wastes.** *Mineralogical Association of Canada*

Okamoto K, Matsuura T, Hosokawa R, Akagawa Y: **RGD peptides regulate the specific adhesion scheme of osteoblasts to hydroxyapatite but not to titanium**. *Journal of Dental Research* 1998, **77**:481-487.

Rimstidt JD, Chermak JA, Gagen PM: **Rates of reaction of galena, sphalerite, chalcopyrite, and arsenopyrite with Fe(III) in acidic solutions.** *Environmental Geochemistry of Sulfide Oxidation*. 1994, 2–13. American Chemical Society.